

## ABSTRACT

Title of dissertation: PLASTIC TEARING ENERGY IN TOUGH STEELS

Xiaohu Chen, Doctor of Philosophy, 2005

Dissertation directed by: Professor Pedro Albrecht  
Department of Civil Engineering

Plastic tearing occurs in compact tension (C(T)) specimens fabricated from ductile steels. This tearing, however, is not an elastic fracture problem governed by a crack tip singularity parameter. The current application of the  $J$ -integral and the  $J$ - $R$  curve to plastic fracture mechanics is misleading. This dissertation reviews the existing energy rate and geometric factor approaches, and then reanalyzes the unloading compliance data for C(T) specimens of various types of steel. The objective of the analysis is to investigate the criteria that can characterize the crack extension under plastic tearing. The author suggests that the energy release rate that remains constant with significant crack growth, in conjunction with the mechanism motion of crack extension to represent the degree of tearing, can serve as the objective parameter in a standard fracture toughness test. Both the energy release rate and the plastic tearing mechanism motion are calculated directly from the test data. The effects of the initial crack length, the specimen size, the testing temperature, and the steel type on the results are investigated. The purpose is to determine the

sensitivity of both parameters to the testing configurations. To discuss the tri-axial stress status ahead of the crack front, a finite element model using non-singular elements is presented and verified by the experimental load-displacement curve. Simplifications to the costly C(T) specimen fabrication are proposed based on the analytical conclusions from both the test data and the finite element model.

# **PLASTIC TEARING ENERGY IN TOUGH STEELS**

by

Xiaohu Chen

Dissertation submitted to the Faculty of the Graduate School of the  
University of Maryland, College Park in partial fulfillment  
of the requirement for the degree of  
Doctor of Philosophy  
2005

Advisory Committee:

Professor Pedro Albrecht, Chairman/Advisor  
Professor Amde M. Amde  
Professor Mark A. Austin  
Professor William L. Fournery  
Professor Ricardo A. Medina

## DEDICATION

To my parents

## ACKNOWLEDGMENTS

The author feels indebted to his advisor, Professor Pedro Albrecht, who initiated the topic of this dissertation, for his guidance and encouragement throughout the entire research. It has been a real pleasure and privilege working with him.

The author would like to thank Dr. Hernando Candra and Dr. William J. Wright of the Structural Laboratory of the Federal Highway Administration, and Professor James A. Joyce of the United States Naval Academy, for providing the fracture toughness test data and for their technical comments. Sincere appreciation is extended to Dr. Akhrawat Lenwari, Post-Doc researcher of the Department of Civil Engineering, for his helpful discussions on many subjects.

Lastly but not least, the author wishes to express his deepest gratitude to his wife, Ying, for her continuous support; and to his parents, for allowing him to pursue his goal overseas.

# TABLE OF CONTENTS

LIST OF TABLES	vii
LIST OF FIGURES	viii
1 INTRODUCTION	1
1.1 Problem	1
1.2 Background	2
1.2.1 Elastic Fracture Mechanics	2
1.2.2 $J$ -integral and $J$ - $R$ Curve	5
1.2.3 Energy Separation	8
1.2.4 Other Approaches in Elastic-Plastic Fracture	8
1.3 Objective	11
2 $J$ -INTEGRAL	17
2.1 Statement	17
2.2 $J$ Is Not Working Theoretically	17
2.2.1 Deformation Theory of Plasticity	17
2.2.2 Small Strain Requirement	19
2.2.3 $J$ as a Measure of Accumulated Work	20
2.2.4 Toughness Continues to Increase With Crack Growth	21
2.3 $J$ Is Not Working Experimentally	22
2.3.1 List of ASTM $J$ Terminologies	22
2.3.2 List of Test Configuration Restrictions	23
2.3.3 List of Data Qualifications for $J$	24

2.4	Summary	25
3	ENERGY RELEASE RATE IN TOUGH STEELS	27
3.1	Previous Energy Release Rate Methods	29
3.2	Compliance Ratio (CR) Method for Energy Release Rate	30
3.3	Comparison of Energy Release Rate Methods	32
3.3.1	Description of Experimental Data	32
3.3.2	Elastic and Plastic Energy Release Rates	34
3.4	Contribution	35
3.4.1	Effect of Steel Type on Energy Release Rate	35
3.4.2	Elastic Energy Release Rate and Stress Intensity Factor	35
3.4.3	Conclusions	37
4	PREVIOUS WORK ON GEOMETRIC FACTORS	53
4.1	CTOD and CTOD-R Curve	53
4.2	CTOA and CTOA-R Curve	56
5	MECHANISM OF PLASTIC TEARING	60
5.1	Plastic Tearing Mechanism Motion Analysis	60
5.1.1	General Theorem of Plastic Limit Load	60
5.1.2	Limit Load Solution for C(T) Specimens	61
5.1.3	Concept of Plastic Tearing Mechanism Motion	65
5.1.4	Mechanism Motion Resistance Curve	67
5.2	Crack Opening Angle / Normalized Displacement	69

5.2.1	Definition	69
5.2.2	COA-R Curve	70
5.3	Discussion	71
6	EFFECT OF TESTING CONFIGURATIONS	80
6.1	Description of Experimental Data	80
6.2	Effect of Initial Crack Length	82
6.3	Effect of Specimen Size	83
6.4	Effect of Testing Temperature	86
6.5	Effect of Steel Type	87
7	DISCUSSIONS AND CONCLUSIONS	102
7.1	Validation of Test Data Range	103
7.1.1	Load Drop Between Load-Displacement Curve and CR Curve	103
7.1.2	Application of SED Method to the Deviation Point Determination	104
7.1.3	Valid Data Range for Energy Release Rate Resistance Curve	105
7.2	Discussions on Finite Element Modeling	106
7.2.1	ABAQUS Model by Non-Singularity Element	106
7.2.2	The Tri-Axial Stress State Ahead of the Crack Front	108
7.3	Conclusions and Future Work	110
	REFERENCES	123



## LIST OF TABLES

Table 3.1 List of Specimens for Energy Release Rate	38
Table 6.1 List of Specimens for Effect of Testing Configurations	89
Table 7.1 Summary of Modeling	112

## LIST OF FIGURES

Fig. 1.1 Elastic and Plastic Energy Released (Mecklenburg et al. 1989)	14
Fig. 1.2 Energy Release Rate and $J$ - $R$ Curve for HY690 Steel, C(T) L-T Specimen (Mecklenburg et al. 1989)	14
Fig. 1.3 Effect of Type of Material on Limit Load (Hu and Albrecht 1991)	15
Fig. 1.4 Elastic, Elastic-Plastic, and Full Plastic Region in a Typical C(T) Specimen Test	15
Fig. 1.5 Comparison of Key Curves for Fatigue-cracked and Blunt-notch Specimens (Candra et al. 2002)	16
Fig. 2.1 Illustrative $J_{lc}$ and Data Qualification; 1T C(T) Specimen B15, A588 Steel, RT (Candra 2001)	26
Fig. 3.1 Load versus Load-Line Displacement with Periodic Unloading	39
Fig. 3.2 Elastic Energy Release Associated with Crack Extension (Irwin and Kies 1954)	39
Fig. 3.3 Energy Dissipation Associated with Crack Extension (Turner 1984)	40
Fig. 3.4 Global Plastic Energy Dissipation Associated with Crack Extension (Watson and Jolles 1986)	40
Fig. 3.5 Separation of Energies into Elastic and Plastic Energy Components (Mecklenburg et al. 1989)	41
Fig. 3.6 Construction of CR Load versus Displacement Curve from the Standard Unloading Compliance Data	41
Fig. 3.7 Calculation of Elastic Energy Release and Plastic Energy Dissipation Associated with Crack Extension by CR Method	42

Fig. 3.8 Details of ASTM Standard 1T C(T) Specimen	42
Fig. 3.9 Comparison of Elastic Energy Release Rate by Different Approaches, A572 Steel (A15)	43
Fig. 3.10 Comparison of Elastic Energy Release Rate by Different Approaches, A588 Steel (B16)	43
Fig. 3.11 Comparison of Elastic Energy Release Rate by Different Approaches, A709 HPS 690 Cu-Ni Steel (G16)	44
Fig. 3.12 Difference of Elastic Energy Release Rate between Method by Mecklenburg et al. (1989) and CR Method in Conventional Steels	44
Fig. 3.13 Difference of Elastic Energy Release Rate between Method by Mecklenburg et al. (1989) and CR Method in HPS	45
Fig. 3.14 Comparison of Plastic Energy Release Rate by Different Approaches, A572 Steel (A15)	45
Fig. 3.15 Comparison of Plastic Energy Release Rate by Different Approaches, A588 Steel (B16)	46
Fig. 3.16 Comparison of Plastic Energy Release Rate by Different Approaches, A709 HPS 690 Cu-Ni Steel (G16)	46
Fig. 3.17 Difference of Plastic Energy Release Rate between Method by Mecklenburg et al. (1989) and CR Method in Conventional Steels	47
Fig. 3.18 Difference of Plastic Energy Release Rate between Method by Mecklenburg et al. (1989) and CR Method in HPS	47
Fig. 3.19 Total Energy Release Rate of Conventional Steels A572, A588, and A913	48
Fig. 3.20 Total Energy Release Rate of High Performance Steels A709	49

Fig. 3.21 Elastic Energy Release Rate of Conventional Steels A572, A588, and A913	50
Fig. 3.22 Elastic Energy Release Rate of High Performance Steels A709	51
Fig. 3.23 Comparison of Elastic Energy Release Rates with ASTM E399-90 Equations	52
Fig. 4.1 The Strip-Yield Model (Dugdale 1960)	59
Fig. 4.2 Calculated Critical CTOA Values of Various Materials Using Elastic-Plastic Finite Element Analyses (Newman et al. 2003)	59
Fig. 5.1 Beam Mechanism for Plastic Limit Load	73
Fig. 5.2 Wedged Notch Bending Bar With Slip Line Field (Green 1953)	73
Fig. 5.3 Circular Slip Line of Modified Green Solution (Hu 1989)	74
Fig. 5.4 Circular Slip Line Field With Crack Extension	74
Fig. 5.5 Load vs. Displacement; 709-690W Cu-Ni, Specimen G16, 1T C(T), 24°C, $a_0/W = 0.60$	75
Fig. 5.6 Load vs. Crack Length, Test Load and Hu's Limit Load; Specimen G16, 1T C(T), 24°C, $a_0/W = 0.60$	75
Fig. 5.7 Plastic Tearing Mechanism Motion vs. Crack Extension; 709-690W Cu-Ni, Specimen G16, 1T C(T), 24°C, $a_0/W = 0.60$	76
Fig. 5.8 Side View of ASTM Standard C(T) Specimen	76
Fig. 5.9 Displacement vs. Crack Extension; 709-690W Cu-Ni, Specimen G16, 1T C(T), 24°C, $a_0/W = 0.60$	77
Fig. 5.10 Crack Opening Angle vs. Crack Extension; 709-690W Cu-Ni, Specimen G16, 1T C(T), 24°C, $a_0/W = 0.60$	77

Fig. 5.11 Plastic Tearing Mechanism Motion, Crack Opening Angle, Energy Release Rate, and ASTM $J$ -Integral vs. Crack Extension; 709-690W Cu-Ni, Specimen G16, 1T C(T), 24°C, $a_0/W = 0.60$	78
Fig. 5.12 Tunneling Effect at the Crack Front, Specimen G16	78
Fig. 5.13 Ratio Between Energy Release Rate, Mechanism Motion, and Crack Opening Angle; 709-690W Cu-Ni, Specimen G16, 1T C(T), 24°C, $a_0/W = 0.60$	79
Fig. 6.1 Unloading Compliance Load versus Load-line Displacement for C(T) Specimens JB4, E3, and 13A	90
Fig. 6.2 Effect of Initial Crack Length on Total Energy Release Rate in C(T) Specimens of A533B Steel	90
Fig. 6.3 Effect of Initial Crack Length on Plastic Tearing Mechanism Motion in C(T) Specimens of A533B Steel	91
Fig. 6.4 Unloading Compliance Load versus Load-line Displacement for C(T) Specimens FYO-N10 and FYO-N4	91
Fig. 6.5 Effect of Initial Crack Length on Total Energy Release Rate in C(T) Specimens of HY100 Steel	92
Fig. 6.6 Effect of Initial Crack Length on Plastic Tearing Mechanism Motion in C(T) Specimens of HY100 Steel	92
Fig. 6.7 Unloading Compliance Load versus Load-line Displacement for C(T) Specimens B1 and B16	93
Fig. 6.8 Effect of Specimen Size on Total Energy Release Rate in C(T) Specimens of A588 Steel	93
Fig. 6.9 Effect of Specimen Size on Plastic Tearing Mechanism Motion in C(T) Specimens of A588 Steel	94

Fig. 6.10 Unloading Compliance Load versus Load-line Displacement for C(T) Specimens C1 and C16	94
Fig. 6.11 Effect of Specimen Size on Total Energy Release Rate in C(T) Specimens of A913-345 Steel	95
Fig. 6.12 Effect of Specimen Size on Plastic Tearing Mechanism Motion in C(T) Specimens of A913-345 Steel	95
Fig. 6.13 Unloading Compliance Load versus Load-line Displacement for C(T) Specimens C11, C13 and C15	96
Fig. 6.14 Effect of Testing Temperature on Total Energy Release Rate in C(T) Specimens of A913-345 Steel	96
Fig. 6.15 Effect of Testing Temperature on Plastic Tearing Mechanism Motion in C(T) Specimens of A913-345 Steel	97
Fig. 6.16 Unloading Compliance Load versus Load-line Displacement for C(T) Specimens H33, H35 and H36	97
Fig. 6.17 Effect of Testing Temperature on Total Energy Release Rate in C(T) Specimens of A709-345W HPS	98
Fig. 6.18 Effect of Testing Temperature on Plastic Tearing Mechanism Motion in C(T) Specimens of A709-345W	98
Fig. 6.19 Unloading Compliance Load versus Load-line Displacement for C(T) Specimens C16, D17 and B16	99
Fig. 6.20 Effect of Steel Type on Total Energy Release Rate in C(T) Specimens of 3 Conventional Steels	99
Fig. 6.21 Effect of Steel Type on Plastic Tearing Mechanism Motion in C(T) Specimens of 3 Conventional Steels	100
Fig. 6.22 Unloading Compliance Load versus Load-line Displacement for C(T) Specimens G16 and E17	100

Fig. 6.23 Effect of Steel Type on Total Energy Release Rate in C(T) Specimens of 2 HPS Steels	101
Fig. 6.24 Effect of Steel Type on Plastic Tearing Mechanism Motion in C(T) Specimens of 2 HPS Steels	101
Fig. 7.1 Load Drop vs. Crack Extension; A533B Steel, Specimen JB4, 1T C(T), 88°C, $a_0/W = 0.56$	113
Fig. 7.2 Load Drop vs. Crack Extension; A533B Steel, Specimen E3, 1T C(T), 88°C, $a_0/W = 0.62$	113
Fig. 7.3 Load Drop vs. Crack Extension; A533B Steel, Specimen 13A, 1T C(T), 88°C, $a_0/W = 0.77$	114
Fig. 7.4 Definition of Strain Energy Density (Lenwari et al. 2005)	114
Fig. 7.5 Accurate Yield Point in Adhesive FM 300K at 15% RH, -15°C and $10^{-4}$ /s strain rate (Lenwari et al. 2005)	115
Fig. 7.6 Deviation Point of Load Drop, A533B Steel, Specimen JB4, 1T C(T), 88°C, $a_0/W = 0.56$	115
Fig. 7.7 Deviation Point of Load Drop, A533B Steel, Specimen E3, 1T C(T), 88°C, $a_0/W = 0.62$	116
Fig. 7.8 Deviation Point of Load Drop, A533B Steel, Specimen 13A, 1T C(T), 88°C, $a_0/W = 0.77$	116
Fig. 7.9 Data Range Validation on Energy Release Rate by Plastic Tearing Mechanism Motion for Specimen JB4	117
Fig. 7.10 Data Range Validation on Energy Release Rate by Plastic Tearing Mechanism Motion for Specimen E3	117

Fig. 7.11 Data Range Validation on Energy Release Rate by Plastic Tearing Mechanism Motion for Specimen 13A	118
Fig. 7.12 Typical ABAQUS Model of Quarter 1T C(T) Specimen	118
Fig. 7.13 True Stress-Strain Curve in FEA Input	119
Fig. 7.14 Load-Displacement Verification for FEA Running With Crack Extension; A913-345, Specimen C15, 1T C(T), 24°C, $a_0/W = 0.50$	119
Fig. 7.15 CR Curve Verification for FEA Running Without Crack Extension; A913-345, Specimen C15, 1T C(T), 24°C, $a_0/W = 0.50$	120
Fig. 7.16 SED From FEA Model Without Side Groove; A913-345, Specimen C15, 1T C(T), 24°C, at $a/W = 0.541$	120
Fig. 7.17 SED From FEA Model Without Side Groove; A913-345, Specimen C15, 1T C(T), 24°C, at $a/W = 0.566$	121
Fig. 7.18 SED From FEA Model With 20% Side Grooves; A913-345, Specimen C15, 1T C(T), 24°C, at $a/W = 0.541$	121
Fig. 7.19 SED From FEA Model With 20% Side Grooves; A913-345, Specimen C15, 1T C(T), 24°C, at $a/W = 0.566$	122



# CHAPTER 1: INTRODUCTION

## 1.1 Problem

On December 15, 1967, the Point Pleasant Bridge, which spanned over the Ohio River and connected West Virginia and Ohio, collapsed claiming 46 lives. The Christmas rush applied an extra load to the 39-year-old bridge causing a cleavage fracture in one of the eyebars, followed by a ductile fracture near the pin (National Transportation Safety Board 1970). The brittle or the elastic fracture is the most undesirable failure mode for steel structures—including bridges and pressure vessels—because it happens without warning and results in catastrophic losses in human life and severe damage to the economy. Each occurrence of this type of failure is reported nationwide in the press and is not tolerated by the public. Hence, construction materials, especially steels, must be tough enough to reach the tearing strength without the slow-stable crack extension being interrupted by instability. Thus, a criterion is needed to determine the minimum required degree of tearing for a given material under certain loading and environmental conditions.

“Tearing” implies that a cracked body or a structure experiences stable crack extension and undergoes extensive plastic deformation. Through the years, the important need has been to understand the crack extension behavior and to predict the stress and the deformations. The  $J$ -integral and the  $J$ -resistance curve ( $J$ - $R$  curve) have been used to determine fracture toughness for more than three decades in the fracture mechanics field. However, they are no longer the appropriate methods to use

in tearing analysis because of their analytical basis. The  $J$ - $R$  curve is not consistent with the energy release rate curve of Mecklenburg et al. (1989), which is calculated directly from experimental data. The slope of the  $J$ - $R$  curve,  $dJ/(B_n da)$ , the so called Tearing Modulus (Paris et al. 1979), does not compare well with the experimental separation of energies.

According to the  $J$ - $R$  curve, the energy released per unit crack extension continues to increase. Yet, it is physically impossible for the material to become progressively tougher as the crack extends. If this were possible, a cracked structural component could be made stronger and safer by simply letting the crack grow. An energy balance criterion does exist, however, it cannot be based on the deformation theory  $J$ . Crack advance in an elastic-plastic material invariably involves elastic unloading and distinctly non-proportional loading in the vicinity of the crack tip, and neither is adequately modeled by the deformation theory  $J$  (Hutchinson 1983).

## **1.2 Background**

### **1.2.1 Elastic Fracture Mechanics**

Fracture mechanics as an engineering discipline dates back to the 1950s when Irwin (1954, 1957) made his fundamental contributions to the stress analysis and to fracture characterization of cracked bodies. Before then, Griffith (1920) first made a quantitative connection between strength and crack size. The basic idea is that the driving force for crack extension results from the release of potential energy as an

inherent resistance to the crack extension. By using the energy balance approach, the fracture condition can be written as:

$$-\frac{d\Pi}{dA} = \frac{dW}{dA} - \frac{dU}{dA} = \gamma \quad (1.1)$$

where,

$\Pi$  = potential energy

$W$  = external work done to the body

$U$  = internal strain energy in the body

$A$  = area of crack surface

$\gamma$  = material surface energy

Eq. (1.1) describes a necessary condition for crack initiation. To sustain the crack extension, the rate change of  $(d\Pi/dA)$  must exceed the rate change of surface energy within the newly cracked area. The shortcoming of Eq. (1.1) is that it does not include a term for plastic deformation energy; therefore, its application is limited to ideally brittle fractures.

Irwin contributed to the key concept required to extend Griffith's theory to the fracture of metals by introducing the strain energy release rate, or crack extension force  $G$

$$G = \frac{dW}{dA} - \frac{dU}{dA} = -\frac{d\Pi}{Bda} \quad (1.2)$$

where,

$B$  = body thickness

$a$  = crack length

Irwin then connected the global energy release rate  $G$  to the stress intensity factor  $K$ , which is a local elastic parameter to characterize the intensity of the stresses and displacements in a small area surrounding the crack tip.

$$G = \frac{K^2}{E'} \quad (1.3)$$

where,

$$E' = E \quad (\text{for plane stress})$$

$$E' = \frac{E}{(1-\nu^2)} \quad (\text{for plane strain})$$

And the stress and displacement field can be written as,

$$\sigma_{ij}(r, \theta) = \frac{K}{\sqrt{r}} f_{ij}(\theta) + H.O.T. \quad (1.4)$$

$$u_i(r, \theta) = K\sqrt{r} g_i(\theta) + H.O.T. \quad (1.5)$$

where,

$\sigma_{ij}$  = component of stress tensor

$u_i$  = component of displacement vector

$r$  = polar distance from crack tip

$\theta$  = polar angle

$f_{ij}, g_i$  = functions of polar angle

This linear elastic fracture mechanics has been successfully applied to many engineering problems, especially those involving Mode *I* plane-strain brittle fractures of low toughness materials. However, by this definition, a stress and strain singularity at the crack tip was assumed in the mathematical model, which does not exist in nature.

### 1.2.2 *J*-integral and *J-R* Curve

It was initially believed that a structural component failed when  $G$  or  $K$  reached their critical values  $G_c$  or  $K_c$ . Later, after substantial crack extension was observed prior to fracture in plane stress, investigators began to describe the resistance to fracture as a function of crack extension. Rice (1968) introduced the *J*-integral as a characterization parameter for elastic-plastic fracture. The *J*-integral in a two-dimensional deformation field free of body forces is defined per unit thickness as

$$J = \int_{\Gamma} W_s dy - T_i \frac{\delta u_i}{\delta x} ds \quad (1.6)$$

where,

$W_s = \int \sigma_{ij} d\varepsilon_{ij}$ , strain energy density

$T_i$  = component of traction vector

$U_i$  = component of displacement vector

$\Gamma$  = any contour surrounding the crack tip within the body

For deformation plasticity, the  $J$ -integral is path independent. For a pure-hardening nonlinear elastic material in which the constitutive relations are given by

$$\frac{\varepsilon_{ij}}{\varepsilon_0} = \phi \left( \frac{\sigma_{ij}}{\sigma_0} \right)^n \quad (1.7)$$

where,

$\varepsilon_0, \sigma_0, \phi$  = material constants

$n$  = strain hardening exponent

Hutchinson (1968), and Rice and Rosengren (1968) have shown that the stresses and strains near the crack tip, the so-called  $HRR$  field, can be written in terms of  $J$ :

$$\sigma_{ij}(r, \theta) = \sigma_0 \left( \frac{J}{r \sigma_0 \varepsilon_0} \right)^{\frac{1}{n+1}} E_{ij}(\theta, n) \quad (1.8)$$

$$\varepsilon_{ij}(r, \theta) = \varepsilon_0 \left( \frac{J}{r \sigma_0 \varepsilon_0} \right)^{\frac{1}{n+1}} F_{ij}(\theta, n) \quad (1.9)$$

where,

$r$  = polar distance from crack tip

$\theta$  = polar angle from crack tip

In a strict sense, all of these estimations of  $J$  are valid only for nonlinear-elastic material or for elastic-plastic materials without unloading (monotonic loading), which is the fundamental hypothesis underlying the derivation of the path-independent  $J$ -integral. The flow theory of plasticity is the preferred theory because it is not restricted to monotonic loading and it is more precise in practice. But unfortunately, it is not used in the  $J$ -integral approach because of its mathematical complexity. Furthermore, the path-independent property of the  $J$ -integral cannot be exactly proven for a material undergoing a large deformation for which the strain-displacement relationship has second order terms. The plot of the  $J$ -integral versus crack extension, called the  $J$ - $R$  curve, was proposed by Landes and Begley (1972) and was later widely adopted to be the size-independent property to stable crack extension and instability behavior of cracked structural components. By assuming that the  $J$ - $R$  curve is a material property, the researchers sidestepped the fact that the stress field around the crack tip unloads as the crack extends, thus violating the monotonic loading requirement of the deformation theory of plasticity.

### 1.2.3 Energy Separation

Mecklenburg et al. (1989) separated the dissipated global energy measured directly from the load versus load-line displacement curve of various tested specimens into its elastic and plastic parts as shown in Fig. 1.1.

The elastic part  $U_e$  was found to be equal to the strain energy release rate  $G$ , showing that the information in Fig 1.1 contains a valid separation. This energy separation provides an upper bound of a  $J$ -integral type quantity, because the dissipation energy rate is the plastic energy dissipated globally in the entire specimen per unit crack extension.

The  $J$ - $R$  curve calculated from the ASTM specification E1820-99a (ASTM 1999) is not consistent with the energy release rate curve by the energy separation as shown in Fig. 1.2. In the figure, the triangles represent the total energy released during crack extension, while the squares and the cross symbols represent the plastic energy and the elastic energy released, respectively.

Unlike the energy release rate curve, the  $J$ - $R$  curve continues to increase without reaching a plateau. Fig. 1.2 shows that the implication of increasing toughness with crack growth in the  $J$ - $R$  or  $G$ - $R$  curves is misleading.

### 1.2.4 Other Approaches in Elastic-Plastic Fracture

Besides the concept of  $G$  and  $J$ , other analyses of energy dissipation in fracture problems continued after Griffith's work. Although the energy method may be a



more suitable approach for elastic-plastic fracture problems than the usual stress and strain analysis in which the singularity at crack tip is involved, the development of this field has been relatively slow. The reason for that has been the need to develop more accurate methods to measure the dissipated energy. Czoboly et al. (1981) studied theoretically and experimentally the absorbed specific energy until fracture (*ASPEF*) from cylindrical tensile specimens. The *ASPEF* for a certain material in the close vicinity of the fracture surface is stated to equal the area under the true stress-strain curve. Then the fracture process was modeled by substituting a fictitious, miniature tensile specimen for the plastic zone ahead of the crack and by assuming that the “rupture” of that specimen was necessary for the initial crack to extend. Expressing the total energy needed for fracture as

$$E_c = \int_V W_c dV = \int_0^L W_c B \Delta a dL \quad (1.10)$$

where,

$L$  = dimension of plastic zone

$B$  = thickness of specimen

leads to the determination of the effective surface energy  $G$

$$G = \frac{E_c}{\Delta a} = \int_0^L W_c B dL \quad (1.11)$$

This resistance  $G$  depends on the value of  $L$ , which is difficult to obtain from an experiment.

Considering that the processes of fracture and yielding were inseparable, Sih (1971) proposed using the strain energy density,  $dW / dV$ , as a single failure criterion. The strain energy density is given by

$$\frac{dW}{dV} = \int \sigma_{ij} d\varepsilon_{ij} \quad (1.12)$$

and varies throughout the body. The direction of the element that initiates fracture or yielding was postulated to coincide with the minimum and maximum values of  $(dW / dV)$ , respectively. Experimental observation on real materials revealed that some elements at a finite distance ahead of the crack fail first prior to the onset of rapid crack growth. Based on these results, Sih (1973) proposed the use of the strain energy factor  $S$  that is defined to  $(dW / dV)$  multiplied by the radius  $r_0$  of the core region ahead of the crack tip. Local instability is assumed to occur when the local energy density factor,  $S$ , reaches a critical value,  $S_{cr}$ , which is characteristic of the material. For a through crack of length  $2a$  subjected to uniform applied stress, Sih has assumed that fracture occurs when

$$\sigma_{cr} a^{\frac{1}{2}} = \left[ \frac{2ES_{cr}}{(1+\nu)(1-2\nu)} \right]^{\frac{1}{2}} \quad (1.13)$$

Although this equation is very similar in form to Griffith's original work, it is based on an entirely different premise. According to Sih, the direction of crack growth is

toward the point near the crack tip with the minimum value of the strain energy density factor  $S$ , which occurs in a region in which the energy of volume change is greater than the energy of distortion.

Researchers also tried to characterize the fracture behavior from the deformation side. Wells (1964) proposed using the crack tip opening displacement (*CTOD*) to describe the capacity of a material near the crack tip to deform before or during crack extension. The *CTOD* includes the crack tip blunting and reflects the material ductility; therefore, it can be applied in elastic-plastic fracture behaviors. Although much experimental and analytical work have been conducted on *CTOD*, its physical basis is not well understood. Recently, Newman et al. (2003) reviewed and suggested another similar parameter crack opening tip angle (*CTOA*) to characterize the crack extension in a metal sheet. Again the measurement of the angle is somewhat arbitrary and lacks an analytical basis.

Based on this information, it becomes apparent that the mechanics of crack extension are not yet completely understood. The role that these different parameters play in characterizing the resistance to crack extension is unclear especially in plastic fracture. Most of the work is geared toward extending the ideas of elastic fracture mechanics into solving elastic-plastic fracture problems.

### **1.3 Objective**

Advances in steel making have led to a continuous increase in the application of tough steels in structural and mechanical fields such as the use of A709 HPS steel for

highway bridges. Hu and Albrecht (1991) found that compact tension specimens made of various types of metals that were used to measure  $J$ - $R$  curves actually reached the limit load while undergoing significant crack extension (Fig. 1.3). The failure of tough steels in which the crack extends in a slow-stable manner is not exactly a “fracture,” instead, it is a plastic tearing.

Realizing that most of the work done to date under the guide of elastic or elastic-plastic fracture now deals in reality with plastic tearing at the limit load, the objective of this research is to replace the fracture criteria on the singularity or weak-singularity basis with the resistance criteria for fully plastic fracture region after the crack extension initiates (Fig. 1.4). For the tearing resistance curve to be a material property, it should be unique for a given specimen thickness, and insensitive to initial crack length and specimen width, but it could depend upon environmental temperature and strain rate. As the processes of crack extension and the yielding of more ductile steels occur simultaneously and are physically inseparable, it is not likely that one single parameter can serve this purpose. Therefore, this dissertation will look for the criteria from both the energy release approach and the crack extension mechanism approaches.

Using a powerful workstation and finite element analysis (FEA) software, it is now possible to simulate in 3-D the fracture specimen toughness test. Another objective of this dissertation is to evaluate the results of FEA to the load versus displacement curve of experimental data by eliminating the singularity element, which is based on the singularity of elastic fracture mechanics and has been the

dominant type of fracture element. Also, the finite element analysis can give us the tri-axial stress status from one energy state to another.

If the criteria were to determine the tearing energy, the high-cost standard unloading compliance test could be greatly simplified because some of the metal shop steps such as polishing of the specimen, pre-cracking by fatigue, and side-grooving may not be necessary. In fact, as shown in Fig. 1.5, Candra et al. (2002) have recently shown that notch type does not affect the key curve (normalized load-displacement curve).

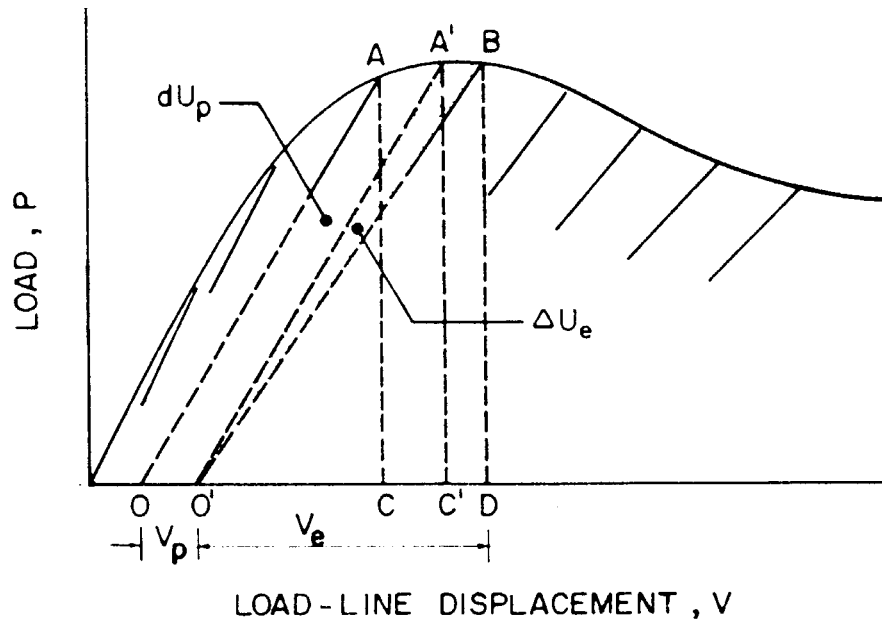


Fig. 1.1 Elastic and Plastic Energy Released (Mecklenburg et al. 1989)

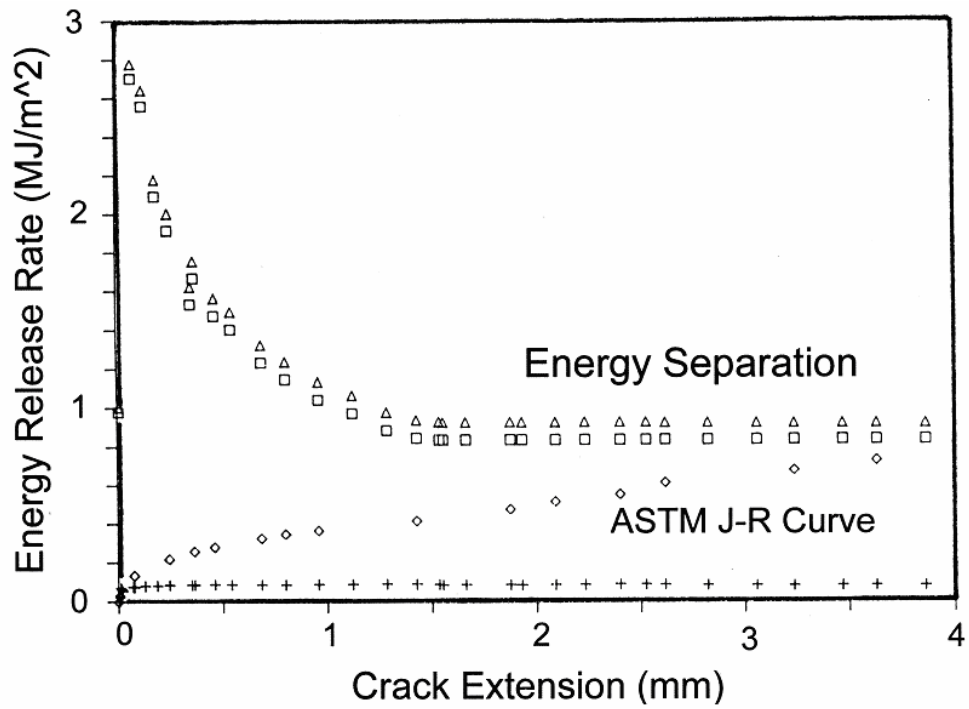


Fig. 1.2 Energy Release Rate and *J-R* Curve for HY690 Steel, C(T) L-T Specimen (Mecklenburg et al. 1989)

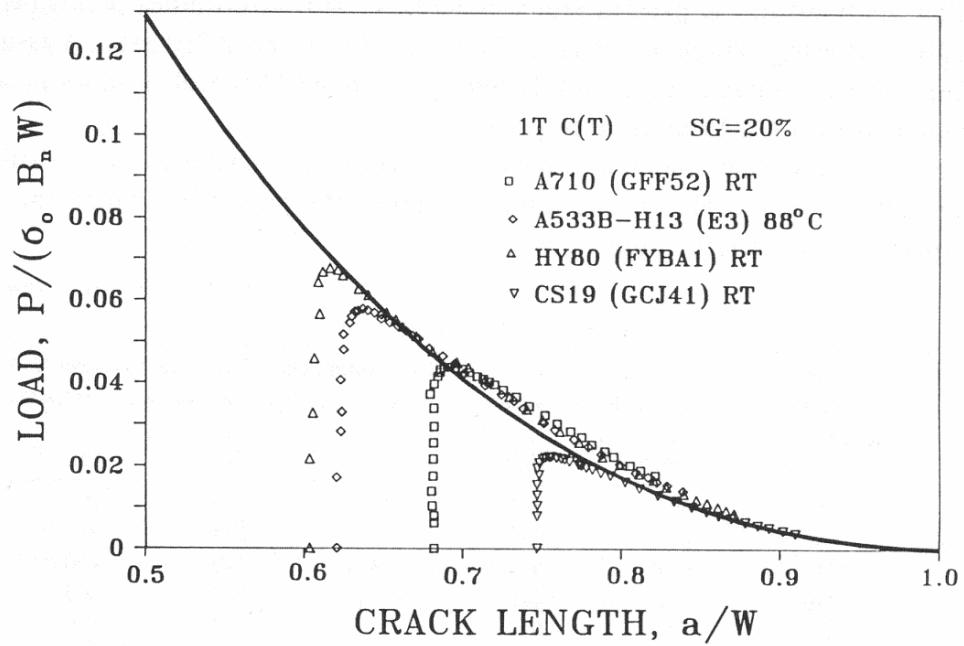


Fig. 1.3 Effect of Type of Material on Limit Load (Hu and Albrecht 1991)

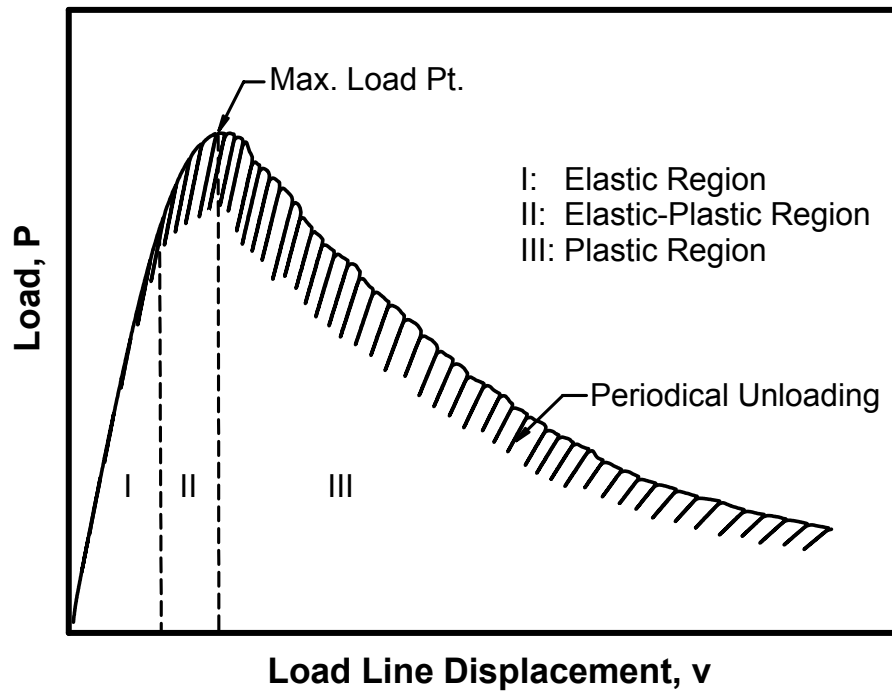


Fig. 1.4 Elastic, Elastic-Plastic, and Full Plastic Region in a Typical C(T) Specimen Test

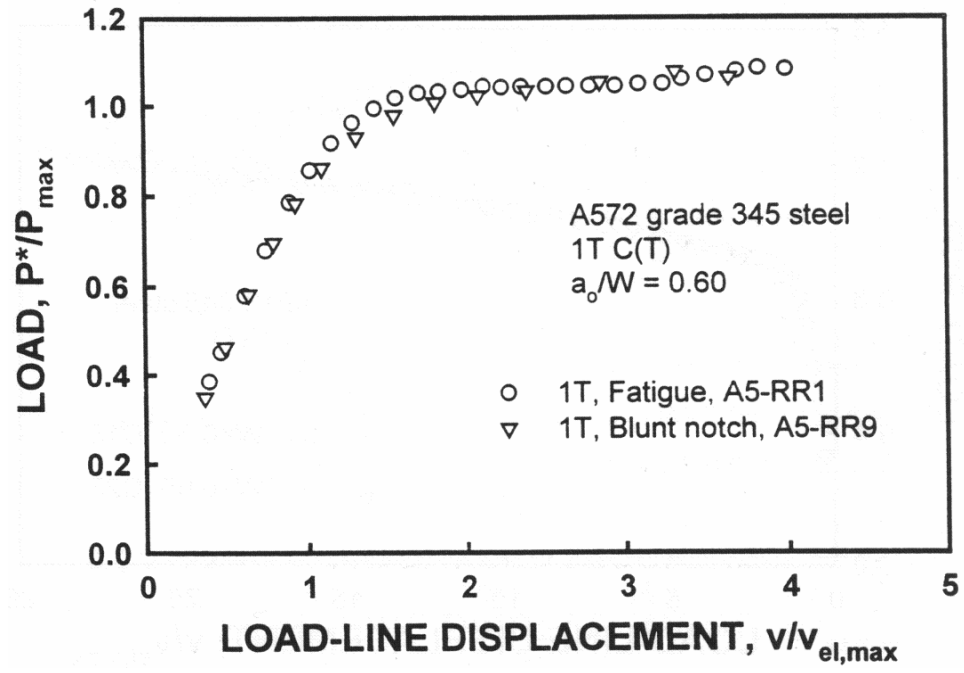


Fig. 1.5 Comparison of Key Curves for Fatigue-cracked and Blunt-notch Specimens (Candra et al. 2002)



## CHAPTER 2: *J*-INTEGRAL

### 2.1 Statement

Despite its early success on the application to crack initiation problems, the *J*-integral or the *J*-*R* curve should not be used as a fracture criterion any more in the plastic regime of fracture mechanics. In the first chapter of this dissertation the mathematical basis of the *J*-integral and its limitations have already been summarized. Yet the author feels it is necessary to make a statement here in a separate chapter that the fracture mechanics should now develop beyond the *J*-integral theory. This is important because the *J*-integral has been dominating the elastic-plastic fracture mechanics both theoretically and experimentally in the United States since 1960's, and it is not easy to overcome its broad use by researchers.

### 2.2 *J* Is Not Working Theoretically

The *J*-integral could be false or misleading in plastic fracture mechanics once any of its analytical bases is lost, which has been happening since it was adapted for characterizing the crack extension. The following quotations on various subjects help to understand why *J* is not working theoretically.

#### 2.2.1 Deformation Theory of Plasticity

- Broek (1982, page 135) “The *J* integral fracture criterion must presently be restricted to crack initiation. There is not yet a methodology to use the *J* integral for stable crack growth. In such case, fracture is always preceded by

slow crack growth. During slow crack growth, unloading of the material behind the crack tip occurs. Path independence of the  $J$  integral has been shown thus far only by using the deformation theory of plasticity which does not allow for unloading.”

- ❑ Hutchinson (1983, page 1048) “Tempting though it may be, to think of the criterion for initiation of crack growth based on  $J$  as an extension of Griffith’s energy-balance criterion, it is nevertheless incorrect to do so. This is not to say that an energy balance does not exist, just that it cannot be based on the deformation theory  $J$ . Crack advance in an elastic-plastic material invariably involves elastic unloading and distinctly nonproportional loading in the vicinity of the crack tip, and neither is adequately modeled by deformation theory.”
- ❑ Thomason (1990, page 260) “It will be shown that the necessary conditions of proportional loading and no unloading, for the validity of the  $J$ -integral, are violated extensively for both small-finite and infinitesimal crack growth conditions.”
- ❑ James (1998, page 11) “Rice defined the  $J$ -integral based on the deformation theory of plasticity, so the integral is strictly only defined for linear or nonlinear elastic solids. For stationary cracks and monotonically increasing loads, the deformation theory of plasticity will accurately model the plastic behavior. However, for growing cracks a region of elastic unloading exists in

the crack tip wake and nonproportional loading occurs in front of the crack tip.”

- Janssen et al. (2002, page 147) “During crack growth the newly formed crack flanks are completely unloaded from stresses as high as yield strength. Therefore,  $J$  is in principle applicable only up to the beginning of crack extension and not for crack growth.”

### 2.2.2 Small Strain Requirement

- Milne (1979, page 358) “Although in the small-scale yielding regime failure can be characterized by a one-parameter criterion, such as the fracture toughness  $K_{IC}$ , it is not clear if this is applicable after appreciable yielding. Experimental evidence based upon evaluation of the  $J$ -integral at failure suggests that under some circumstances this maybe the case. Alternatively, there is an increasing amount of evidence demonstrating situations in which this is not so, and a geometry effect is apparent.”
- Hutchinson (1983, page 1046) “It is clear from (Begley and Landes, 1972) that  $J$  can be regarded as a measure of the intensity of the crack-tip singularity fields. However, before it can be assumed that  $J$  can be used to correlate the initiation of crack growth in true elastic-plastic solids, one must be sure that the following two conditions are met. First, the deformation theory of plasticity must be an adequate model of the small-strain behavior of real elastic-plastic materials under the monotonic loads being considered. Second,

the regions in which finite strain effects are important and in which the microscopic processes occur must each be contained well within the region of the small-strain solution dominated by the singularity fields.”

- James (1998, page 11) “The HRR singularity, which neither considers the effect of blunting of the crack tip on the stress fields, nor takes into account the large strains present near the crack tip, is invalid in a small region near the crack tip.”

### **2.2.3 $J$ as a Measure of Accumulated Work**

- Sumpter (1999, page 162) “The literature attached to the  $J$ - $R$  curves has been criticized by many who pointed out that  $J$  is simply a measure of accumulated work (Kolednik 1991), and that any crack tip characterizing role attached to the parameter must be lost after a small amount of crack growth (Thomason 1990).”
- Chapuliot (2001, page 231) “However, despite these advantages and the fact that  $J$  is accepted as a criterion for characterizing crack initiation, there has been and still substantial opposition to using the  $J$ -integral for characterizing the ductile propagation of cracks. This is because, during this phase,  $J$  only represents a measurement of the work accumulated in the specimen or structure and is no longer a variable characteristic of the loading at the crack tip as a result of local relief. The associated criterion is then dependent on the size or the thickness of the structure analyzed.”

- Brocks and Anuschewski (2004, page 128) “In fact, the cumulative quantity  $J$ , which rises with increasing crack length, is not the true driving force for ductile tearing as Turner [7] pointed out.”

#### 2.2.4 Toughness Continues to Increase With Crack Growth

- Etemad (1990, page 303) “The present discussion emphasizes the obvious, namely that whatever was intended, the value of a  $J$ -based  $R$ -curve reflects the dissipation of work associated with the whole plastic region of deformation. With increasing plasticity this spreads from local to the tip when characterized by LEFM, to the final limit of fully plasticity where slip patterns and component geometry govern the behavior. The commonly used presentation in which an  $R$ -curve rises reflects total work dissipation. If an incremental,  $d/da$ , work or energy term, is used, consistent with the LEFM concept of work and energy rates, it will decrease once the maximum size of plastic zone has been reached.”
- Etemad (1990, page 304) “Clearly the Griffith concept characterizes the increment or  $d/da$  rate of either potential energy or work done. On the other hand, the Charpy-type test uses total work quantity and  $J$ - $R$  curves as conventionally measured use either total work or an inferred non-linear elastic energy as normalized quantities (which increase) rather than as  $d/da$  rates (which decrease). The distinction is not crucial in LEFM where they are directly related, but it is argued here that, despite it not apparently being

widely recognized, it is crucial in EPFM where the one term increases whilst the other decreases with growth.”

- James (1998, page 11) “Anderson (1995) notes that steady state crack growth is necessary, and that even when  $J$ -controlled crack growth is obtained (valid), steady state values of  $J$  are rarely reached.”
- Sumpter (1999, page161) “All current  $R$ -curve approaches pose the same major unsolved problem. Why does toughness continue to increase with crack growth without reaching a plateau value?”
- Sumpter (2004a, page17) “It is shown that the implication of increasing toughness with crack growth in  $G_R$  and  $J_R$  curves is misleading.”

### **2.3 $J$ Is Not Working Experimentally**

The current experimentally derived  $J$  value or  $J$  resistance curve is based on the summation of functions of the increments of work normalized by the net section thickness, the remaining ligament, and a correction factor. In an ASTM standard fracture toughness test, the specimen and loading configurations are subjected to various limitations to keep the  $J$ - $R$  curve substantially invariant.

#### **2.3.1 List of ASTM $J$ Terminologies**

This section lists the  $J$  terminologies defined with different conditions in a standard fracture toughness test. To ensure the validity of these  $J$  values, various restrictions are applied to specimen and loading preparation.

- ❑  $J_c$  : Measure of fracture toughness at instability without significant stable crack extension
- ❑  $J_u$  : Measure of fracture instability after the onset of significant stable tearing crack extension
- ❑  $J_{el}$  : Elastic Component of  $J$
- ❑  $J_{pl}$  : Plastic Component of  $J$
- ❑  $J_{Ic}$  : Represents initial toughness  $J$
- ❑  $J_{Qc}$  : Labeled final point of instability, a provisional  $J_c$  value
- ❑  $J_{max}$  : Maximum  $J$ -integral capacity of a specimen

### 2.3.2 List of Test Configuration Restrictions

Despite restrictions listed in this section to the standard fracture toughness test, the modified ASTM  $J$ - $R$  curves are still very size dependent beyond 30% crack extension except for the case of very high toughness materials (Joyce 1990).

- ❑ The surface of all specimens shall be polished.
- ❑  $B$  and  $b$  must be equal or greater than  $20J_{max}/\sigma_y$ .
- ❑ All specimens shall be pre-cracked in fatigue starting with a narrow notch.

- ❑ The fatigue crack length (total length of the crack starter configuration plus the fatigue crack) shall be between 0.45 and 0.70  $W$  for  $J$  determination.
- ❑ Side grooves may be necessary to ensure a straight crack front.
- ❑ Crack growth must not exceed 25% of the initial remaining ligament.

### 2.3.3 List of Data Qualifications for $J$

Only a limited amount of crack growth in small specimens can be considered valid as to the data qualifications listed in this section, and thus consequently, the full resistance curve of large but stable crack extension can only be inferred by extrapolation. Smaller size specimens generally gave higher  $dJ/da$  than larger specimens (Joyce 1990, Wilkowski 1990, Sumpter 2004b), which makes  $J$ - $R$  curve extrapolations from small scale specimen non-conservative for large structural crack growth.

- ❑ The spacing of unload/reload sequence shall be less than 0.01  $W$ .
- ❑ The average spacing of unload/reload sequence shall be less than 0.005  $W$ .
- ❑ To obtain  $J_{lc}$ , at least one data point shall lie between the 0.15-mm exclusion line and the 0.5-mm offset line. At least one data point shall lie between the 0.5-mm offset line and the 1.5-mm offset line.
- ❑ The number of data between  $0.4J_Q$  and  $J_Q$  shall be more than 3.



- The correlation coefficient of the least squares fit shall be greater than 0.96.
- To qualify  $J_Q$  as  $J_{Ic}$ , the specimen thickness shall be  $B > 25J_Q/\sigma_y$ , and the initial ligament shall be  $b_0 > 25J_Q/\sigma_y$ .
- To qualify  $J_{Qc}$  as  $J_c$ ,  $B$  and  $b_0$  shall be greater than  $200J_Q/\sigma_y$ , and  $\Delta a_p < 0.2mm + J_Q/(2\sigma_y)$ .
- To qualify  $J_{Qu}$  as  $J_u$ ,  $\Delta a_p$  shall be equal or greater than  $0.2mm + J_Q/(2\sigma_y)$ .
- Candra (2001) illustrated the data qualifications for  $J_{Ic}$  and  $J$ - $R$  curve as shown in Fig. 2.1.

## 2.4 Summary

Hu and Albrecht (1991) found various metal specimens that were used to measure  $J$ - $R$  curves actually reach the limit load while undergoing significant crack extension. Thus, singularity is not associated to the failure of plastic tearing in those specimens.

European researchers don't use  $J$  values anymore in fracture toughness testing. Instead, CTOD and its operational quantity  $\delta_5$  (Schwalbe 1995, Schwalbe et al. 2004) are widely adopted. A new standard method which is under ballot by ASTM international technical committee, uses CTOA and CTOD to determine the resistance to stable crack extension under low-constraint conditions,  $J$ -integral excluded.

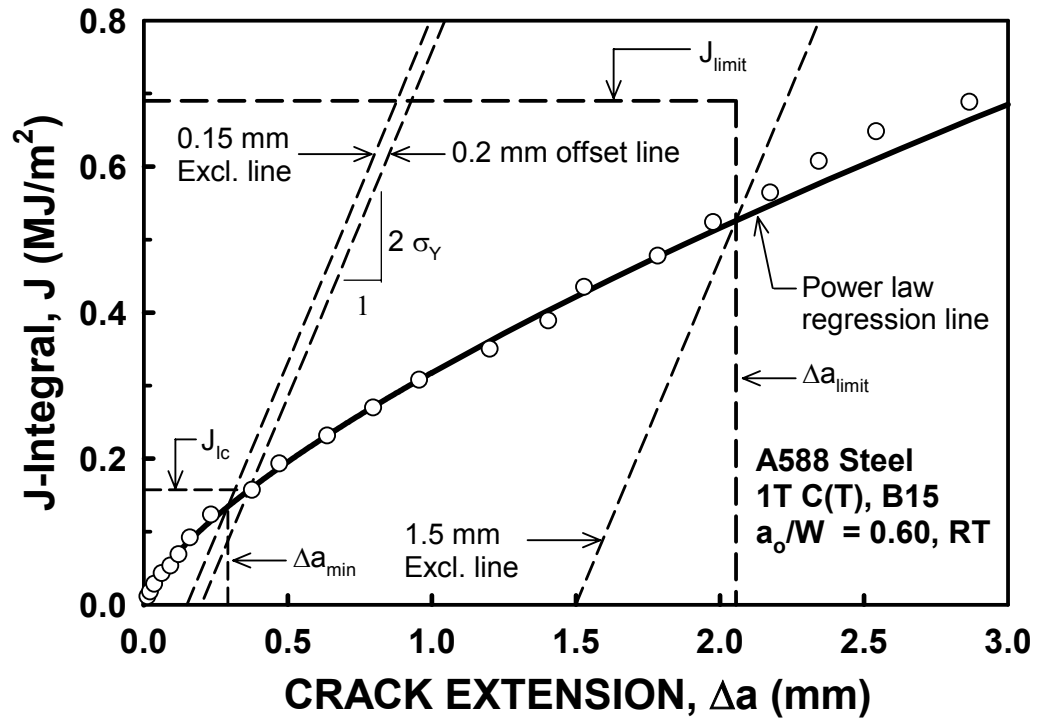


Fig. 2.1 Illustrative  $J_{Ic}$  and Data Qualification; 1T C(T) Specimen B15, A588 Steel, RT (Candra 2001)

### CHAPTER 3: ENERGY RELEASE RATE IN TOUGH STEELS

Irwin and Kies (1954) developed the energy release rate concept, which is related to the Griffith theory but is in a form that is more useful for solving engineering problems. Practical use of the energy release rate, or so-called crack extension force, was illustrated by Irwin (1956). The energy release rate is defined as the rate of change in potential energy per unit crack area for linear elastic materials. In the concept, crack extension (i.e. elastic fracture) will occur when the energy release rate reaches a critical value. Subsequently, Irwin (1957) used the Westergaard approach to show that stresses and displacements near the crack tip in elastic materials can be described by a single parameter called the stress intensity factor, which is proportional to the square root of the energy release rate.

For elastic-plastic materials, Rice (1968) presented a path-independent contour integral called  $J$ -integral. This parameter has been conventionally used to characterize the crack extension in an elastic-plastic material. However, there are some concerns regarding the use of  $J$ -integral. First, the large plastic deformations and unloading of the material in the wake of crack extension when crack extension occurs violate the basic assumptions of the  $J$ -integral. This concern has been incorporated into the test standards (ASTM E1820-99, BS7448 Part 4:1997) by restricting the maximum allowable  $J$  in terms of specimen dimensions and flow stress, and by limiting the allowable extent of crack growth as a function of ligament (Sumpter 2004a). Secondly, a crack growth correction factor is added in the calculation of the  $J$ -integral in the standard to flatten the  $J$ - $R$  curve as the crack extension progresses. The

lack of clarity in the definition of the  $J$ -integral after crack extension is emphasized by the fact that there have been different  $J$  validity limits and different crack growth correction factors among the test standards (Sumpter 2004a). Thirdly, the implication of increasing toughness with crack growth in the  $J$ - $R$  curve is misleading. It is physically impossible for the material to become progressively tougher as the crack extends. Turner and Kolednik (1994) state that “the widely used  $R$ -curve method based on a  $J$  value derived from normalized work rather than from the original contour integral definition”. Finally, the fact that the  $J$ -integral does not permit unloading to elastic-plastic materials contradicts the standard unloading compliance test procedure used to obtain the  $J$ - $R$  curve from a single specimen.

In many ductile materials such as some aluminums and steels, crack extension occurs when the structural component reaches the “limit load”. Stable crack extension is a process of continuous plastic collapse at the limit load for the current crack length. Because all  $J$ - $R$  curve tests were performed under displacement control, the load gradually dropped in a slow and stable manner as the crack extended. For a compact tension C(T) specimen, a plastic hinge is formed at the limit load and a considerable amount of plastic energy that was dissipated in the specimen was on the compression side of the neutral axis of the specimen (Hu and Albrecht 1991).

After some previous energy release rate methods are reviewed, this dissertation proposes a new definition of the energy release rate associated with elastic-plastic crack extension. The standard unloading compliance load versus load-line displacement record, as shown in Fig. 3.1, is analyzed. The method is then applied to

evaluate the energy release rate in both conventional and high performance structural steels.

### 3.1 Previous Energy Release Rate Methods

Irwin and Kies (1954) explained the unstable fracture in terms of the energy release rate. The energy release rate can be calculated from the compliance of the cracked body, where the compliance is the inverse of the stiffness. The elastic energy release  $\Delta U_e$  associated with crack extension amount  $\Delta a$  can be determined from the standard unloading compliance record as shown Fig. 3.2. Elastic fracture occurs when the elastic energy release rate reaches a critical value.

For elastic-plastic fracture, many attempts have been made to compute the energy release rate. Turner (1984) estimated the elastic energy release,  $\Delta U_e$ , and the plastic energy dissipation,  $\Delta U_p$ , associated with crack extension amount  $\Delta a$  as shown in Fig. 3.3. The area ABC was considered a second order term.

Watson and Jolles (1986) determined the total energy release from the area under the load versus load-line displacement curve as shown in Fig. 3.4. The total energy release associated with crack extension  $\Delta a$  is  $\Delta(U_p + U_{cg})$ , where  $\Delta U_p$  is the global plastic energy dissipates and  $\Delta U_{cg}$  is the crack tip work as the crack extends, which is much smaller. No attempt was made to separate the total energy into the elastic and the plastic components.

Mecklenburg et al. (1989) separated the total energy release into the elastic and the plastic components. The total energy release associated with crack extension  $\Delta a$  was partitioned into the elastic energy release,  $\Delta U_e$ , and the plastic energy dissipation,  $\Delta U_p$ , as shown in Fig. 3.5.

For three steels in the investigation, the elastic energy release rate and the plastic energy dissipation rate were found to be dependent on the specimen size and the initial crack length. Also, the total energy release rate was large at early stage and fell to a near constant value as the steady-state crack growth developed.

### **3.2 Compliance Ratio (CR) Method for Energy Release Rate**

Fig. 3.6 illustrates the CR method for constructing the load-displacement curve without crack extension, called the CR load-displacement curve, from the standard unloading compliance data. Developed by Candra et al. (2002), the method assumed that the crack was able to heal to its “initial” crack length, so the reloading compliance at any crack length was equal to the initial compliance,  $C_0$ .

In a present study, the objective is to calculate the energy release rate. A new assumption made is that the crack at the any unloading point heals to its “previous” crack length. Therefore, the reloading compliance at the any crack length is equal to the previous compliance. Therefore, the load  $P'_{i+1}$  on the curve at the unloading point  $(i+1)^{th}$  is given by

$$P'_{i+1} C_i = P_{i+1} C_{i+1} \quad (3.1)$$

or,

$$P'_{i+1} = \frac{C_{i+1}}{C_i} P_{i+1} \quad (3.2)$$

where  $P_{i+1}$  is the actual load at the unloading point  $(i+1)^{th}$ .  $C_i$  and  $C_{i+1}$  are the compliances at unloading points  $i^{th}$  and  $(i+1)^{th}$ , respectively.

The total energy released consist of the elastic energy release,  $\Delta U_e$ , and the plastic energy dissipation,  $\Delta U_p$ . It is proposed that  $\Delta U_e$  and  $\Delta U_p$  associated with crack extension  $\Delta a$  are represented by the area  $ABP_{i+1}P'_{i+1}$  and area  $ABCP_iP'_{i+1}$  respectively under the CR load-displacement curve as shown in Fig. 3.7. This definition is different from Mecklenburg et al. (1989) by the small triangular areas  $AP_{i+1}P'_{i+1}$  and  $AP_iP'_{i+1}$  between the CR load-displacement curve and the actual load-displacement curve for elastic and plastic cases, respectively.

The elastic energy release rate and the plastic energy dissipation rate are determined as  $\Delta U_e / B_n \Delta a$  and  $\Delta U_p / B_n \Delta a$ , where  $B_n$  is the net specimen thickness between side grooves. The crack length  $a_i$  at any unloading point  $i^{th}$  was determined from the compliance  $C_i$  using the equation in ASTM Standard Test Method for Measurement of Fracture Toughness (ASTM E1820-99):

$$a_i / W = 1.000196 - 4.06319u + 11.242u^2 - 106.043u^3 + 464.335 u^4 - 650.677u^5 \quad (3.3)$$

where,

$$u = \frac{1}{(B_e E C_i)^{1/2} + 1}$$

$W$  = specimen width

$$B_e = B - (B - B_n)^2 / B$$

$E$  = modulus of elasticity

### 3.3 Comparison of Energy Release Rate Methods

#### 3.3.1 Description of Experimental Data

The standard unloading compliance load versus load-line displacement records of compact tension specimens were analyzed. The configuration of the standard 1T C(T) Specimen is shown in Fig. 3.8. The test data were obtained from the test procedure specified in the ASTM E1820-99 specification. All specimens had fatigue pre-cracked notches, were side-grooved 10% per side (total of 20%), and were tested at room temperature. Table 3.1 shows the specimen details. Four types of conventional steels were investigated:

- ASTM designation A572 grade 345, *High-strength Low-Alloy Columbium-Vanadium Structural Steel*.



- ASTM designation A588, *High-strength Low-Alloy Structural Steel with 345 MPa Minimum Yield Point to 100 mm Thick.*
- ASTM designation A913 grade 345, *High-strength Low-Alloy Steel Plates of Structural Quality, Produced by Quenching and Self-Tempering Process (QST).*
- ASTM designation A913 grade 450, *High-strength Low-Alloy Steel Plates of Structural Quality, Produced by Quenching and Self-Tempering Process (QST).*

In addition, four high performance steels were investigated. These steels are:

- ASTM designation A709 grades HPS 345W, HPS 485W, and HPS 690W, *High-Strength Low-Alloy Structural Steel Shapes, Produced by Quenching and Tempering Process.*
- Two new versions of A709 grade HPS 690W which are currently still in “mill trial” – being developed by Lehigh University. The first version is designated as “A709 grade HPS-690W Cu-Ni Steel” and the second version is called as “Improved A709 grade HPS-690W Cu-Ni Steel”. These steels use the Cu-Ni base elements in the composition to achieve better performance.

### 3.3.2 Elastic and Plastic Energy Release Rates

Fig. 3.9 to 3.11 compare the elastic component of energy release rate among the three methods -- the method by Turner (1984), by Mecklenburg et al. (1989), and CR method – for A572 steel (A15), A588 steel (B16), and A709 HPS 690W Cu-Ni steel (G16), respectively. It is found that the CR method gives the results close to those of Turner and Mecklenburg methods. The difference between the CR method the Mecklenburg method is mostly within 5% for conventional steels and high performance steels, as shown in Fig. 3.12 and 3.13, respectively.

Fig. 3.14 to 3.16 compare the plastic energy component of energy release rate among the three methods for A572 steel (A15), A588 steel (B16), and A709 HPS 690W Cu-Ni steel (G16), respectively. These results were averaged by 5-point moving average. It is found that the method by Turner gives the lowest values of the plastic energy dissipation rate. The differences of plastic energy dissipation rate between the CR method and the Mecklenburg method are within 5% in all steels, as shown in Fig. 3.17 and 3.18.

In all steels investigated, the amount of plastic energy dissipation rate is larger than the elastic energy release rate during crack extension. Therefore, the plastic energy dissipation rate was the dominant part of the total energy releases.

## **3.4 Contribution**

### **3.4.1 Effect of Steel Type on Energy Release Rate**

Fig. 3.19 and 3.20 show the total energy release rate in conventional steels and HPS, respectively. Most conventional steels (except specimen B16) have relatively shorter crack extension than HPS. In specimens with long crack extension (B16, G16, J6, and S6), the total energy release rate stabilizes to a constant value after some extents of crack extension. However, the total energy release rate in HPS is not much different from the conventional steels for specimens with the same size (1T). The addition of Cu-Ni elements seems to decrease the resistance to crack extension in HPS (G16 and J6).

Effect of specimen size is realized by the considering the large energy release rate in specimen H36 (size 2T) and S6 (size 1.5T). When the specimen size increases, the energy release rate in the entire specimen is higher.

Fig. 3.21 and 3.22 show the elastic component of energy release rate in conventional steels and HPS, respectively. The elastic energy release rates in HPS are higher than conventional steels.

### **3.4.2 Elastic Energy Release Rate and Stress Intensity Factor**

The elastic component of energy release rate obtained from the CR method is compared with the elastic energy release rate from the standard elastic singularity equation in ASTM Standard Test Method for Plane-Strain Fracture Toughness of Metallic Materials (ASTM E399-90) for a compact specimen. By using the load

value at any unloading point  $i^{th}$  on the load-displacement record, the stress intensity factor is expressed as,

$$K_i = \frac{P_i}{B_n W^{1/2}} f(a/W) \quad (3.4)$$

where,

$$f(a/W) = \frac{(2 + a/W)}{(1 - a/W)^{3/2}} [0.886 + 4.64 a/W - 13.32 a^2/W^2 + 14.72 a^3/W^3 - 5.6 a^4/W^4]$$

and  $P_i$  is the load value at unloading point  $i^{th}$ .  $a$ ,  $B_n$ , and  $W$  are the crack length, specimen net thickness, and specimen width, respectively. The elastic energy release rate  $G_i$  is given as,

$$G_i = \frac{K_i^2}{E^*} \quad (3.5)$$

where  $E^*$  is equal to  $E/(1 - \nu^2)$  and  $E$  under plane strain and plane stress, respectively.  $\nu$  is the Poisson's ratio.

Fig. 3.23 shows the elastic energy release rate of A572 steel (A15) from the CR method and the above equations assuming both plane stress and plane strain conditions. Poisson's ratio of steel was assumed to be 0.3. Reasonable agreement was found.

### 3.4.3 Conclusions

The objective of the energy release rate approach proposed above is to determine the energy release rate during the elastic-plastic crack extension, thus to provide an understanding to the plastic fracture in ductile steels. The approach is applied to both conventional and high performance structural steels. The main conclusions are:

- The total energy release rate approaches a constant value during stable crack extension in specimens with long crack extension.
- The elastic energy release rate is smaller than the plastic energy dissipation rate during elastic-plastic crack extension.
- The total energy release rates in high performance steels (HPS) are not different from the conventional steels.
- The elastic energy release rate obtained from the CR method is in good agreement with the elastic strain energy release rate calculated from the standard elastic singularity equation in ASTM Test E399-90, using the load value at the unloading point on the load-displacement record.

Table 3.1 List of Specimens for Energy Release Rate

Specimen ID	Steel Designation	Specimen Size	Testing Temperature (°C)	Initial crack length $a_0 / W$
A15	A572	1T	24	0.60
B16	A588	1T	24	0.60
C16	A913 Gr. 345	1T	24	0.60
D17	A913 Gr. 450	1T	24	0.60
H36	A709 HPS 345W	2T	24	0.50
E17	A709 HPS 485W	1T	24	0.60
S6	A709 HPS 690W	1.5T	24	0.50
G16	A709 HPS 690W Cu-Ni	1T	24	0.60
J6	Improved A709 HPS 690W Cu-Ni	1T	24	0.55

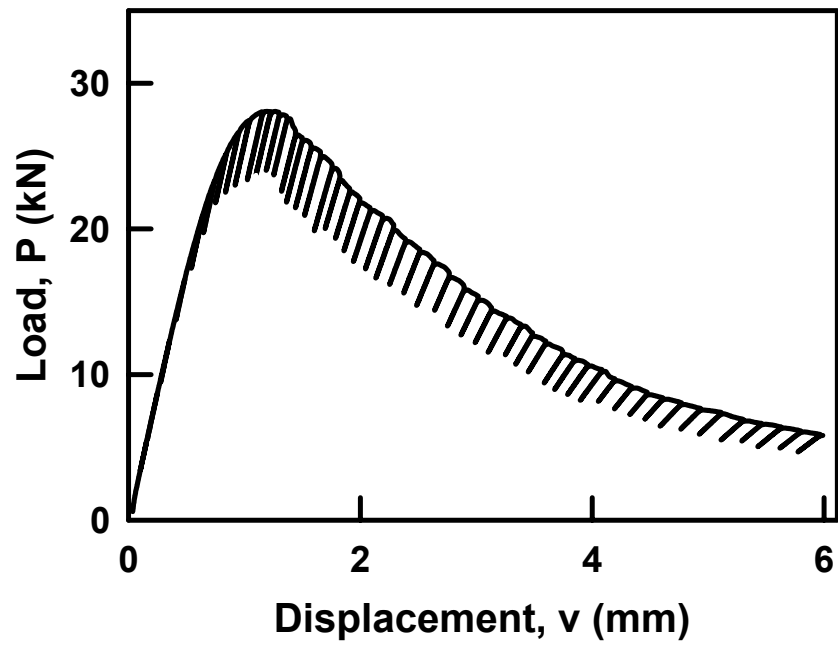


Fig. 3.1 Load versus Load-Line Displacement with Periodic Unloading

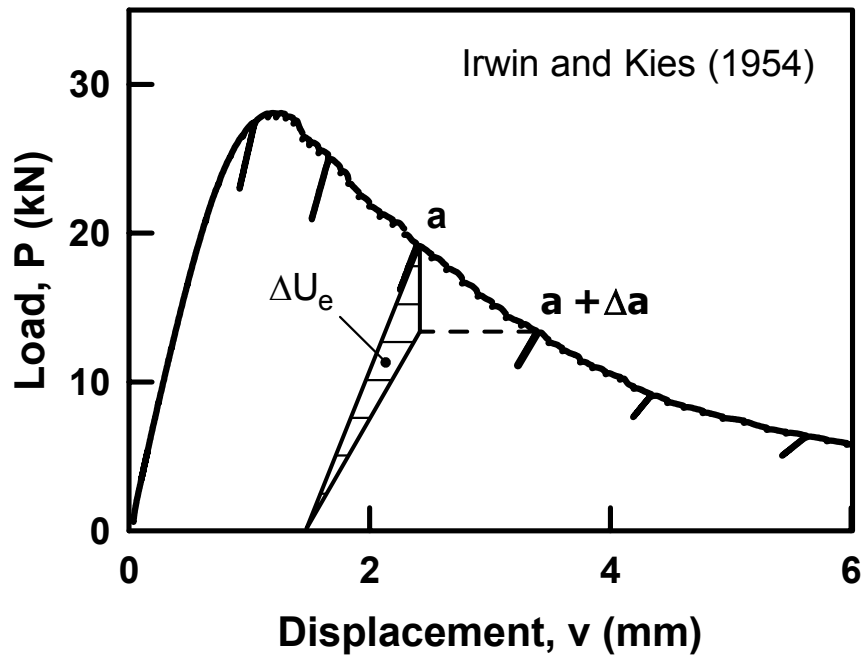


Fig. 3.2 Elastic Energy Release Associated with Crack Extension (Irwin and Kies 1954)

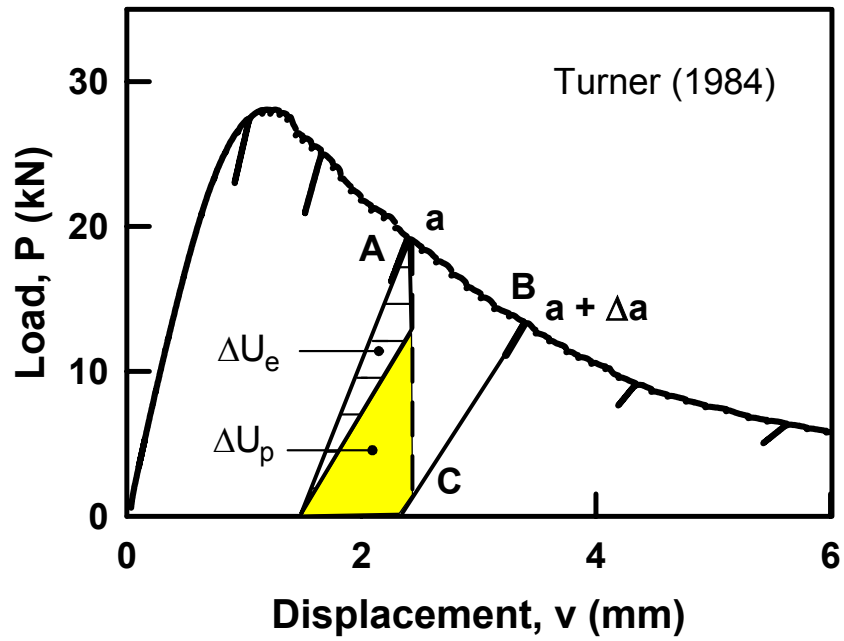


Fig. 3.3 Energy Dissipation Associated with Crack Extension (Turner 1984)

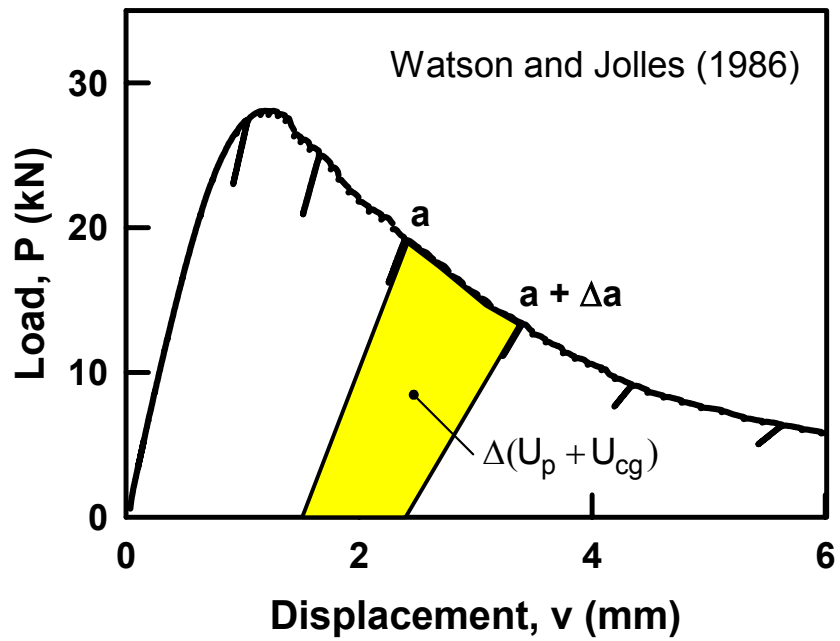


Fig. 3.4 Global Plastic Energy Dissipation Associated with Crack Extension (Watson and Jolles 1986)



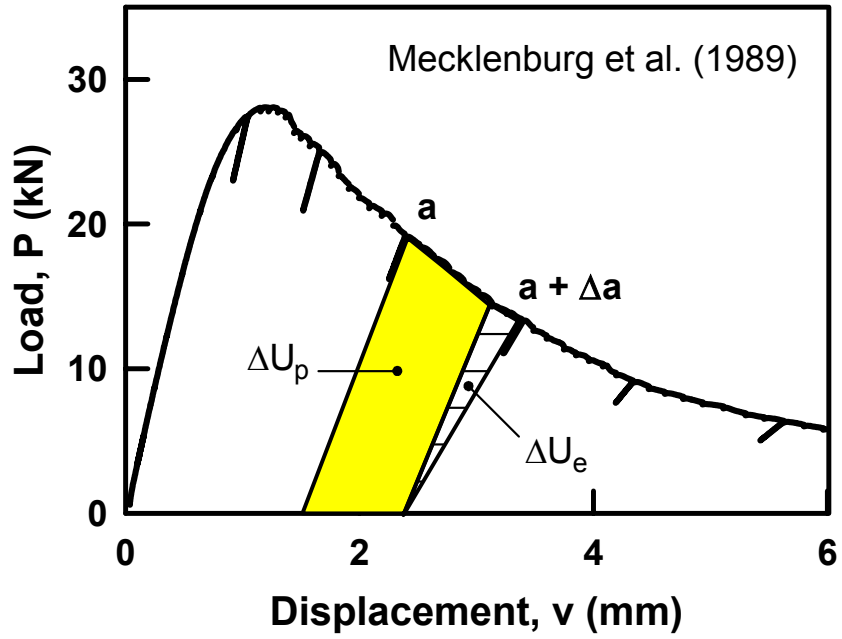


Fig. 3.5 Separation of Energies into Elastic and Plastic Energy Components (Mecklenburg et al. 1989)

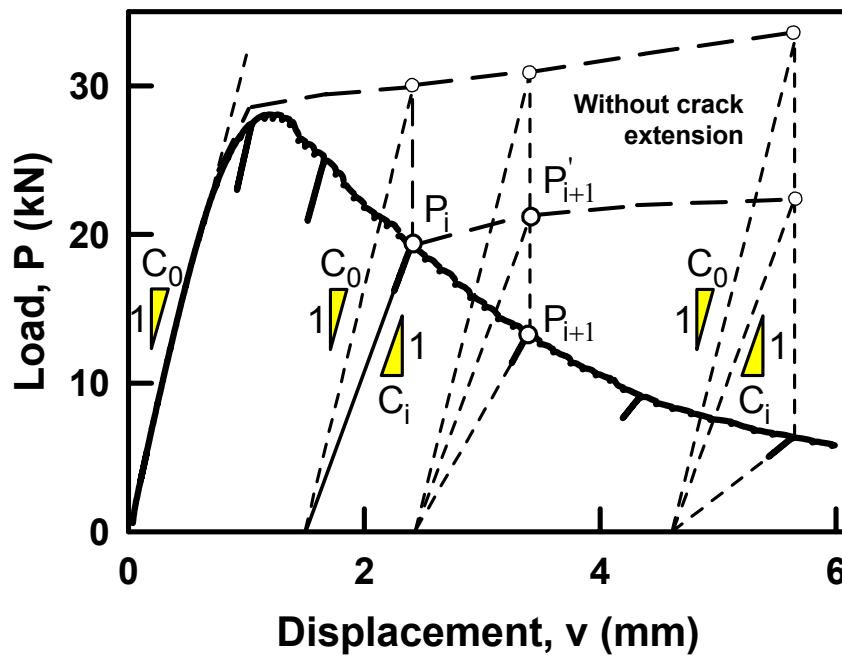


Fig. 3.6 Construction of CR Load versus Displacement Curve from the Standard Unloading Compliance Data

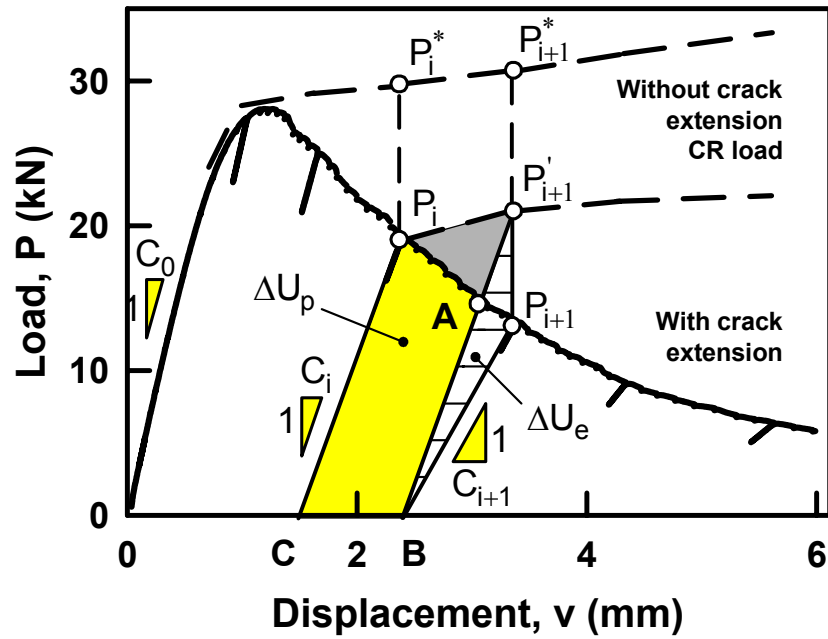


Fig. 3.7 Calculation of Elastic Energy Release and Plastic Energy Dissipation Associated with Crack Extension by CR Method

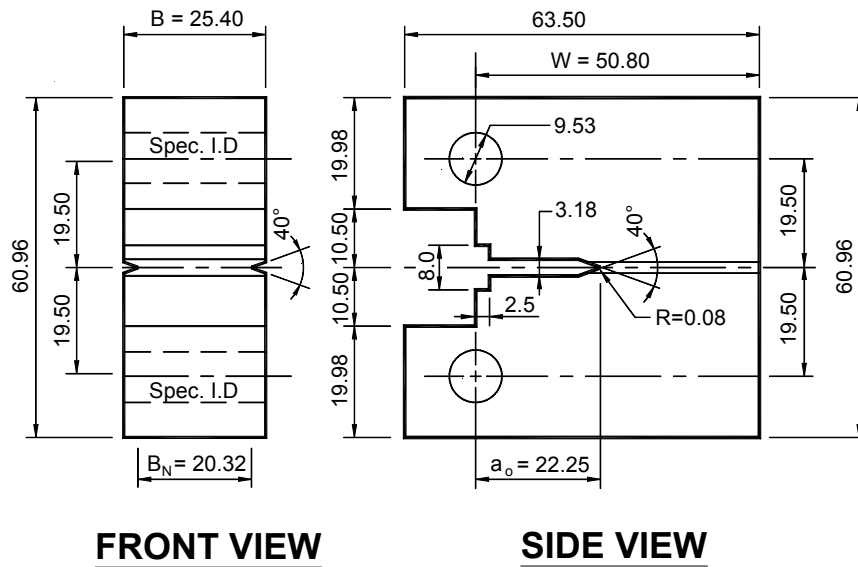


Fig. 3.8 Details of ASTM Standard 1T C(T) Specimen

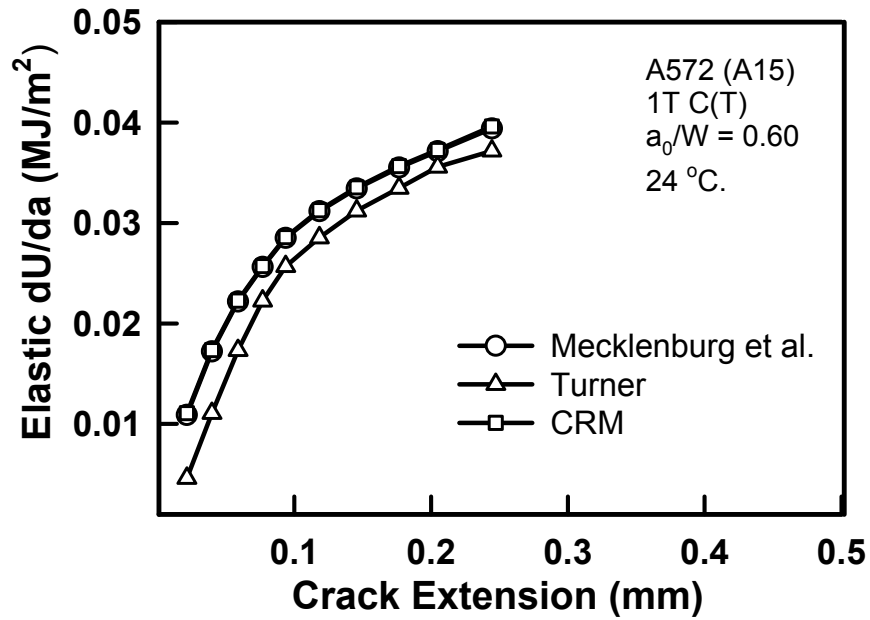


Fig. 3.9 Comparison of Elastic Energy Release Rate by Different Approaches, A572 Steel (A15)

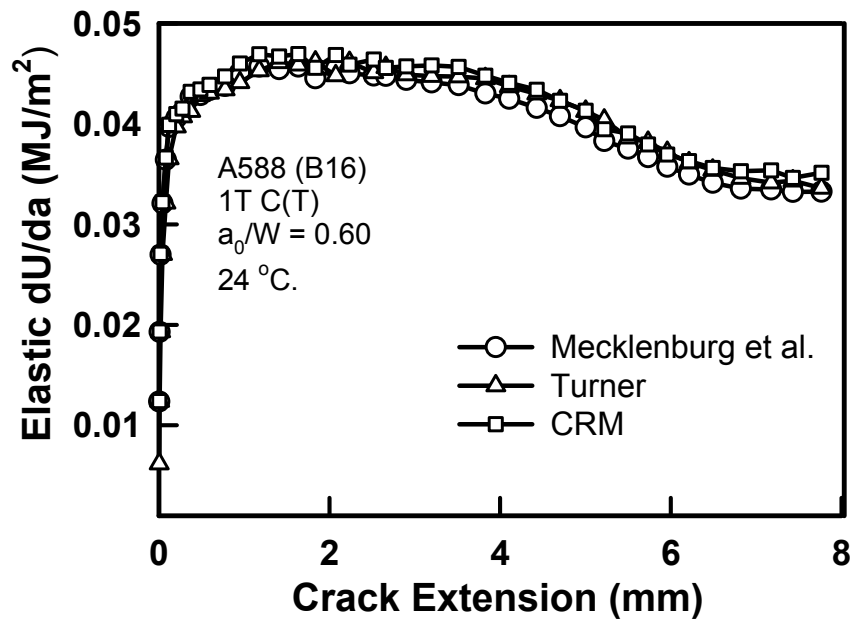


Fig. 3.10 Comparison of Elastic Energy Release Rate by Different Approaches, A588 Steel (B16)

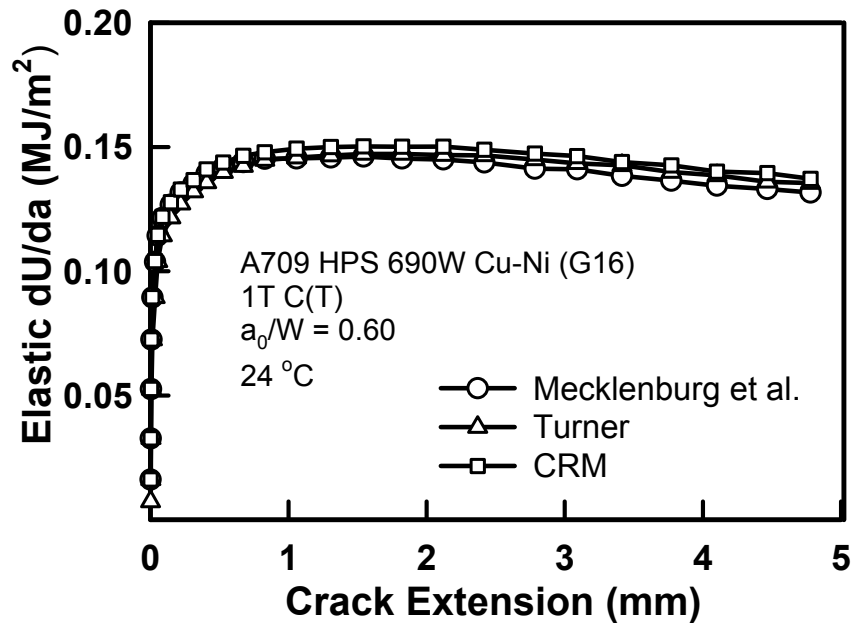


Fig. 3.11 Comparison of Elastic Energy Release Rate by Different Approaches, A709 HPS 690 Cu-Ni Steel (G16)

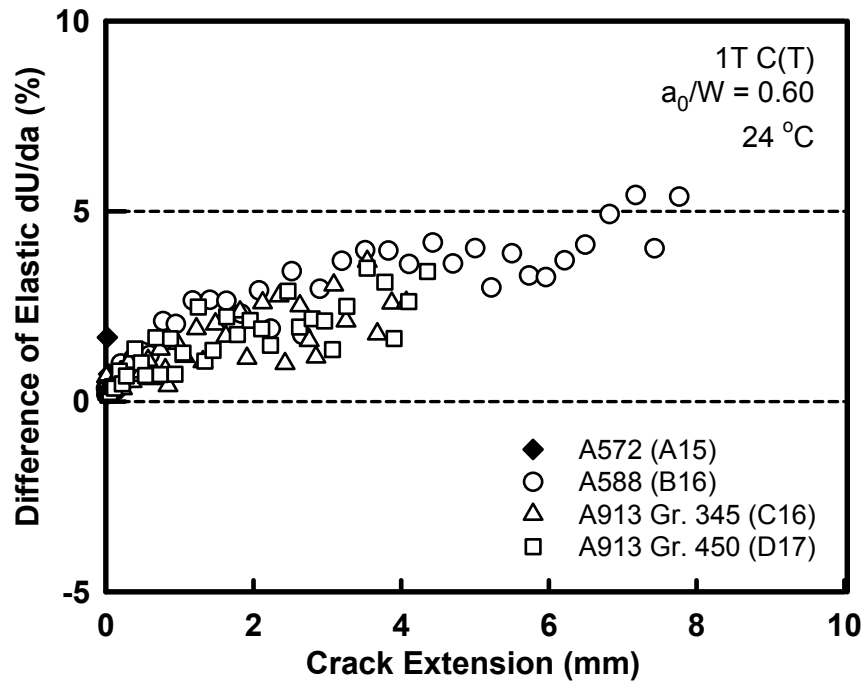


Fig. 3.12 Difference of Elastic Energy Release Rate between Method by Mecklenburg et al. (1989) and CR Method in Conventional Steels

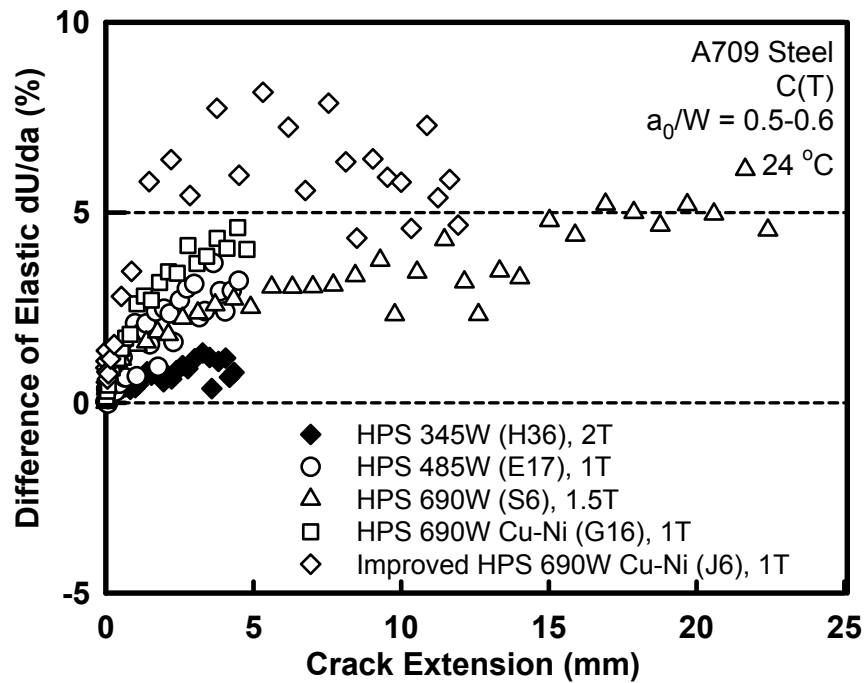


Fig. 3.13 Difference of Elastic Energy Release Rate between Method by Mecklenburg et al. (1989) and CR Method in HPS

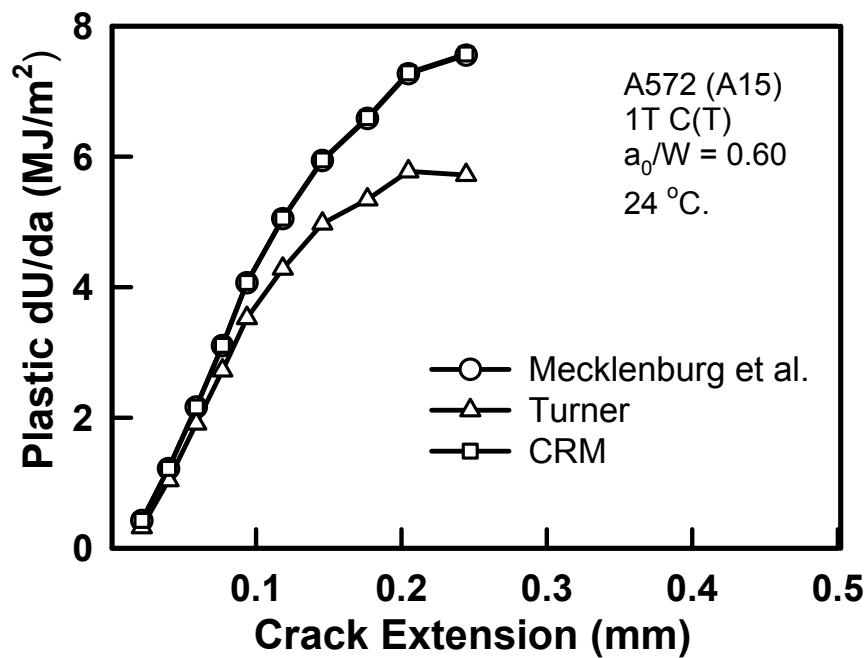


Fig. 3.14 Comparison of Plastic Energy Release Rate by Different Approaches, A572 Steel (A15)

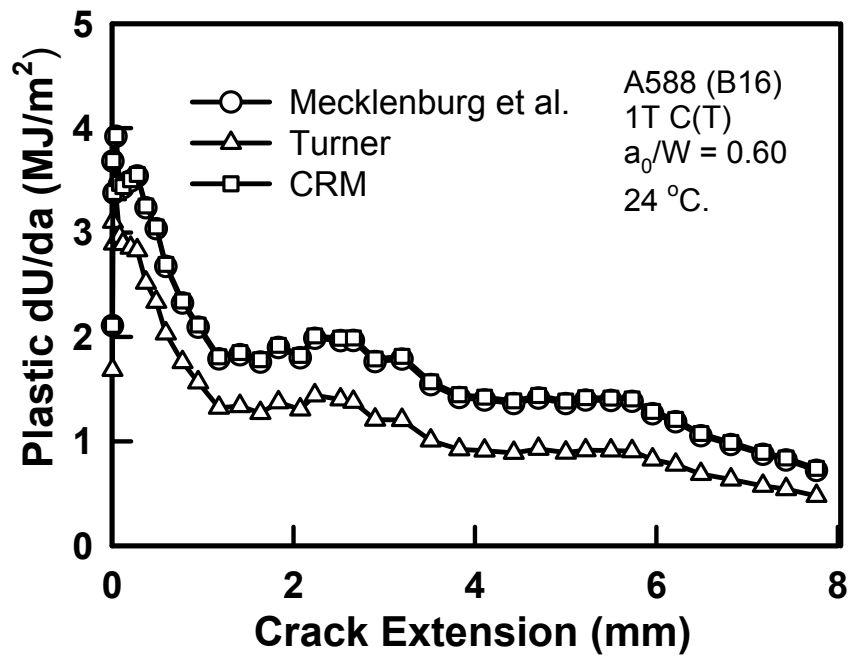


Fig. 3.15 Comparison of Plastic Energy Release Rate by Different Approaches, A588 Steel (B16)

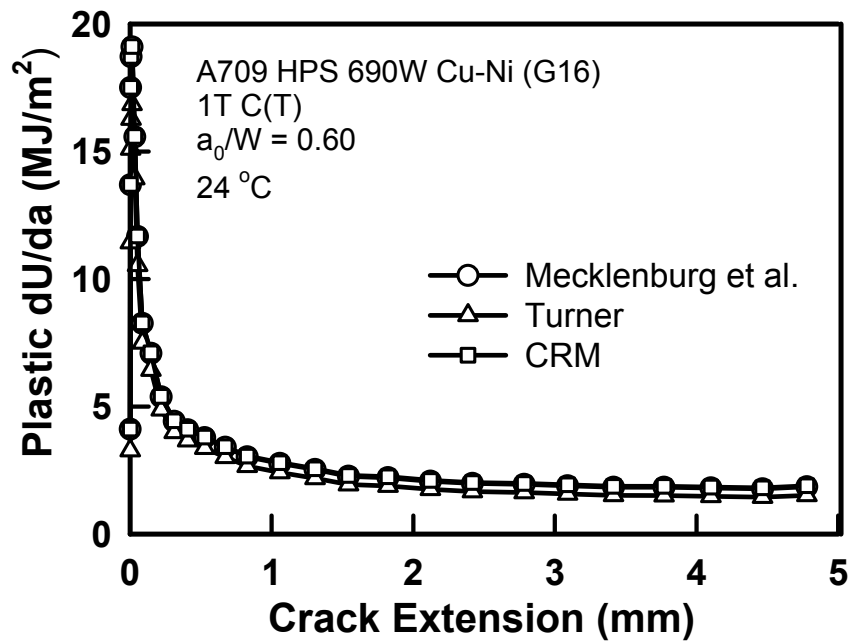


Fig. 3.16 Comparison of Plastic Energy Release Rate by Different Approaches, A709 HPS 690 Cu-Ni Steel (G16)

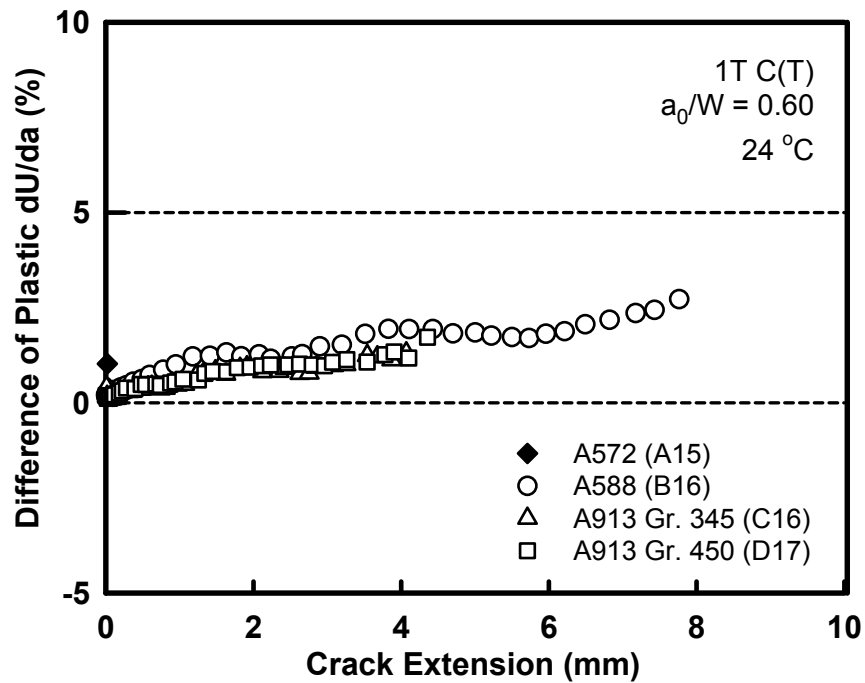


Fig. 3.17 Difference of Plastic Energy Release Rate between Method by Mecklenburg et al. (1989) and CR Method in Conventional Steels

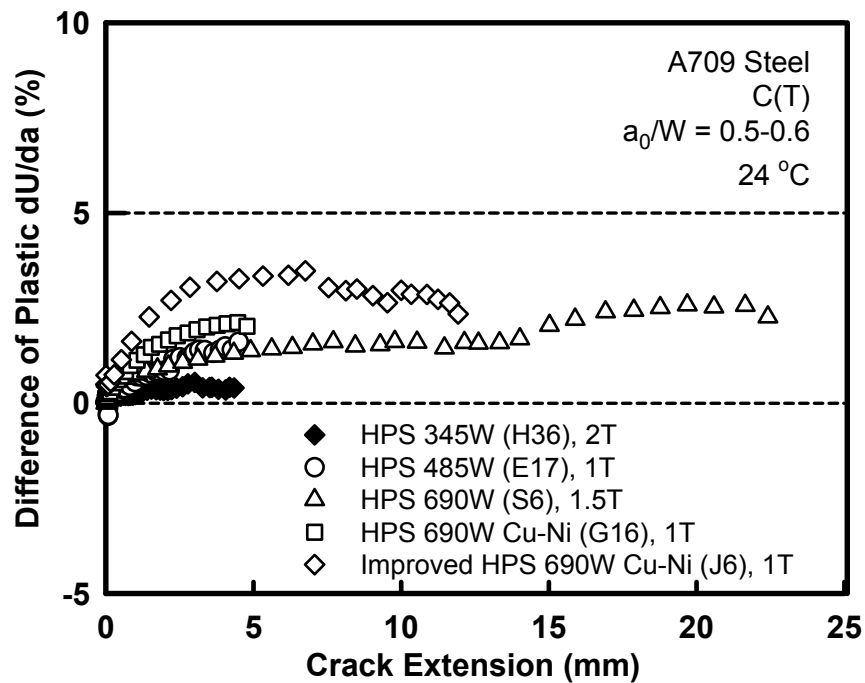


Fig. 3.18 Difference of Plastic Energy Release Rate between Method by Mecklenburg et al. (1989) and CR Method in HPS

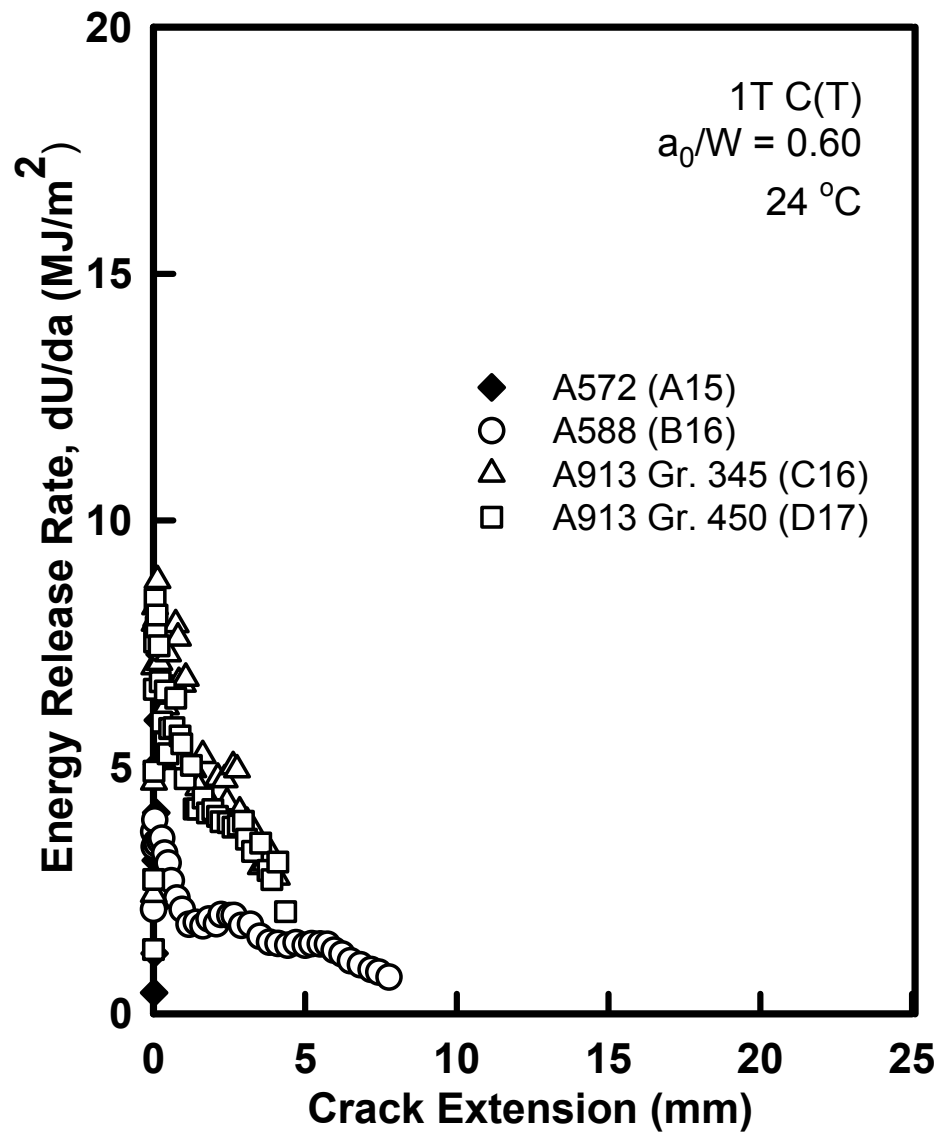


Fig. 3.19 Total Energy Release Rate of Conventional Steels A572, A588, and A913



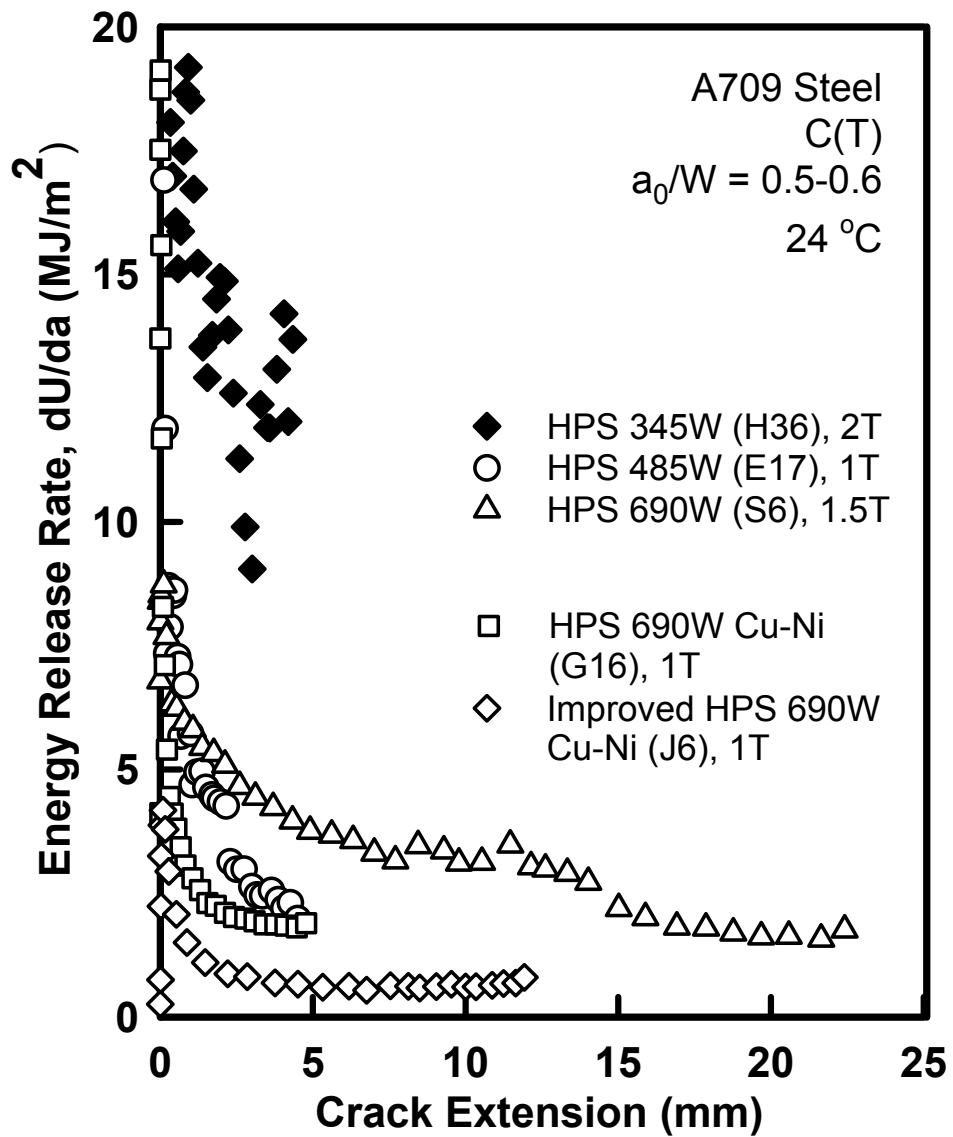


Fig. 3.20 Total Energy Release Rate of High Performance Steels A709

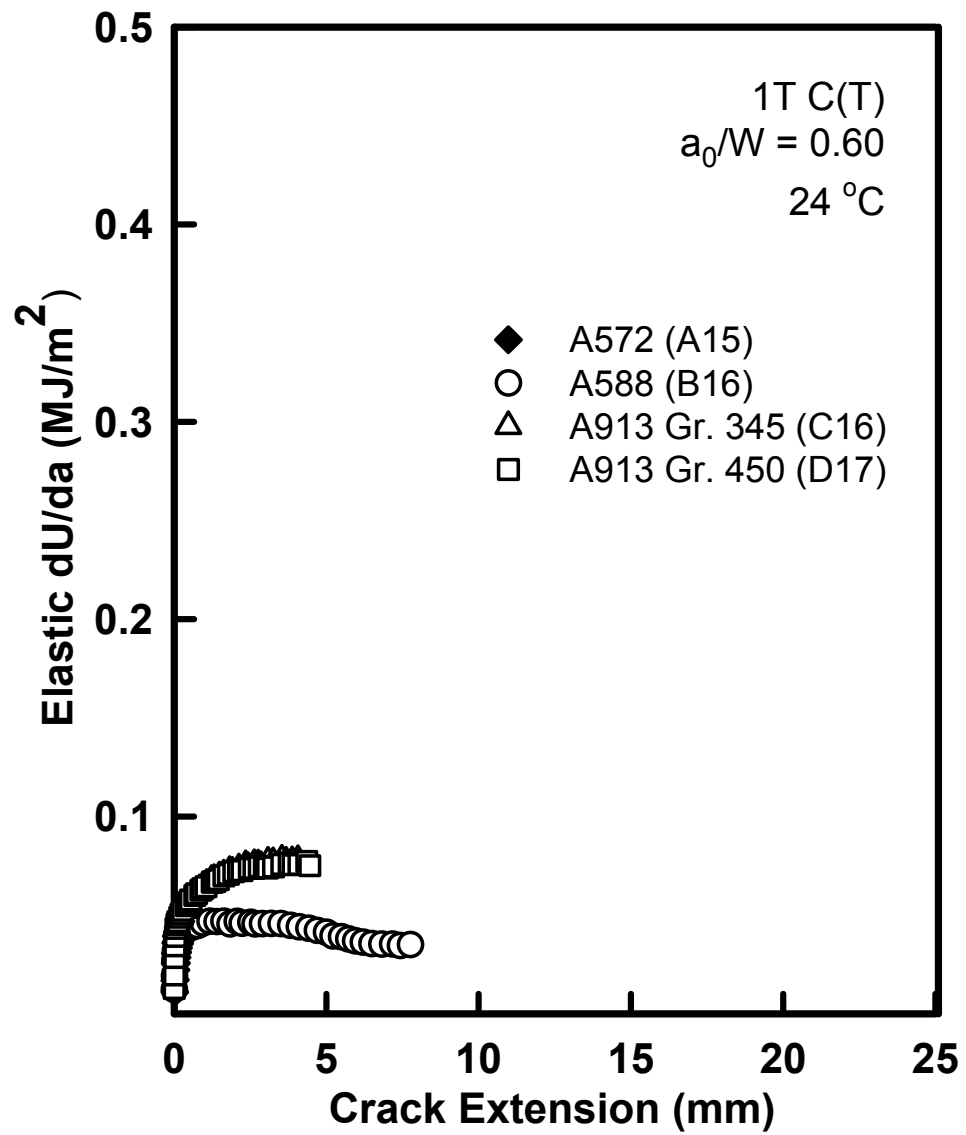


Fig. 3.21 Elastic Energy Release Rate of Conventional Steels A572, A588, and A913

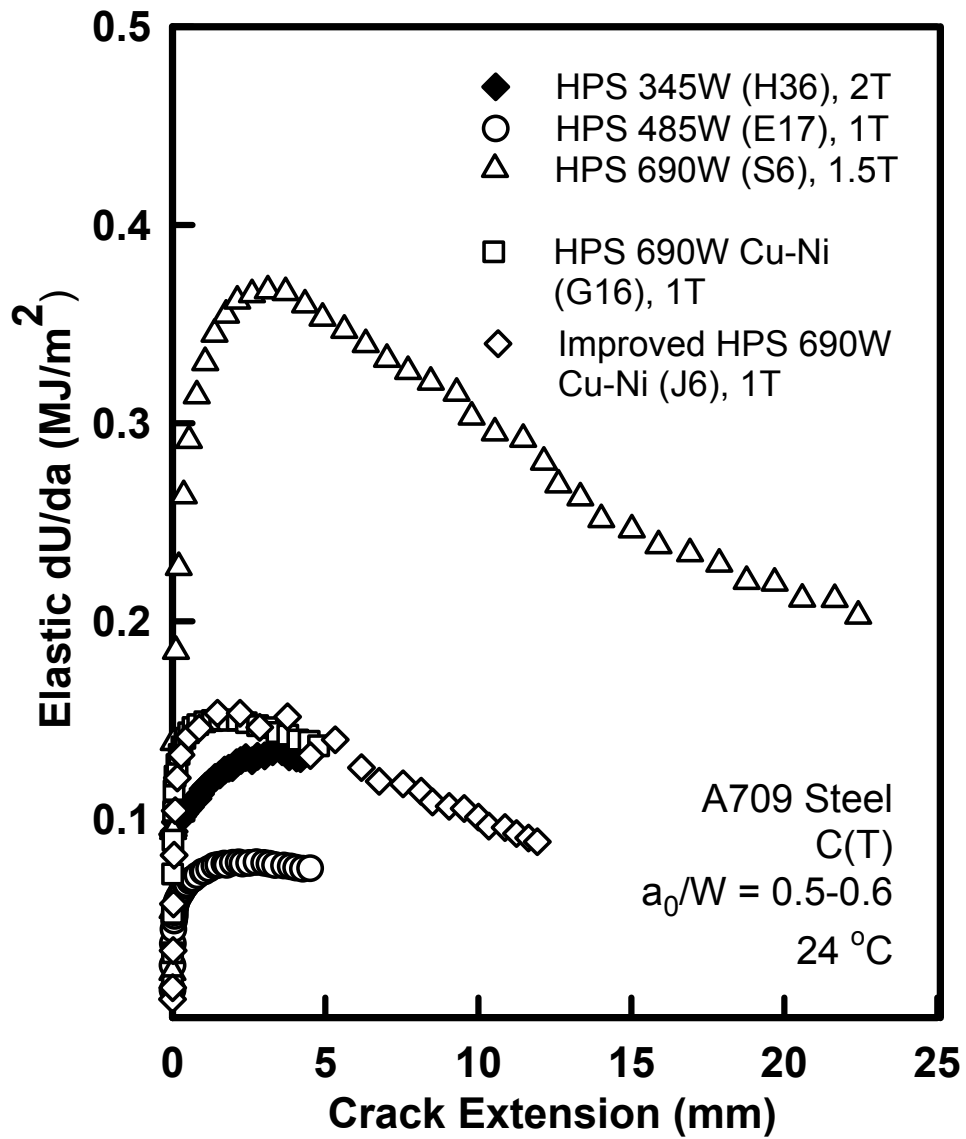


Fig. 3.22 Elastic Energy Release Rate of High Performance Steels A709

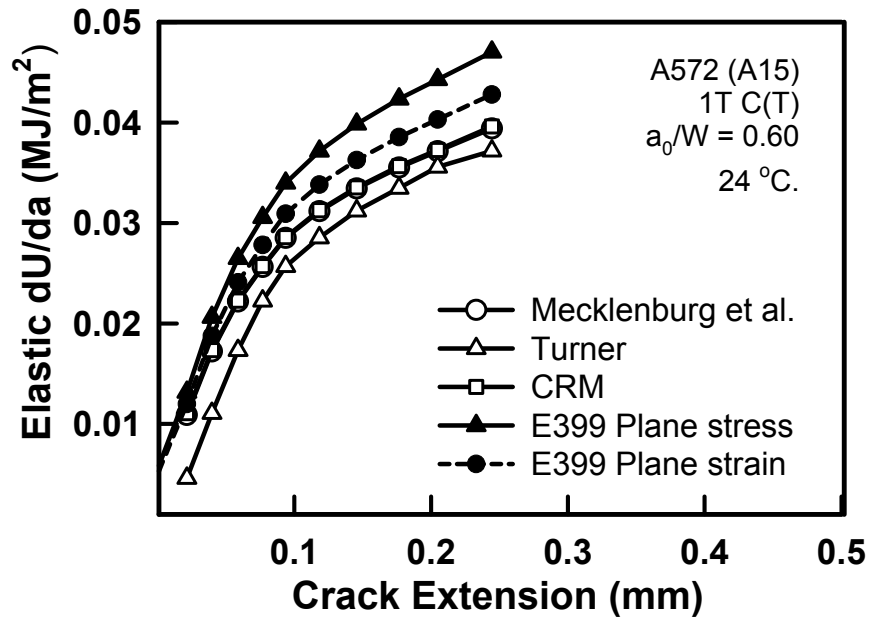


Fig. 3.23 Comparison of Elastic Energy Release Rates with ASTM E399-90 Equations

## CHAPTER 4: PREVIOUS WORK ON GEOMETRIC FACTORS

After the fundamentals of fracture mechanics were established around 1960, scientists and engineers began to concentrate on the plasticity of the crack tip. The biggest difficulty with the energy approaches such as the  $J$ -integral is that direct measurements cannot be obtained from experiments. Naturally, some researchers started searching for the criterion on the deformation side that is physically ready for measurement and could characterize the crack extension geometrically. Most of the work has been conducted on the Crack Tip Opening Displacement (CTOD) and on the Crack Tip Opening Angle (CTOA).

### 4.1 CTOD and CTOD-R Curve

While Rice's  $J$ -integral theory has dominated the development of fracture mechanics in the United States, Wells (1961, 1963, 1964) proposed a parameter called the Crack Tip Opening Displacement (CTOD) that led Europe in the field of fracture mechanics for tough materials.

The CTOD method characterizes the fracture behavior by measuring the opening of the crack surfaces at the original crack tip, and describes the capacity of a material near the crack tip to deform before or during crack extension. It was hypothesized that crack extension can take place when the material at the crack tip has reached a maximum permissible plastic strain. The crack tip strain then can be related to the crack opening displacement, which is a measurable quantity. Because the CTOD method is based on the determination of a critical strain at the fracture

from a load-displacement record, which does not require a stress analysis, it can be used to characterize the resistance to crack extension from elastic to fully plastic behaviors.

CTOD can be related to the applied stress and crack length in the crack tip strip-yield model proposed by Dugdale (1960) and Bilby et al. (1963). As shown in Fig. 4.1, the strip-yield model consists of a through-thickness crack in an infinite plate that is subjected to a uniform closing stress,  $\sigma_{ys}$ , normal to the crack plane. The crack length is  $2a$  and the yield zone length ahead of the physical crack tip is  $r_y$ .

$$CTOD = \frac{\pi\sigma^2 a}{E\sigma_{ys}} = \frac{K^2}{E\sigma_{ys}} = \frac{G}{\sigma_{ys}} \quad (4.1)$$

CTOD will reach the critical value  $CTOD_C$  when the stress intensity factor  $K$  reaches  $K_C$ .  $CTOD_C$  was found to be dependent on the crack size when the temperature was higher than a certain transition range (Castro et al. 1979).  $CTOD_C$  appears to have three possible values: the value at the onset of crack extension, at the maximum load, and at the point of instability. It is not clear to researchers which value is correct for use in determining the  $CTOD_C$ . A single edge, three-point-bend specimen was used to obtain the critical CTOD in the British standard test method (BSI 1979). The specimen has a large plastic constraint, which gave the following equation consisting of both elastic and plastic parts:

$$CTOD = \frac{K^2(1-\nu^2)}{2E\sigma_{ys}} + \frac{r_p(W-a)}{r_p(W-a)+a} V_p \quad (4.2)$$

where,

$r_p$  = plastic rotation factor

$V_p$  = plastic component of clip gauge displacement

In this case, a rigid body rotation around a plastic hinge was assumed at 40% of the ligament ahead of the crack tip for the SE(B) specimen, which resulted in  $r_p = 0.4$ .

Later the ASTM standard (ASTM 1988) adopted Eq. (4.2) for both the SE(B) and the compact tension (C(T)) specimens. For the C(T) specimen,  $r_p$  has different values for different ranges of  $a_0/W$ .

Instead of using the average intensity of stress around the crack tip in the case of the  $J$ -integral, the CTOD method takes the blunting at the crack tip as a direct measure of crack deformation. Miller and Kfoury (1979) showed in a finite element analysis that the  $J$ -integral is more relevant to crack initiation while CTOD is more relevant to crack extension. Unlike the blunted parabolic shape established before the onset of crack extension, the crack tip becomes relatively sharp as the crack extends. So the measurement and the interpretation of the CTOD-R curve become more complex.

Rice and Sorensen (1978) postulated a plastic deformation zone along with the advancing crack tip and defined the CTOD as the opening distance between two points moving with the crack extension. Dawes (1979) suggested that CTOD should be defined as the opening displacement at the original crack tip position. This

definition recognized the formation of a stretch zone ahead of the original crack front and avoided the ambiguity of the CTOD definition based on the advancing crack tip profile. Newman (1985) proposed a methodology using the CTOD-R curve to predict stable crack growth and instability under plane stress condition. The method is similar to the  $J$ - $R$  curve approach, with the crack extension drive force written in terms of CTOD. Newman et al. (1988) further showed that after the maximum load was reached on the CTOD-R curve, the CTOD had a nearly constant value that depended on specimen type, specimen width, and initial crack length. Garwood (1988) used the CTOD-R curve to predict the nominal stress and crack growth behavior of wide steel plates. The accuracy was reported to be heavily dependent on the estimation of the plastic limit load.

## **4.2 CTOA and CTOA-R Curve**

Similar to the CTOD, the Crack Tip Opening Angle (CTOA) parameter is appealing because it is physically ready for measurement. Recent interest has developed in the CTOA as a criterion of fracture toughness or resistance, especially in the research of thin-sheet alloys (Newman et al. 2003).

However, an agreement has not be reached regarding the definition of CTOA. In the past, researchers have made several distinct definitions. Green and Knot (1975) defined CTOA as the ratio of CTOD at the initial crack tip position to the current crack extension value



$$CTOA = \frac{\Delta CTOD}{\Delta a} = \frac{(CTOD_i - CTOD_0)}{(a_i - a_0)} \quad (4.3)$$

Thus, CTOA can be indirectly measured through CTOD. Yet the relationship between the so defined initial crack front CTOD and the events occurring at the current crack tip is somewhat ambiguous. De Koning (1975) used an angle that reflects the actual slope of the crack surfaces at the crack front

$$CTOA = d(CTOD) / da \quad (4.4)$$

By using a local Cartesian coordinate system with the x-axis parallel to the crack plane, Eq. (4.4) becomes

$$CTOA = -\frac{d(CTOD)}{dx} \quad (4.5)$$

According to Shih et al. (1979), based on the flow theory of plasticity, the incremental strain in the immediate vicinity of the crack tip for perfect plastic materials can be uniquely characterized by the local slope of the crack faces, provided that the CTOA is large in comparison with the proportion of the material flow stress and the modulus of elasticity  $\sigma_o / E$ . However, for an ideally plastic material, the CTOA defined in Eq. (4.5) will theoretically approach  $90^\circ$ , which cannot realistically occur.

Some researchers observed constant value and geometric independence of the CTOA-R curve during the entire process of crack extension (De Koning 1975), while

others (Shih et al. 1979, Kanninen and Popelar 1979) reported the non-constant CTOA for different crack configurations. Two-dimensional finite element analyses (Brocks and Yuan 1991, Newman et al. 1991) showed that CTOA was larger at crack initiation, in some cases much larger than the value needed for stable crack growth. The results were discouraging and indicated that CTOA was not a constant. Newman et al. (2003) argued that some of the problems associated with the early finite element analyses using the CTOD/CTOA criterion were triggered by the improper setting of either the plane-stress or the plane-strain condition around the crack tip. He further explained the phenomena of large CTOA at crack initiation for various materials in Fig. 4.2 to the severe crack front tunneling at the early stage of stable tearing. Dawicke et al. (1999) and Gullerud et al. (1999) analyzed thin-sheet metals by using the three-dimensional finite element method, and demonstrated that the constraint effects around the crack front must be modeled properly to obtain accurate failure predictions with the constant critical CTOA value.

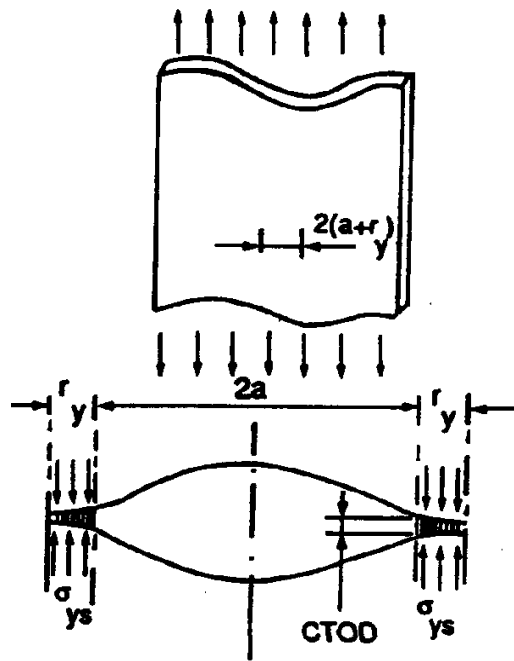


Fig. 4.1 The Strip-Yield Model (Dugdale 1960)

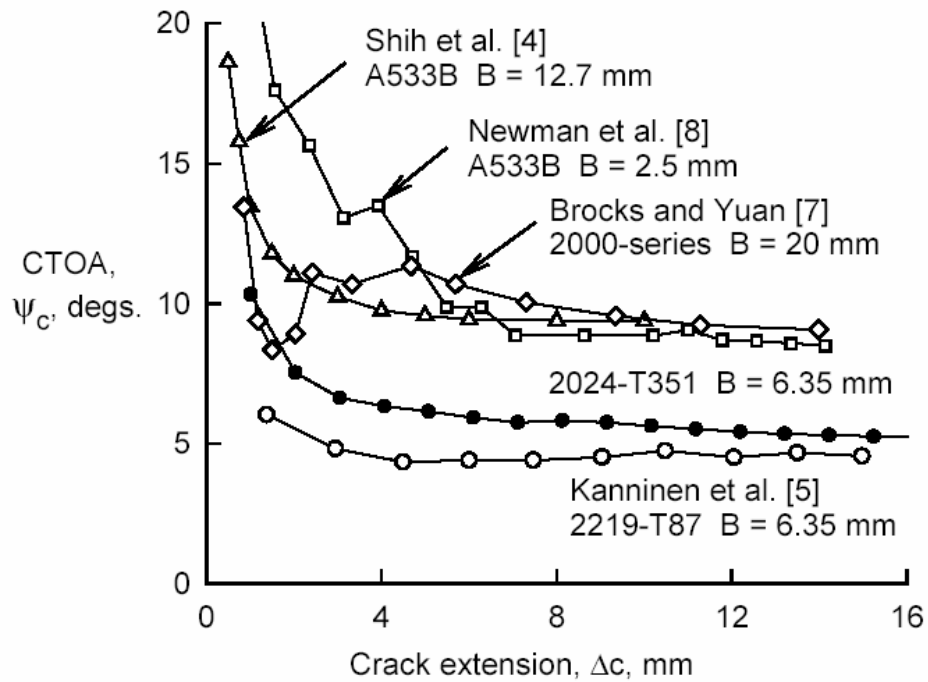


Fig. 4.2 Calculated Critical CTOA Values of Various Materials Using Elastic-Plastic Finite Element Analyses (Newman et al. 2003)

## CHAPTER 5: MECHANISM OF PLASTIC TEARING

### 5.1 Plastic Tearing Mechanism Motion Analysis

#### 5.1.1 General Theorem of Plastic Limit Load

The *Plastic Limit Load* of a structure is the corresponding load at which the plastic flow is unrestrained by the elastic material surrounding the plastic hinge. The mechanism method can be employed to solve the limit load in the frame structure analysis. Fig. 5.1 shows the only possible plastic mechanism for a beam with both ends fixed and with a concentrate load  $P$  applied in the mid-span. In the virtual motion, the external work should be equal to the total internal work by the plastic bending moment in all three hinges, and the equation can be written as

$$P_L \cdot \frac{\theta L}{2} = M_{PA} \cdot \theta + M_{PB} \cdot 2\theta + M_{PC} \cdot \theta \quad (5.1)$$

where,

$\theta$  = unit angle of virtual rotation at plastic hinges

$M_{PA}, M_{PB}, M_{PC}$  = plastic moment capacity at hinges A, B, and C, respectively

The plastic limit load can be solved using Eq. (5.1)

$$P_L = \frac{2(M_{PA} + M_{PB} + M_{PC})}{L} \quad (5.2)$$

The exact plastic limit load can only be found for a few simple cases such as the beam mechanism shown above. For a general structure, determining the limit load is usually quite difficult and requires the simultaneous satisfaction of the equilibrium equations, the stress-strain functions, the compatibility relations, and the yield criteria. Therefore, using the approximate lower-bound and upper-bound solution approaches is necessary to bracket the correct limit load for complicated stress fields. Generally, the lower-bound solution is obtained from stress distributions that are in equilibrium with the external loads and that satisfy the yield condition, while the upper-bound solution is determined from the work of energy balance corresponding to a displacement distribution that satisfies the compatibility. If the lower and upper bounds on the limit load only differ by an amount practically insignificant, the limit load can be regarded as having been determined for the purpose of engineering applications.

### **5.1.2 Limit Load Solution for C(T) Specimens**

Green (1953) calculated the limit moment for the pure bending bar with a wedged notch, as shown in Fig. 5.2. With increased loading, the bar is bent to open so that the stress is tensile near the wedge-shaped root and is compressive in the back face. The elastic-plastic interface in the vicinity of the notch gradually spreads into the remaining elastic field. At some loading stage another plastic region starts and grows from the back face. When the two plastic fields eventually join each other, a plastic hinge is formed and large strains are free to develop without further changes in loading. Fig. 5.2(a) shows the slip-line field constructed by Green with a plane-strain

assumption. In the vicinity of the notch, the slip lines determined by the stress-free face are straight and meet the back surface by  $45^\circ$ . The plastic limit moment of the notched bar increases as the wedge angle  $\Omega$  decreases. When  $\Omega$  approaches zero, the limit moment  $M_L$  can be written as

$$M_L = 1.2606\left(\frac{kb^2}{2}\right) \quad (5.3)$$

where the term  $(kb^2 / 2)$  is the elastic limit moment of a non-notched bending bar with a depth  $b$ . The constant 1.2606 is the constraint factor representing the ratio of the plastic limit moment with a notch to the yield moment without the notch. In this case, the radius  $R$  of the circular arc equals  $0.389b$  and the angle of the arc,  $2\Phi$ , satisfies the following equation

$$\tan(2\Phi) = \frac{2\Phi}{1 - 2\Phi} \quad (5.4)$$

Solving Eq. (5.4) results in  $2\Phi$  being equal to  $117.02^\circ$ .

The theoretically assumed slip-line field satisfied the stress and velocity boundary conditions and was experimentally confirmed by Green and Hundy (1956). Fig. 5.2(b) shows the photographed deformation for a pure bending bar with a V-notch that has the same pattern as the assumed slip-line field.

The compact tension (C(T)) specimen (Fig. 5.8) is recommended by the ASTM E24 committee as the standard specimen in fracture toughness and resistance testing. Kumar and Shih (1980) applied Green's results to the C(T) specimen by neglecting

the effect of the tension force and by dividing Eq. (5.3) by the moment lever arm taken from the load line to the rotation center of the plastic hinge for pure bending

$$P_L = \frac{0.364\sigma_o B(W - a)^2}{a + 0.37(W - a)} \quad (5.5)$$

where,

$\sigma_o$  = material flow stress

$a$  = crack length

$W$  = specimen width

$B$  = specimen thickness

In the equation, the lever arm is written as the crack length plus the horizontal projection of the distance from the crack tip to the plastic rotation center. Eq. (5.5) is hereafter referred to as Green's limit load for the C(T) specimen, and the coefficient "0.37" in the equation is called the plastic rotation factor.

Hu (1989) reviewed all the past limit load solutions for the C(T) specimen and proposed including both bending and tension effects in the Modified Green Solution. Fig. 5.3 shows the slip line in the upper half of the specimen, which consists of a circular segment of the angle  $(\alpha + \beta)$  and a linear segment that intersects the back face of the specimen at an angle of  $45^\circ$ . The lower part of the slip line would be

symmetrical to the upper one about the x-axis. According to Eq. (5.4), the angle subtended by the circular segment to its rotation center O is

$$\alpha + \beta = 2\Phi = 117.02^\circ \quad (5.6)$$

The above equation can be solved further from the geometry of the slip line with

$$\beta = 45^\circ \text{ and } \alpha = 72.02^\circ$$

From the assumed slip-line field of Fig. 5.3 and from the Von Mises yield criterion, Hu derived the limit load of a C(T) specimen including both bending moment and tension force

$$P_L = \frac{2}{\sqrt{3}}WB\sigma(2.572\frac{R}{b}-1)(1-\frac{a}{W}) \quad (5.7)$$

where,

$P_L$  = limit load

$\sigma = \sigma_{YS}$  or  $\sigma_o$ , material yield stress or flow stress

$a$  = crack length

$b = W - a$  = remaining ligament

$R = \sqrt{(1.052a)^2 + 0.409(2ab + b^2)} - 1.052a$ , radius of the circular segment of the

Green slip line



The shear stress at any point on the boundary of the slip line field reaches its maximum value, which corresponds to the term  $\sigma/\sqrt{3}$  in the equation. If the tension force effect is neglected, that is  $P_L = 0$ , Eq. (5.7) will yield to Green's limit moment solution for the pure bending bar with the expression of Eq. (5.3).

### **5.1.3 Concept of Plastic Tearing Mechanism Motion**

The modified Green solution can be considered to give a lower-bound limit load because the equation is based on the stress equilibrium of the slip-line field. It could also be considered as an upper-bound solution because the moment equilibrium in the derivation can be interpreted using the balance of external work and internal energy with each term multiplied by a virtual rotation. Furthermore, this limit load is lower than all existing upper-bound solutions and higher than all lower-bound solutions (Hu 1989). Because the difference between the closest lower and upper bound solutions is practically insignificant, Hu's equation is an accurately determined engineering solution for the C(T) specimen.

A large amount of specimens made of various steels and alloys have been shown (Hu and Albrecht 1991) to reach the limit load after the crack initiation and to keep following the limit load curve with stable crack growth. These results indicate that the failure of tough steels when the crack extends in a slow-stable-ductile manner is a plastic tearing problem governed by essential material properties instead of a "fracture" problem determined by singularity or weak-singularity parameters.

The difference between a regular plastic stress flow and a plastic fracture stress flow is the crack extension in the latter case. For a regular structure, the plastic limit load or moment keeps constant, and every plastic hinge stays in the original place where it forms despite the “virtually” applied rotation. In a plastic tearing problem, the hinge or plastic rotation center moves with the advancing crack front; therefore, the deformation mechanism is more complicated. Fig. 5.4 introduces the dynamic change of the slip-line field in a C(T) specimen with an initial crack length of  $a_0/W = 0.5$ . In Fig. 5.4, the two symmetric rotation centers move forward and become closer when the crack length grows to  $0.7W$  and  $0.9W$ . Referring to the term  $R$  in Eq. (5.7) and in Fig. 5.3, the distance  $d$  between the upper and lower rotation center can be calculated by

$$d = 2R \sin \alpha \quad (5.8)$$

where  $R$  is determined through the current crack length and the remaining ligament. With continuous crack growth, the opening load-line displacement in the back of the crack front increases and the closing distance between rotation centers in the front decreases. So the plastic mechanism for a C(T) specimen can be simply defined as

$$\text{Plastic Tearing Mechanism Motion} = \frac{\Delta v}{\Delta d} \quad (5.9)$$

The use of the distance  $d$  is essential and crucial in Eq. (5.9) to characterize the mechanism of plastic tearing because the current information of crack length and slip-line field configurations are incorporated in this term. Because this mechanism keeps

changing with each increment of crack length  $\Delta a$ , it is named “Mechanism Motion” to emphasize its differences from the general mechanism method.

#### 5.1.4 Mechanism Motion Resistance Curve

The definition of the Mechanism Motion fits the crack extension resistance curve because the change of the mechanism and the moving of the slip-line field are essentially triggered by a crack growth.

Fig. 5.5 shows the experimental Load-Displacement curve of a newly developed high performance structural steel C(T) specimen (A709-690W Cu-Ni, specimen ID G16). In Fig. 5.5, the gray diamond locates the maximum load point. The unloading cycles with the Load-Displacement curve can be used to construct the Compliance Ratio (CR) curve without crack extension (Candra et al. 2002). Using Eq. (5.7) with the measured material yield strength (756MPa), Fig. 5.6 compares the experimental load and Hu’s limit load versus the crack length for specimen G16. The current crack length  $a_i$  or  $a_i/W$  required to obtain the limit load is calculated from the unloading compliance (ASTM 1999), which can be determined directly from the Load-Displacement curve.

$$\frac{a_i}{W} = (1.000196 - 4.06319u + 11.242u^2 - 106.043u^3 + 464.335u^4 - 650.677u^5) \quad (5.10)$$

where,

$$u = \frac{1}{[B_e E C_{c(i)}]^{1/2} + 1}$$

$$B_e = B - \frac{(B - B_N)^2}{B} = \text{effective specimen thickness}$$

$B_N$  = net specimen thickness

$E$  = modulus of elasticity

$$C_{c(i)} = \frac{\Delta v}{\Delta P} = \text{specimen load-line crack opening elastic compliance on an}$$

unloading/reloading sequence corrected for rotation

The result shows that the specimen follows the limit load track while undergoing significant crack extension. This phenomenon is plastic tearing. The discrepancy between the theoretical value and the test data after the crack initiation can be explained by the strain hardening.

With its unloading compliances shown in Fig. 5.5, the crack length at each unloading cycle can easily be determined by using Eq. (5.10). Therefore, the plastic tearing mechanism motion at each stage can be solved using Eq. (5.8) and (5.9). Fig. 5.7 shows the plots for the Mechanism Motion of specimen G16 versus the crack extension in terms of  $a/W$ . The gray-shaded circle represents the data location of maximum loading. The data series have a relatively large value in the crack initiation and decrease after the maximum load point. The data tend to stay constant during stable growth indicating that the Mechanism Motion could be a potential plastic tearing resistance parameter.

The Plastic Tearing Mechanism Motion has a better physical meaning and analytical base than other deformation variables such as CTOD/CTOA. Furthermore, it can be determined directly from the ASTM standard fracture toughness test.

## **5.2 Crack Opening Angle/Normalized Displacement**

### **5.2.1 Definition**

Determining the Crack Tip Opening Angle (CTOA) in the experiment is actually very difficult and often requires expensive high-resolution photographic equipment regardless if the measurement is taken from the original crack front or is based on a certain constant distance from the current crack tip, not to mention the nebulous definition described in Chapter 4.

In a standard ASTM (1999) fracture toughness test for the compact tension specimen, the load-line displacement measured by a clip gauge is the only deformation variable recorded directly in the experiment. As sketched in Fig. 5.8, symmetric loadings are applied to the two pinholes, and the clip gauge measures the movement at each end of the load line for a total amount of  $v$ .

For every crack growth increment  $\delta(\Delta a)$ , there is a corresponding change of displacement  $\Delta v$ . Here,

$$\Delta a = a_i - a_0 \quad (5.11)$$

where,

$a_i$  = current crack length

$a_0$  = initial crack length

Fig. 5.9 shows the plot of Load-Line Displacement versus the crack extension  $\Delta a$  of specimen G16. The displacement  $v$  is directly measured in the experiment while  $\Delta a$  is calculated by plugging the compliances from Fig. 5.5 into Eq. (5.10) and Eq. (5.11). Clearly the data proportion on the curve tends to be a straight line starting from the gray-shaded circle, which corresponds to the maximum load point. This leads to the definition of the *Crack Opening Angle* (COA)

$$COA = \frac{\Delta V}{\delta(\Delta a)} \quad (5.12)$$

The COA can be considered as a modified CTOA or as its operational value. The COA no longer represents the deformation angle in the crack tip, which is hard to find. Instead, it is a remote displacement from the crack front normalized by the local effect of crack growth increment. So in a strict sense, the COA should be called *Normalized Displacement*, but it has the same dimension of the CTOA.

### 5.2.2 COA-R Curve

The newly defined COA reflects the degree of deformation at the moving crack tip by incorporating the crack growth increment  $\delta(\Delta a)$  in Eq. (5.12).

Fig. 5.10 shows the plot of the COA versus the crack extension of specimen G16. Similar to the Mechanism Motion, the data series again have a relatively large

value in the crack initiation and a decreased value after the maximum load point. The curve keeps constant with stable crack growth.

The biggest improvement of the COA or Normalized Displacement to CTOA is that this new concept avoids the difficult measurement for the actual angle at the crack tip. The measurement can be determined directly from the ASTM standard test in a regular mechanical lab without using any extra costly equipment.

### **5.3 Discussion**

Using the same specimen G16, Fig. 5.11 shows the plots of two newly developed geometric resistance factors for the Mechanism Motion and the COA versus crack extension in terms of  $a/W$ , with a conjunction of the Energy Release Rate (ERR) from Chapter 3 and the ASTM  $J$ -integral. The gray-shaded points represent the data locations of maximum loading. Among the four resistance curves, the ASTM  $J$ - $R$  curve keeps climbing with the crack extension while the others remain at a constant value after the maximum loading. It is physically impossible for a material to become progressively tougher as a crack extends. Were it so, a cracked structural component could be made stronger and safer by simply letting the cracks grow.

The relatively high values on the curves of the Mechanism Motion (MM), the COA, and the ERR before the maximum loading point can be explained by the severe tunneling effect at the crack initiation stage. When the crack starts to extend the crack front lags at the free surface because of the low constraint conditions. Once the crack

switches from a flat fracture to the shear mode fracture, the crack front tends to straighten out with much slighter tunneling, as shown in Fig. 5.12.

Obviously, if plastic tearing controls the failure of a specimen, the data in the fully plastic region become more interesting. Fig. 5.13 shows the ratios between the ERR, the MM, and the COA versus the crack extension starting from the maximum loading. The ratio curve of MM/COA is constant with crack extension, which indicates that the two variables may have identical characterization. The MM, however, is more consistent with the ERR because the ratio curve of ERR/MM is constant while the ratio of ERR/COA drops with the crack growth. This result implies that the MM is better than the COA as a geometric resistance factor to plastic tearing.



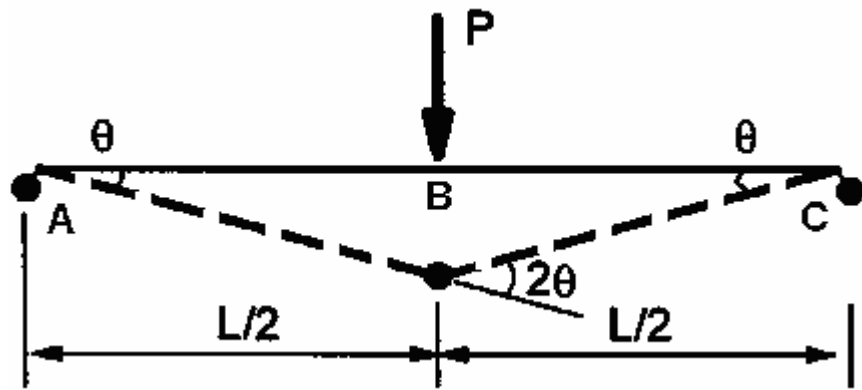
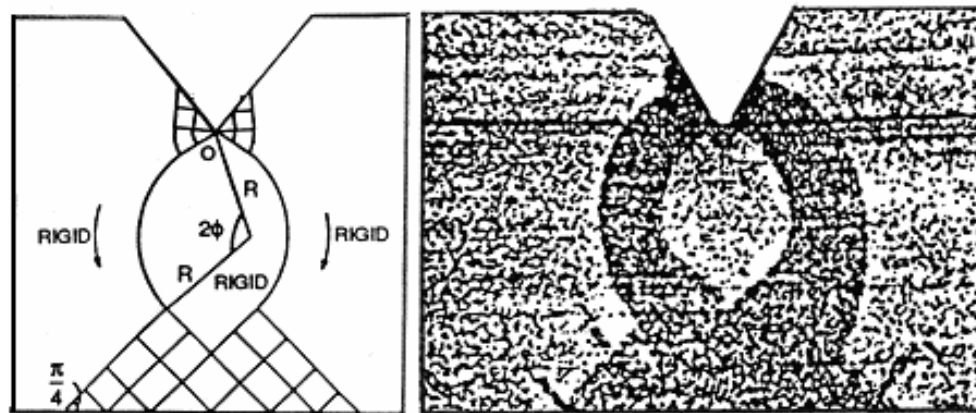


Fig. 5.1 Beam Mechanism for Plastic Limit Load



(a) Assumed Slip Line Field (b) Observed Deformation Pattern

Fig. 5.2 Wedged Notch Bending Bar With Slip Line Field (Green 1953)

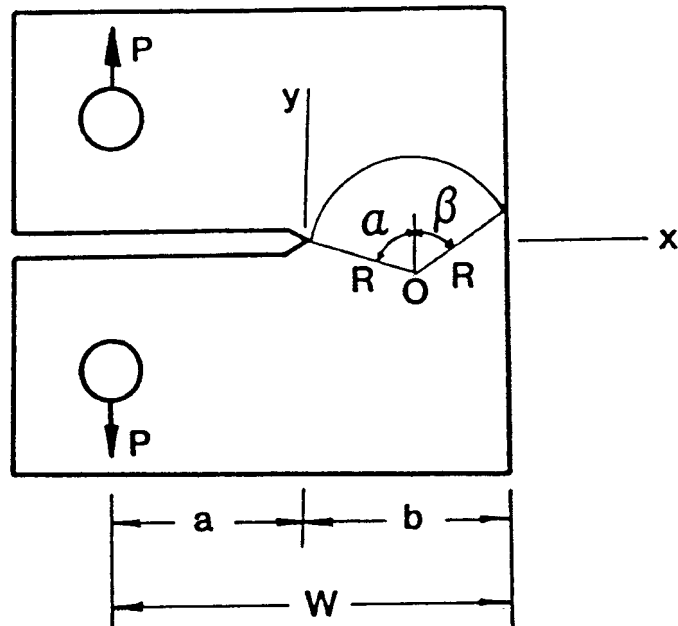


Fig. 5.3 Circular Slip Line of Modified Green Solution (Hu 1989)

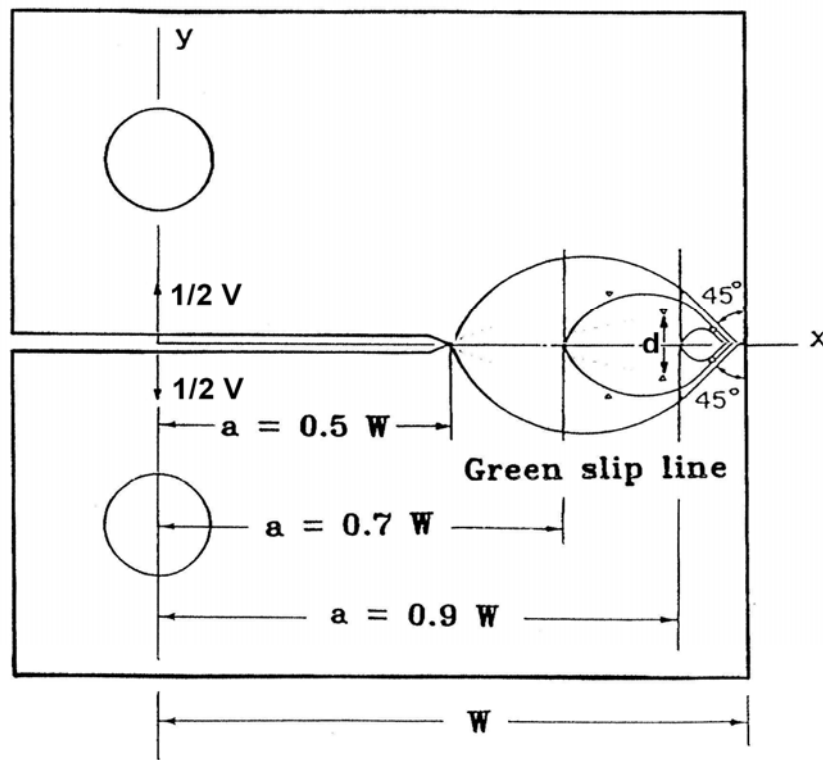


Fig. 5.4 Circular Slip Line Field With Crack Extension

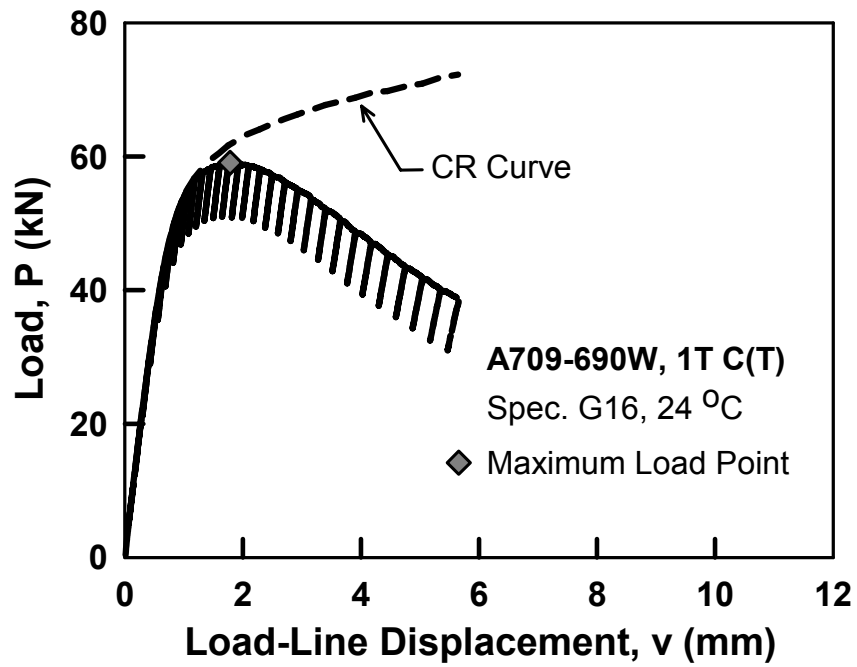


Fig. 5.5 Load vs. Displacement; 709-690W Cu-Ni, Specimen G16, 1T C(T), 24°C,  $a_0/W = 0.60$

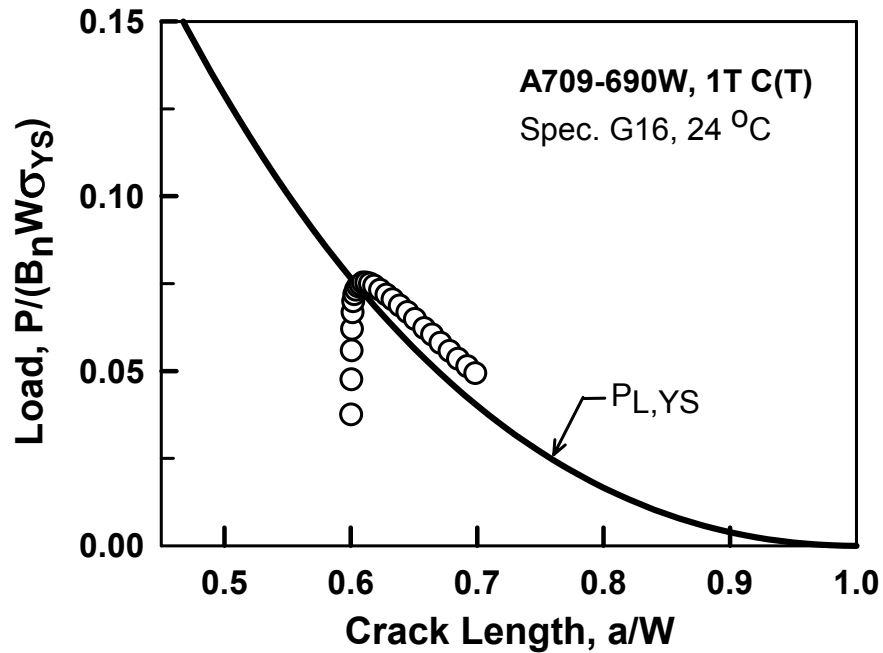


Fig. 5.6 Load vs. Crack Length, Test Load and Hu's Limit Load; Specimen G16, 1T C(T), 24°C,  $a_0/W = 0.60$

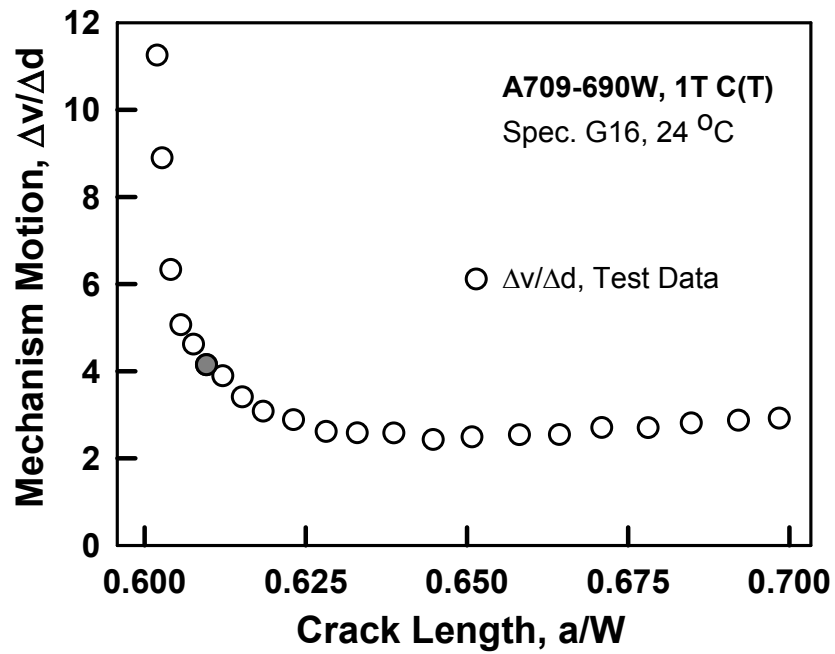


Fig. 5.7 Plastic Tearing Mechanism Motion vs. Crack Extension; 709-690W Cu-Ni, Specimen G16, 1T C(T), 24°C,  $a_0/W = 0.60$

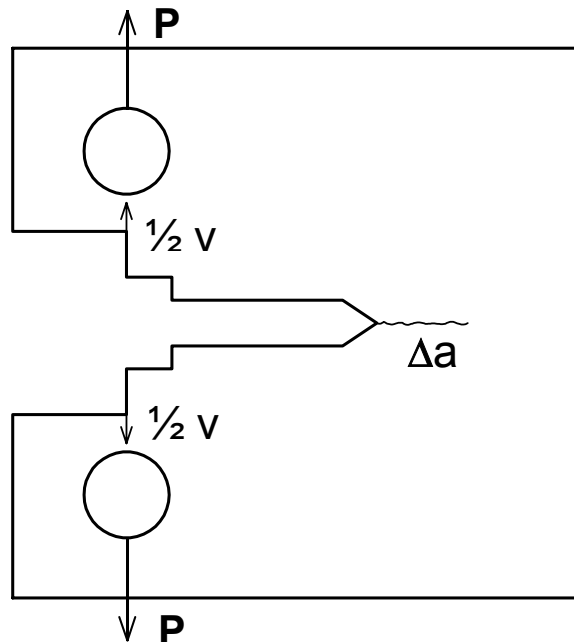


Fig. 5.8 Side View of ASTM Standard C(T) Specimen

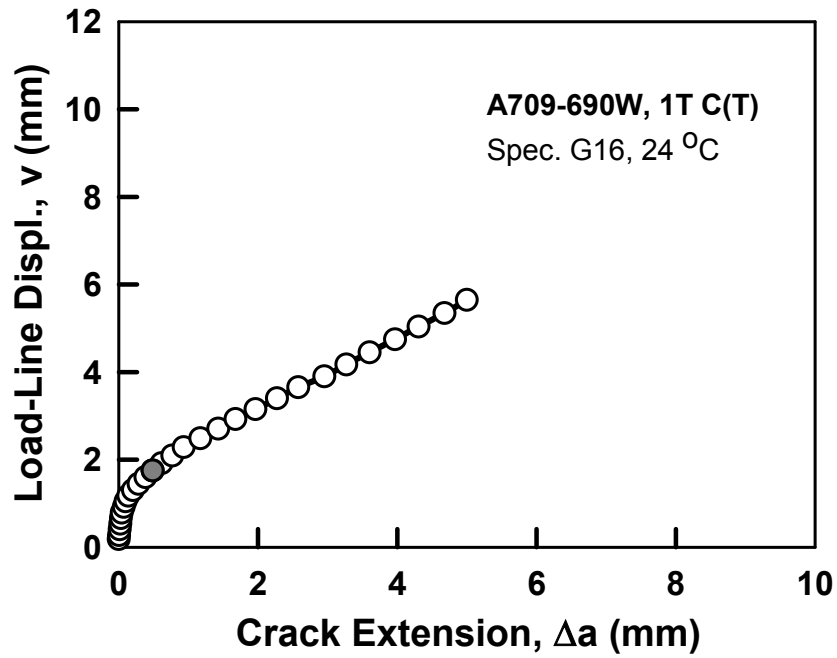


Fig. 5.9 Displacement vs. Crack Extension; 709-690W Cu-Ni, Specimen G16, 1T C(T), 24°C,  $a_0/W = 0.60$

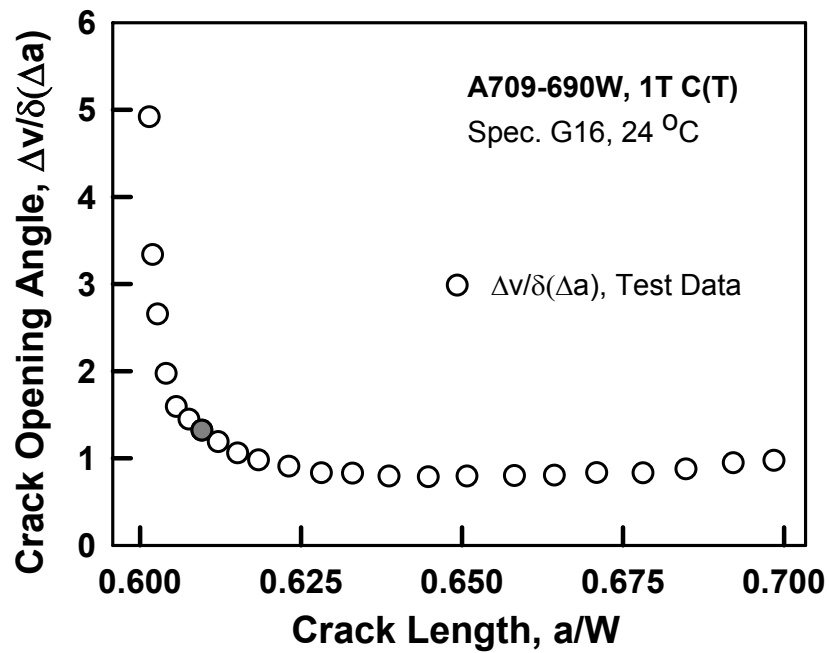


Fig. 5.10 Crack Opening Angle vs. Crack Extension; 709-690W Cu-Ni, Specimen G16, 1T C(T), 24°C,  $a_0/W = 0.60$

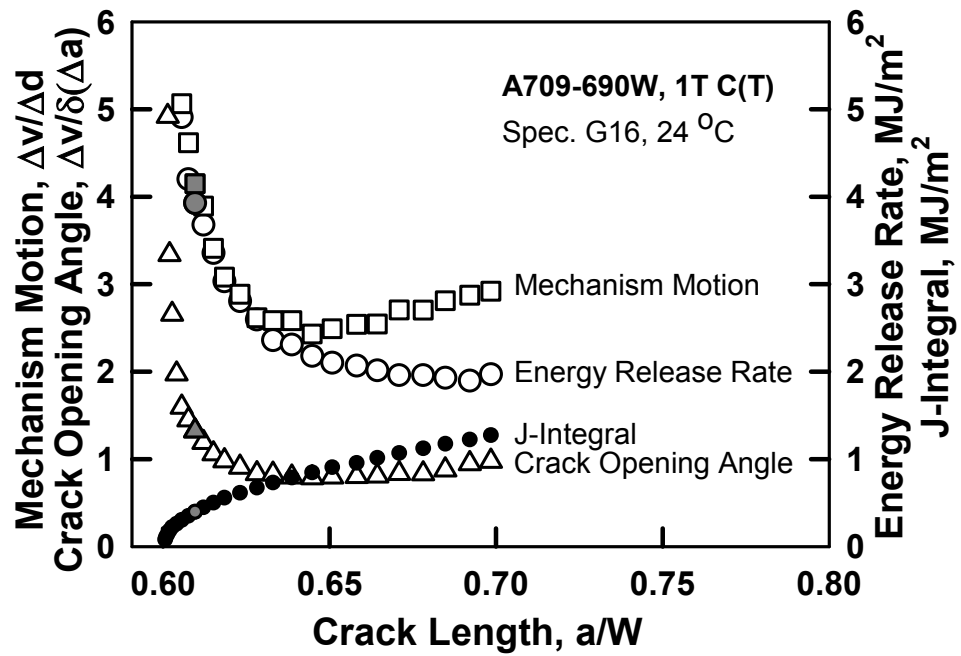


Fig. 5.11 Plastic Tearing Mechanism Motion, Crack Opening Angle, Energy Release Rate, and ASTM J-Integral vs. Crack Extension; 709-690W Cu-Ni, Specimen G16, 1T C(T), 24°C,  $a_0/W = 0.60$

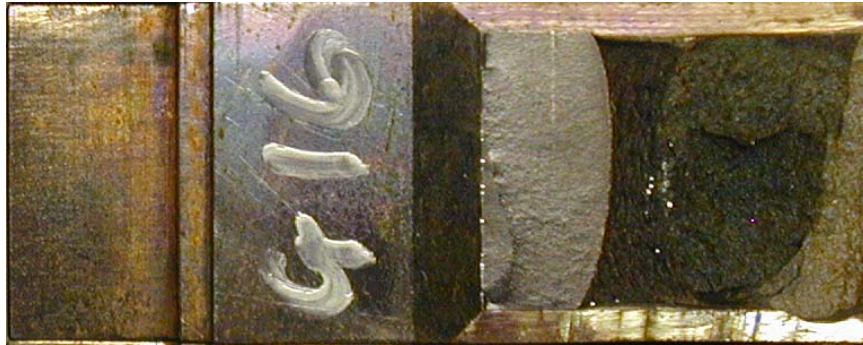


Fig. 5.12 Tunneling Effect at the Crack Front, Specimen G16

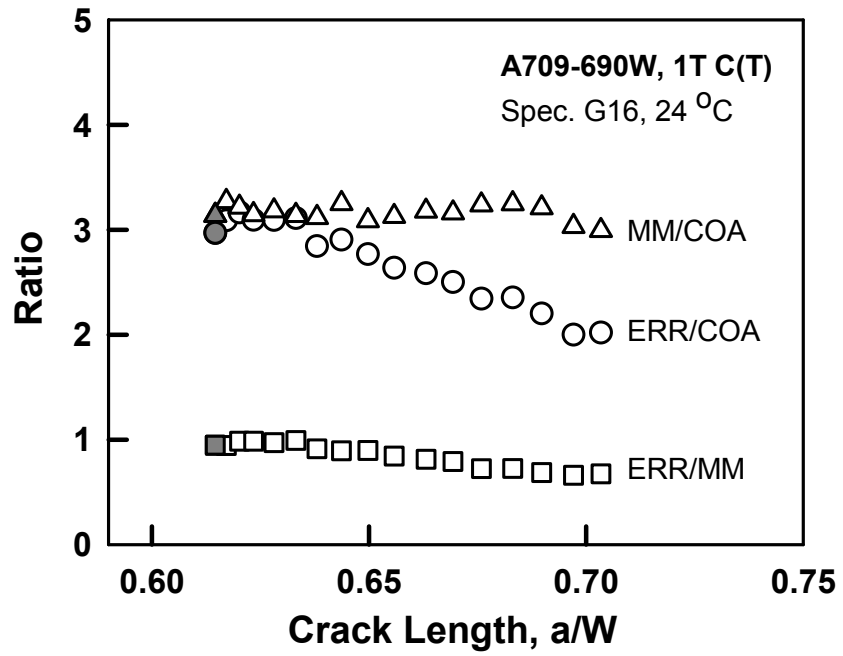


Fig. 5.13 Ratio Between Energy Release Rate, Mechanism Motion, and Crack Opening Angle; 709-690W Cu-Ni, Specimen G16, 1T C(T), 24°C,  $a_0/W = 0.60$

## **CHAPTER 6: EFFECT OF TESTING CONFIGURATIONS**

Fracture toughness tests for steels or other types of metals have to comply with the procedures and guidelines of the ASTM E1820 specification. Each testing matrix usually consists of a multi-way partial factorial design with variables that consist of specimen configurations and testing environments. Researchers determine the number and types of variables based on their experimental objectives. The analysis of this dissertation has already shown that both the energy release rate and the plastic tearing mechanism motion tend to keep constant with significant crack extension in certain testing environments. To characterize the plastic tearing in a given material, the sensitivity of a fracture resistance curve to the testing configurations must be verified. This chapter will investigate the effect of all major parameters, specifically, the initial crack length, the specimen size, the testing temperature, and the types of steel.

### **6.1 Description of Experimental Data**

All results in this chapter are interpreted directly from the standard unloading compliance load versus load-line displacement record compact tension C(T) specimens. All specimens have a total of a 20 percent side groove and a fatigue pre-crack notch. Detailed dimensions of a standard ASTM 1T (thickness = 1 inch) C(T) are shown in Fig. 3.1.

Table 6.1 lists all specimen configurations, steel designations, yield strengths, and testing temperatures. A total of eight types of steel will be analyzed: A588 grade



345 steel for bridges; A913 grade 345 and grade 450 structural steel; A709 grade 345, 485, and 690 HPS weathering steel for bridges; HY100 grade 690 steel for ships; and A533B grade 465 steel for reactor pressure vessels. The description for the structural and bridge steels can be found in section 3.3.1 in this dissertation. In addition, the following steels will be analyzed:

- HY100 (ASTM A543), *High Yield Strength, Low Carbon, Low Alloy Steel with Nickel, Molybdenum, and Chromium*
- ASTM designation A533B, *Alloy Steel, Quenched and Tempered, Manganese-Molybdenum and Manganese-Molybdenum-Nickel*

The tests of conventional structural steels (A588 and A913) and high performance steel for bridges (A709 HPS) were performed at the Structural Laboratory of the Federal Highway Administration. The data were provided by Dr. Hernando Candra and Dr. William J. Wright. The tests of naval steels (HY100 and A533B) were performed at the Naval Academy, and the data were provided by Dr. James A. Joyce.

To investigate the effect of a given testing configuration, only one parameter should be chosen as the variable for a group of specimens. For example, in the analysis, each specimen in a group has different initial crack lengths. All other parameters, however, have to remain identical including specimen size, temperature, and steel type. Two sets of specimens will be analyzed for each parameter.

## 6.2 Effect of Initial Crack Length

The effect of initial crack length on two sets of C(T) specimens is analyzed in this section.

Fig. 6.1 shows the load versus load line displacement curves for the first set of specimens. The set includes three 1T C(T) specimens that were fabricated from the same plate of A533B steel and were tested at 88° C. The specimens have initial crack lengths of  $a_0 = 0.56, 0.62$  and  $0.77W$ . Their material properties are listed in Table 6.1.

Fig. 6.2 shows the total energy release rate with extensive crack growth in these specimens. The data in this figure show that the test of one specimen from  $a_0/W = 0.56$  to  $a_0/W = 0.88$  would give the same overall energy elastic rate versus normalized crack extension ( $a/W$ ) curve as the three tests combined.

Fig. 6.3 shows the plastic tearing mechanism motion  $\Delta v/\Delta d$  defined in Chapter 5 versus  $a/W$  curves. While the three curves do reach a plateau after the initiation of crack growth, they all rise again after a certain point of crack extension. The curve of mechanism motion in the specimen with a longer initial crack length has two characteristics. First, the curve has a shorter constant value range. Second, the curve becomes higher at an earlier take-off point. These results can be explained as follows. When the tearing process is stable, the change in distance between the two plastic zones at the rear part of the specimen is linear to the increase of the displacement. After excessive crack growth, when the two plastic zones intersect each other and the

remainder of the specimen cannot take any external loading, the specimen becomes unstable if unloading does not occur. At this stage, the clip gage can still take equal pace readings because the test is displacement controlled, and the specimen is undergoing an unloading process as the crack continues to grow. So one fully plastic zone emerges in the rear part the specimen and  $\Delta d$  varies nonlinearly in a concave curve relative to  $\Delta v$ . Another observation from Fig. 6.3 is that the specimen with a longer initial crack length ( $a_0$ ) has an overall larger mechanism motion. This result is reasonable because, in this case, the initial positions of the plastic zones are closer due to the shorter remaining segment in the rear part of the specimen.

Similarly, Fig. 6.4 shows the load versus load line displacement curves for the second set of two 1T C(T) specimens. These specimens are made out of HY100 steel and were tested at 24° C (room temperature). The specimens have initial crack lengths of  $a_0 = 0.60$  and  $0.70W$ . Their material properties are listed in Table 6.1. HY100 is a high strength steel with a specified yield stress of 690 MPa (100 ksi) and with good ductility. Fig. 6.5 shows the total energy release rate versus plastic tearing in these specimens. The same conclusion that was made in Fig. 6.2 can also be made in this case: One specimen with a short initial crack length  $a_0$  would give the same energy resistance curve as multiple specimens with different  $a_0$  combined. Fig. 6.6 shows the plastic tearing mechanism motion  $\Delta v / \Delta d$  versus  $a / W$  curves. The same observations can be made for both Fig. 6.3 and Fig. 6.6. The rising part of the curve indicates that the data are not valid on energy resistance curves in the region of

excessive crack growth, specifically, when  $a/W$  is beyond the range of 0.75 to 0.80. These results will be discussed further in Chapter 7 of this dissertation.

### **6.3 Effect of Specimen Size**

Two sets of C(T) specimens are analyzed in this section to determine the effect of specimen size. The material properties of these specimens are listed in Table 6.1.

Fig. 6.7 shows the load versus load line displacement curves for the first set of the two C(T) specimens. These specimens have an initial crack length of  $0.60W$ , are fabricated from A588 steel, and were tested at room temperature. The specimens have two different sizes of 1/2T and 1T. Fig. 6.8 and Fig 6.9 show the crack extension resistance curves of total energy release rate and the plastic tearing mechanism motion, respectively.

Fig. 6.10 shows the load versus load line displacement curves for the second set of two C(T) specimens. These specimens have an initial crack length of  $0.60W$ , are fabricated from A913-345 steel, and were tested at room temperature. The specimens have two different sizes of 1/2T and 1T. Fig. 6.11 and Fig 6.12 show the crack extension resistance curves of the total energy release rate and the plastic tearing mechanism motion, respectively.

Both Fig. 6.8 and Fig. 6.11 show that the larger specimen (1T) has a higher energy release rate than the smaller specimen (1/2T) at the same point of crack extension  $a/W$ . The energy release rate is the total energy normalized by the newly

created crack face. Therefore, one can expect that the specimen size would not be a factor in this case as long as the ligament of the rear part of the specimen remains proportional. This is true only when the specimens being compared are thick or thin enough to approach the pure plane-strain or plane-stress condition. This condition is not part of the normal scope of fracture toughness tests. All the dimensions remain proportional for the specimen thickness from  $1/2T$  to  $1T$ . However, as the thickness increases, the plane-strain portion of the crack front that is located away from the side grooves increases relative to the plane-stress portions of the crack front close to the side grooves. A higher tri-axial state of stress in the plane-strain region elevates the material strength, and thus, the load applied. For both A588 and A913 steels, the load in  $1T$  specimen is three times higher, while the energy release rate is only 30 percent higher than for the  $1/2T$ . Therefore, it is reasonable to predict that the variance due to the specimen size would be less significant in the  $2T$ ,  $4T$ , and other thicker specimens.

Both Fig. 6.9 and Fig. 6.12 show that the larger specimen also has a higher curve for the tearing mechanism motion. This result is expected because the initial plastic zones are closer in the smaller specimen. Unlike the specimen dimensions, the term  $\Delta v$  is not normalized for the difference in specimen thickness.

## 6.4 Effect of Testing Temperature

Two sets of C(T) specimens are analyzed in this section for the effect of testing temperature. The material properties of these specimens are listed in Table 6.1.

Fig. 6.13 shows the load versus load line displacement curves for the first set of three 1T C(T) specimens. These specimens have an initial crack length  $0.50W$  and are fabricated from A913-345 steel. The specimens were tested at  $-20^{\circ}\text{C}$ ,  $0^{\circ}\text{C}$ , and  $24^{\circ}\text{C}$ . Fig. 6.14 and Fig 6.15 show the crack extension resistance curves of the total energy release rate and the plastic tearing mechanism motion, respectively.

Fig. 6.16 shows the load versus load line displacement curves for the second set of three 2T C(T) specimens. These specimens have an initial crack length  $0.50W$  and are fabricated from A709-345W high performance steel. The specimens were tested at  $-34^{\circ}\text{C}$ ,  $0^{\circ}\text{C}$ , and  $24^{\circ}\text{C}$ . Fig. 6.17 and Fig 6.18 show the crack extension resistance curves of the total energy release rate and the plastic tearing mechanism motion, respectively.

Clearly, the testing temperature does not affect the energy release rate or the tearing mechanism motion resistance curve, at least for the mild range of  $-20^{\circ}\text{C}$  to room temperature. The strength of the steels may increase to a certain degree with the drop in temperature, which can be concluded from the load versus displacement curve. The decrease in temperature, however, is not significant enough to change the rate of energy to create the crack growth. Investigating the fracture toughness transition point for the variation of temperature change is worthwhile for construction

materials that will be exposed to extreme environments, such as a reactor pressure vessel.

## **6.5 Effect of Steel Type**

Two sets of C(T) specimens are analyzed in this section for the effect of steel type. The material properties of these specimens are listed in Table 6.1.

Fig. 6.19 shows the load versus load line displacement curves for the first set of three 1T C(T) specimens. These specimens have an initial crack length of  $0.60W$  and were tested at room temperature. The specimens were fabricated from conventional structural steels A913-345, A913-450, and A588. Fig. 6.20 and Fig 6.21 show the crack extension resistance curves of the total energy release rate and the plastic tearing mechanism motion, respectively.

Fig. 6.22 shows the load versus load line displacement curves for the second set of two 1T C(T) specimens. These specimens have an initial crack length of  $0.60W$  and were tested at room temperature. The specimens were fabricated from high performance structural steels A709-485W and A709-690W Cu-Ni. Fig. 6.23 and Fig 6.24 show the crack extension resistance curves of the total energy release rate and the plastic tearing mechanism motion, respectively.

Although specimens C16 and B16 have the same specified grade (345MPa), Fig. 6.20 shows that specimen C16, which is made out of A913 steel, has about a 50 percent higher energy release rate resistance curve than specimen B16, which is made

out of A588 steel. The original unloading compliance load versus load line displacement curve in Fig. 6.19 also shows that B16 has a much lower loading level. Meanwhile, specimens C16 and D17, which are made out of the same category of steel but with different grades, have identical resistance curves. This result indicates that the material strength is not the controlling factor when we investigate the effect of steel type on plastic tearing. In the author's opinion, the re-arrangement in the atomic structure level when the crack front grows plays a more important role in determining the toughness in plastic tearing. The modified chemical composition and the quenching process can greatly change the performance in the level of crystal structure and its interfacial and volumetric defects (Meyers and Chawla 1999). Although this topic is beyond the scope of this dissertation, there has been recent interest in the stochastic computational mechanics field for modeling the fracture problem at a microstructure level using the finite element method (Shi 2004).

Fig. 6.23 also shows that even though the specified yield strength of specimen G16 (fabricated from A709-690W Cu-Ni) is more than 40 percent higher than specimen E17 (fabricated from A709-485W,) its energy release rate curve is 10 percent lower. Unlike the comparison of specimen C16 and B16, specimen G16 has a higher external loading level than specimen E17.

Fig. 6.22 and Fig. 6.24 show that when the type of steel is the only variable, the plastic tearing mechanism motion curves keep an identical relative level with the responding energy release rate resistance curves.



Table 6.1 List of Specimens for Effect of Testing Configurations

Specimen ID	Steel Designation	Specimen Size	Nominal Yield Strength $\sigma_y$ (MPa)	Initial Crack Length $a_0/W$	Testing Temperature (°C)
<b>Effect of Initial Crack Length</b>					
JB4	A533B	1T	465	0.56	88
E3	A533B	1T	465	0.62	88
13A	A533B	1T	465	0.77	88
FYO-N10	HY100	1T	690	0.60	24
FYO-N4	HY100	1T	690	0.70	24
<b>Effect of Specimen Size</b>					
B1	A588	1/2 T	345	0.60	24
B16	A588	1T	345	0.60	24
C1	A913-345	1/2 T	345	0.60	24
C16	A913-345	1T	345	0.60	24
<b>Effect of Testing Temperature</b>					
C11	A913-345	1T	345	0.50	-20
C13	A913-345	1T	345	0.50	0
C15	A913-345	1T	345	0.50	24
H33	A709-345W	2T	345	0.50	-34
H35	A709-345W	2T	345	0.50	0
H36	A709-345W	2T	345	0.50	24
<b>Effect of Steel Type</b>					
C16	A913-345	1T	345	0.60	24
D17	A913-450	1T	450	0.60	24
B16	A588	1T	345	0.60	24
E17	A709-485W	1T	485	0.60	24
G16	A709-690W Cu-Ni	1T	690	0.60	24

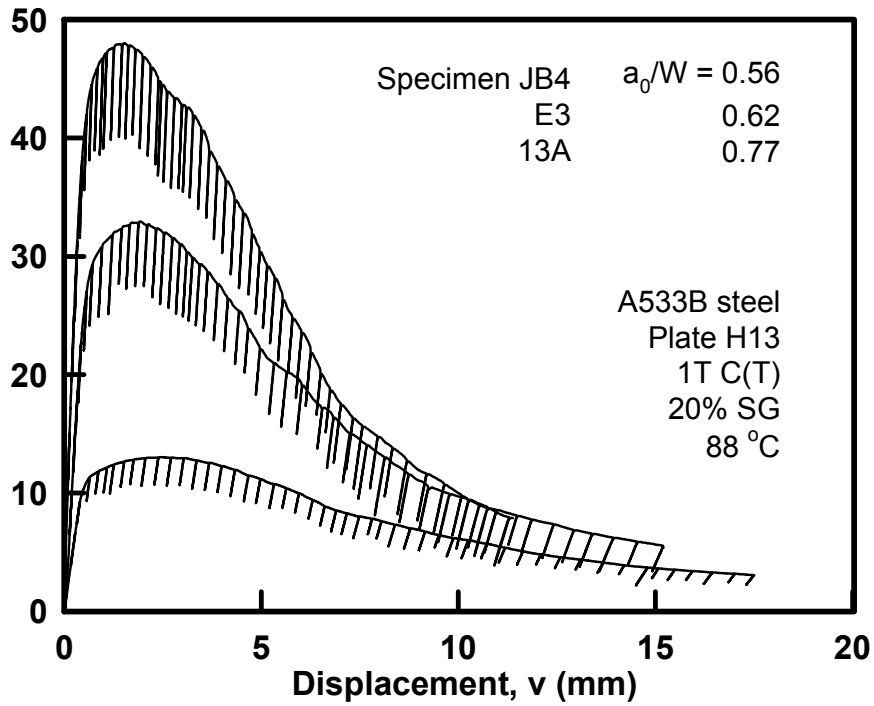


Fig. 6.1 Unloading Compliance Load versus Load-line Displacement for C(T) Specimens JB4, E3, and 13A

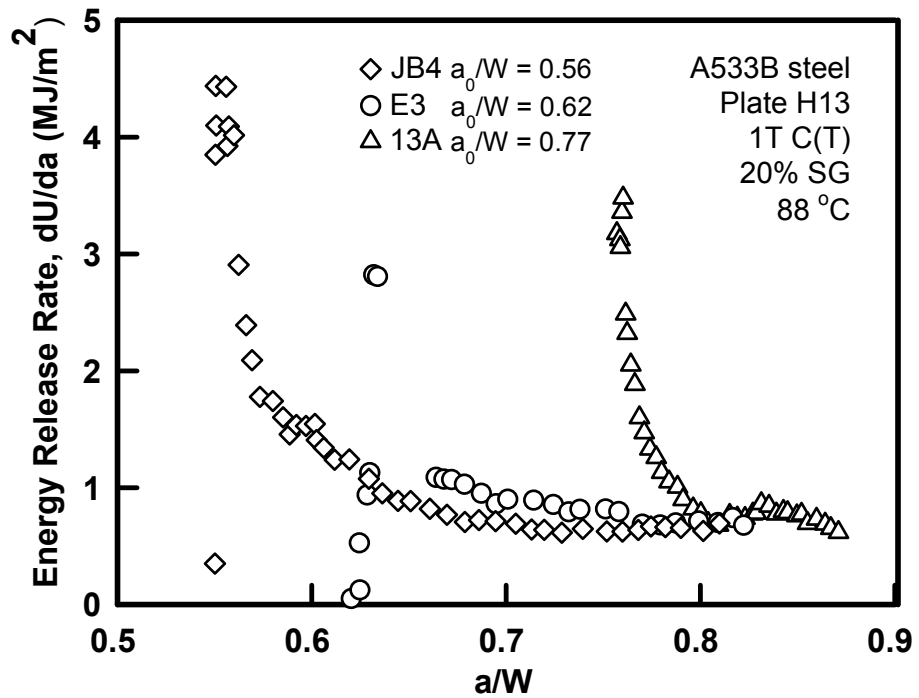


Fig. 6.2 Effect of Initial Crack Length on Total Energy Release Rate in C(T) Specimens of A533B Steel

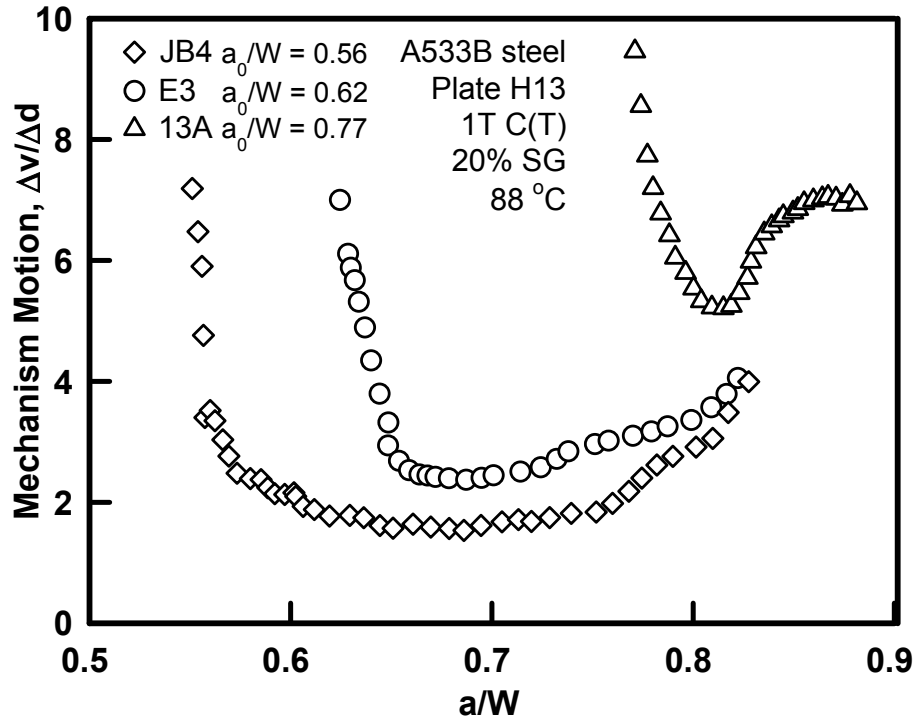


Fig. 6.3 Effect of Initial Crack Length on Plastic Tearing Mechanism Motion in C(T) Specimens of A533B Steel

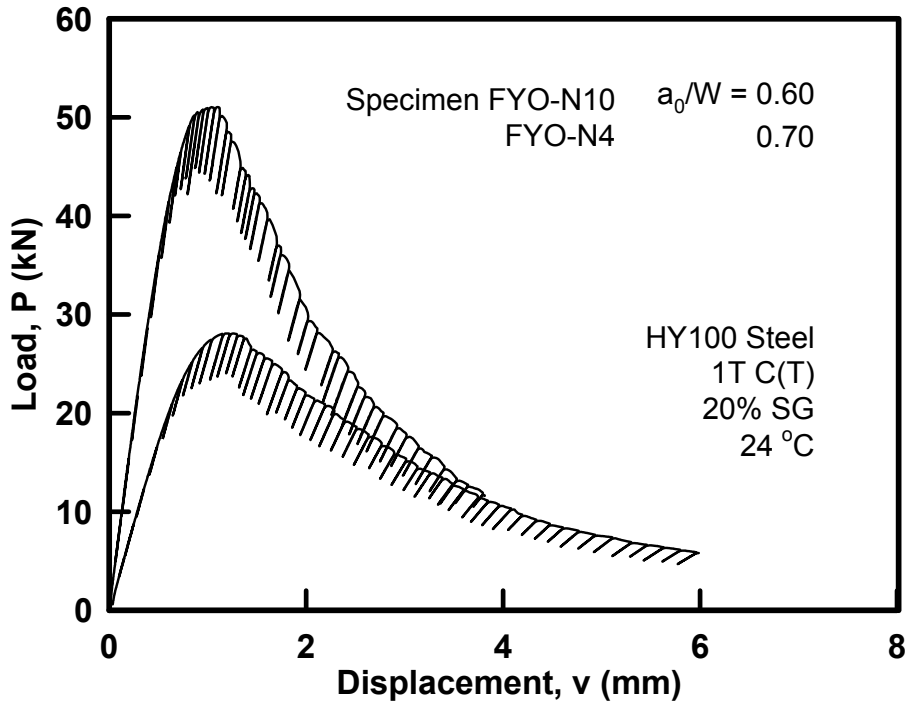


Fig. 6.4 Unloading Compliance Load versus Load-line Displacement for C(T) Specimens FYO-N10 and FYO-N4

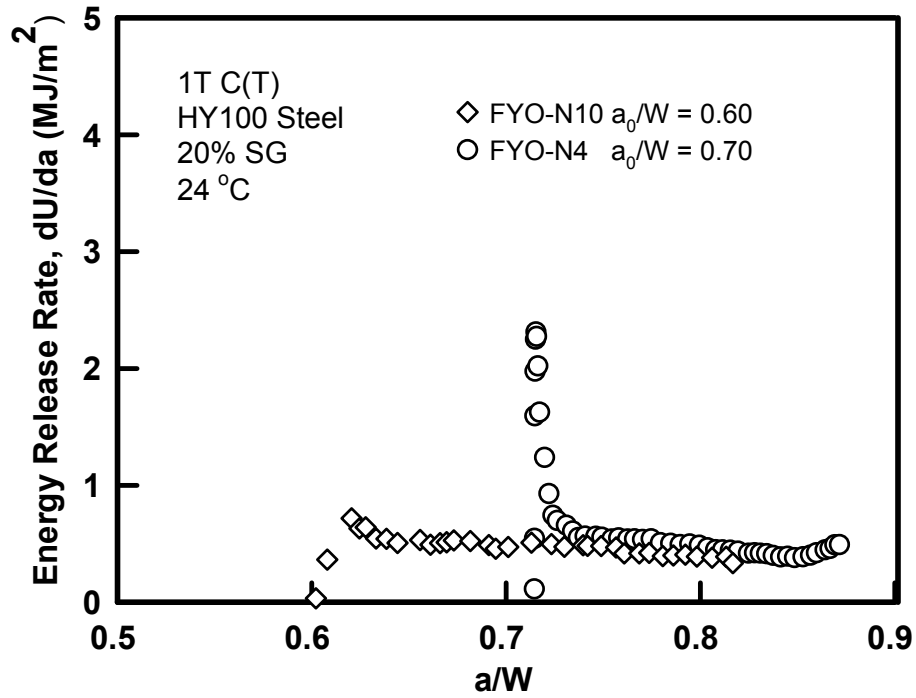


Fig. 6.5 Effect of Initial Crack Length on Total Energy Release Rate in C(T) Specimens of HY100 Steel

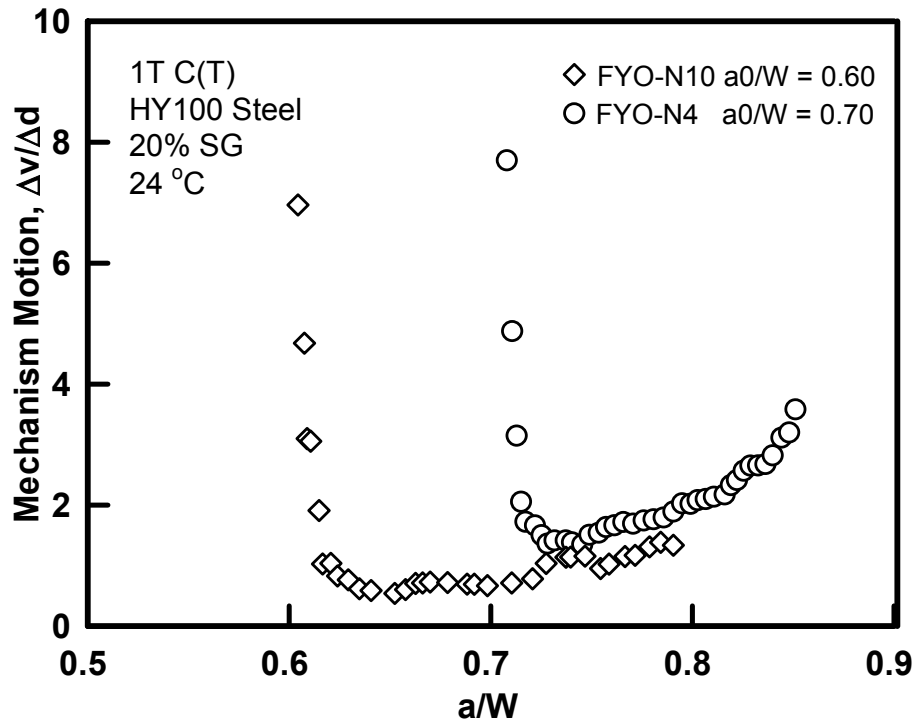


Fig. 6.6 Effect of Initial Crack Length on Plastic Tearing Mechanism Motion in C(T) Specimens of HY100 Steel

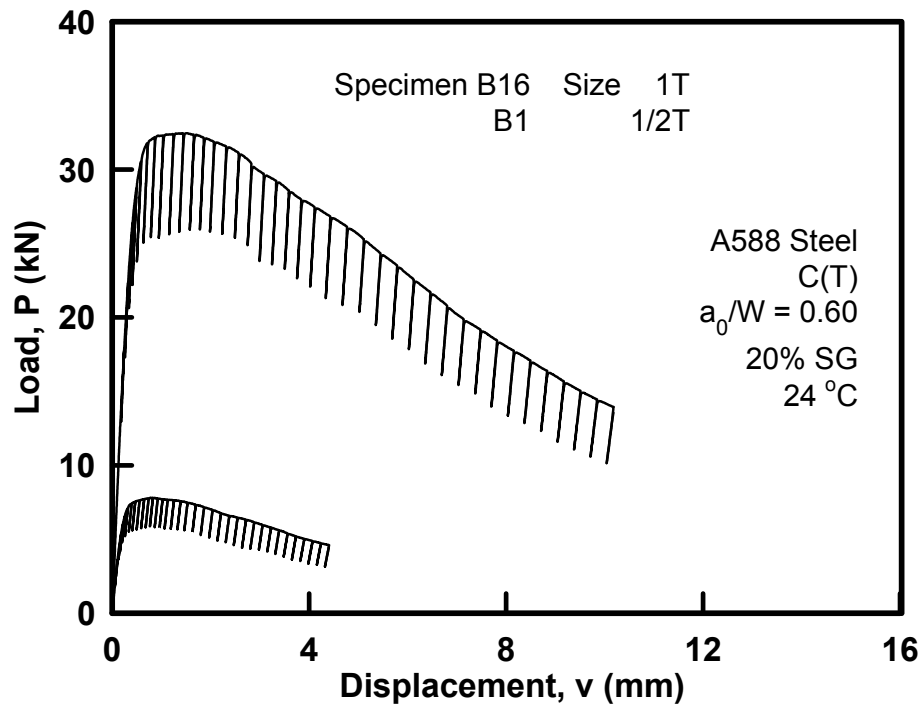


Fig. 6.7 Unloading Compliance Load versus Load-line Displacement for C(T) Specimens B1 and B16

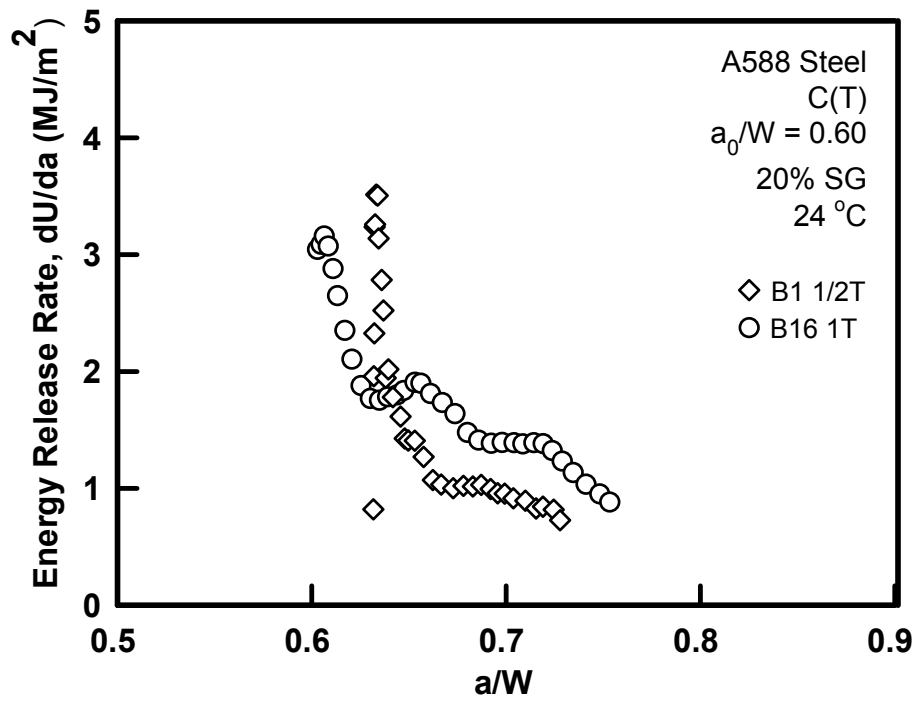


Fig. 6.8 Effect of Specimen Size on Total Energy Release Rate in C(T) Specimens of A588 Steel

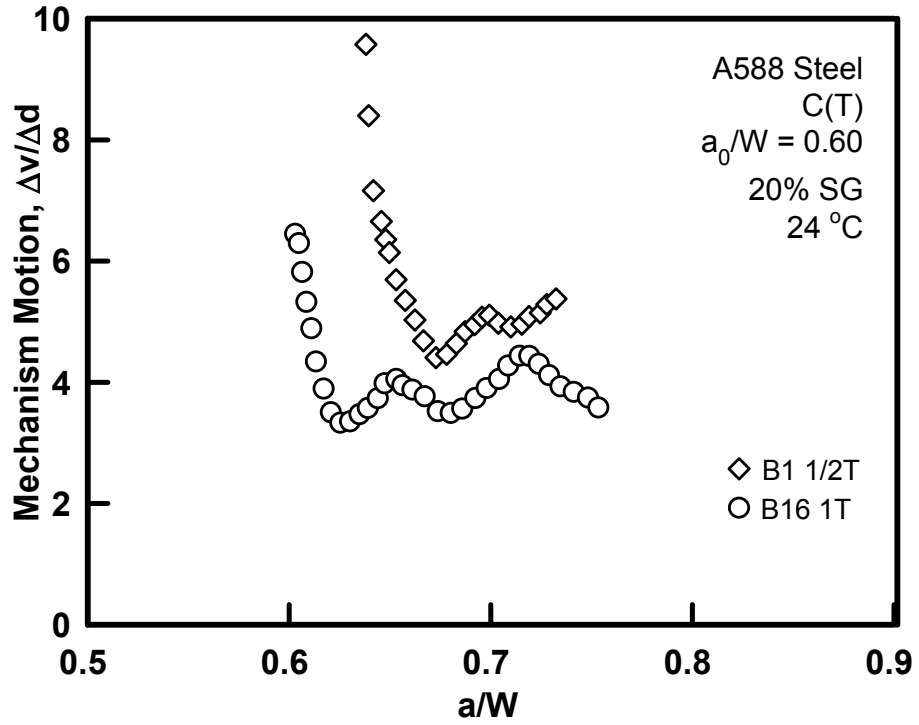


Fig. 6.9 Effect of Specimen Size on Plastic Tearing Mechanism Motion in C(T) Specimens of A588 Steel

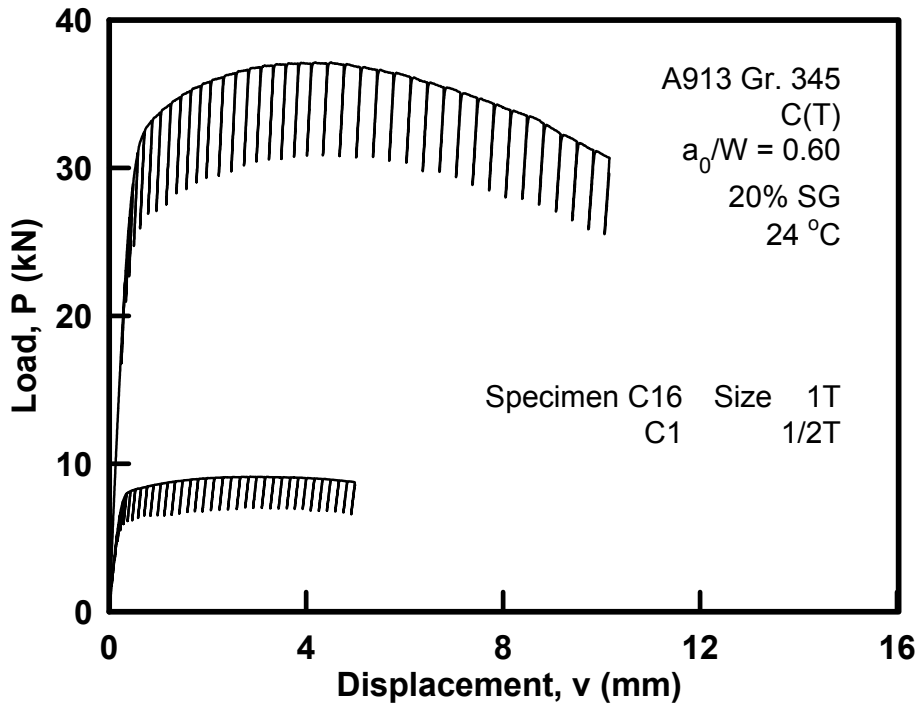


Fig. 6.10 Unloading Compliance Load versus Load-line Displacement for C(T) Specimens C1 and C16

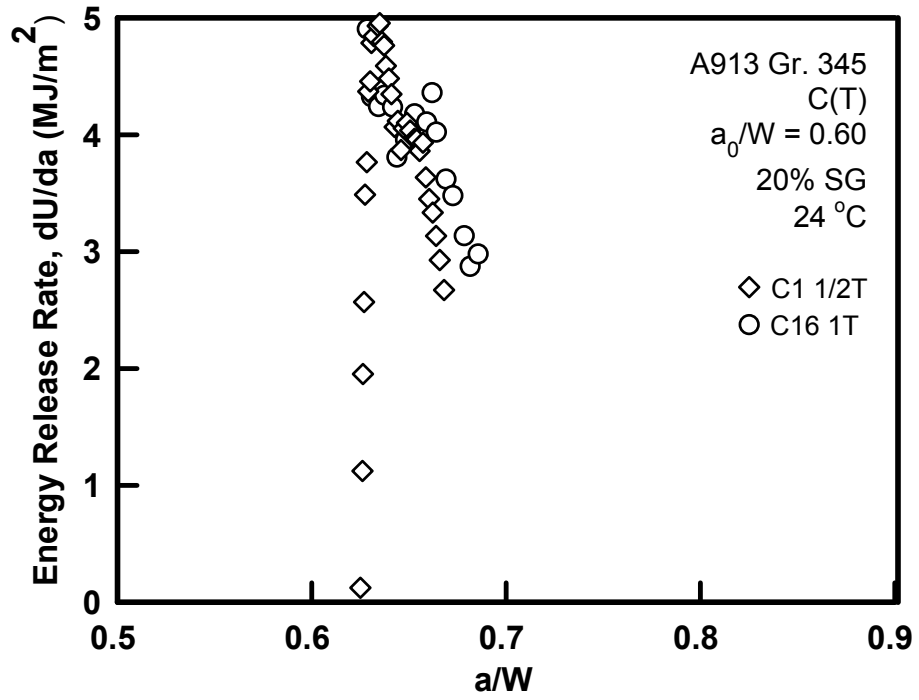


Fig. 6.11 Effect of Specimen Size on Total Energy Release Rate in C(T) Specimens of A913-345 Steel

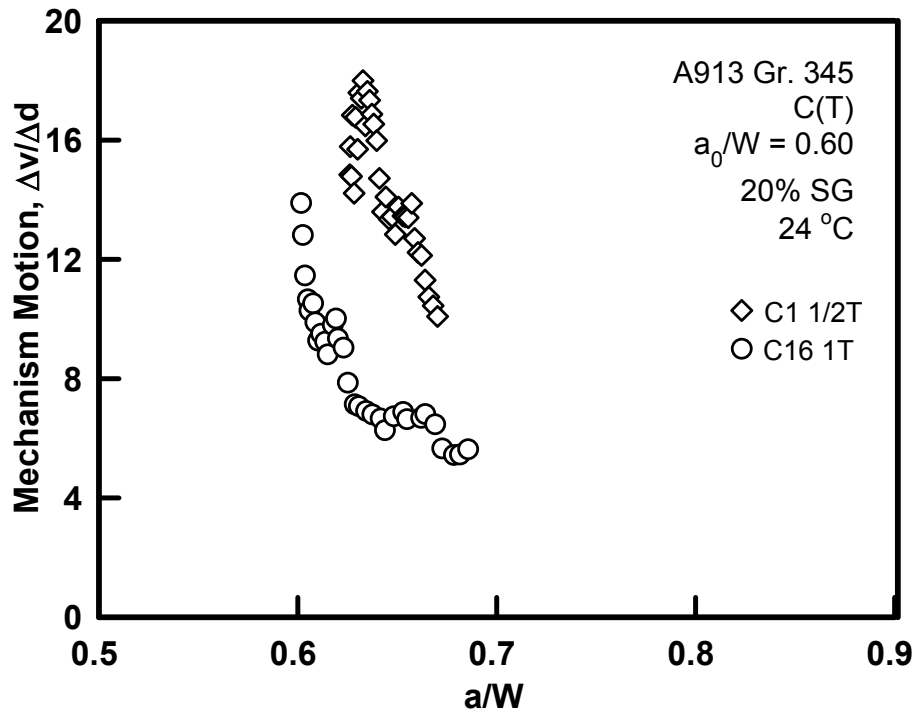


Fig. 6.12 Effect of Specimen Size on Plastic Tearing Mechanism Motion in C(T) Specimens of A913-345 Steel

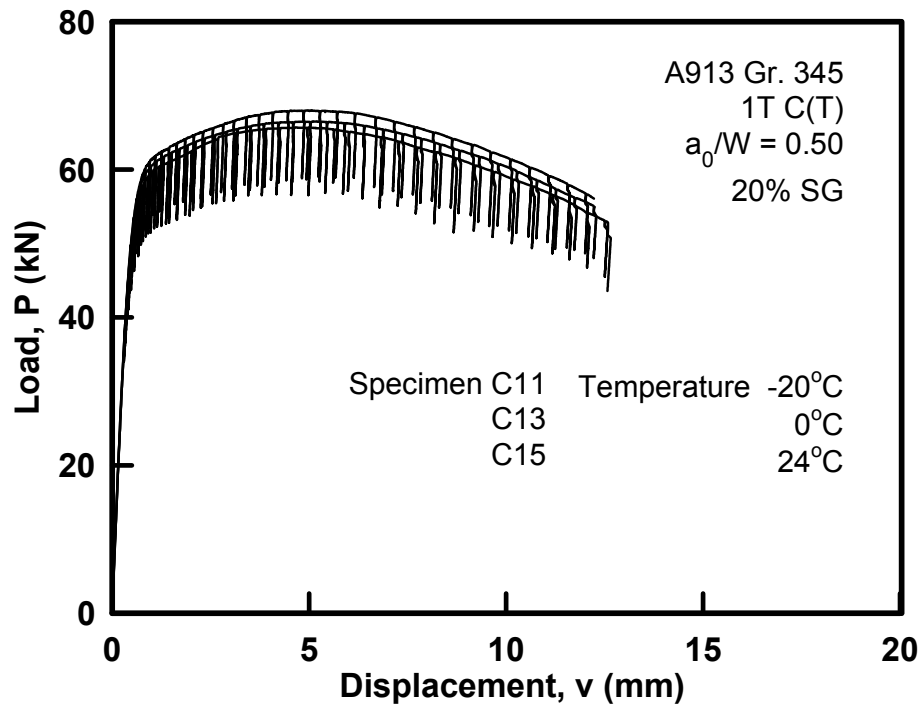


Fig. 6.13 Unloading Compliance Load versus Load-line Displacement for C(T) Specimens C11, C13 and C15

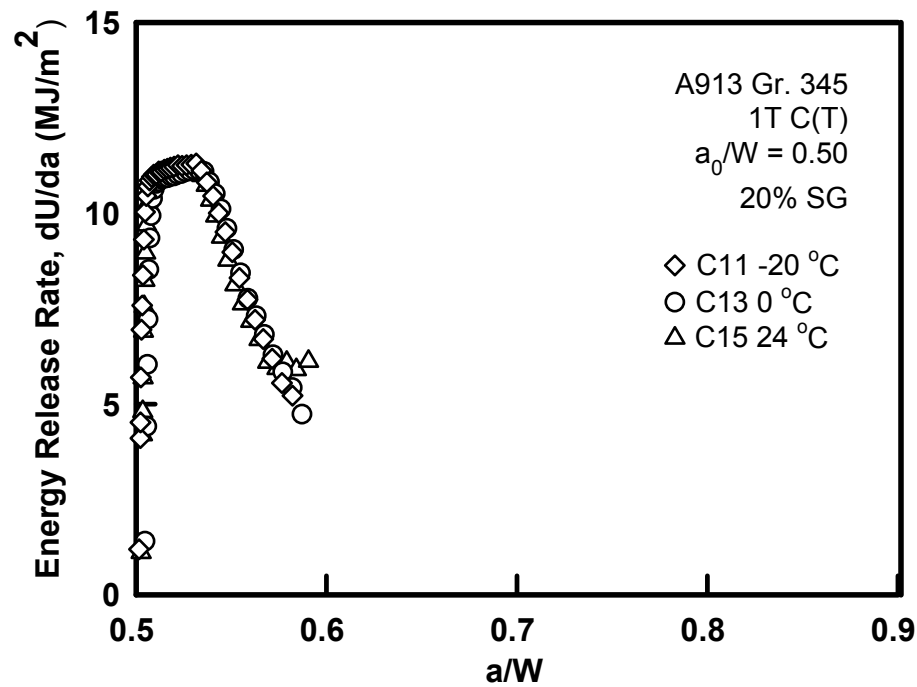


Fig. 6.14 Effect of Testing Temperature on Total Energy Release Rate in C(T) Specimens of A913-345 Steel



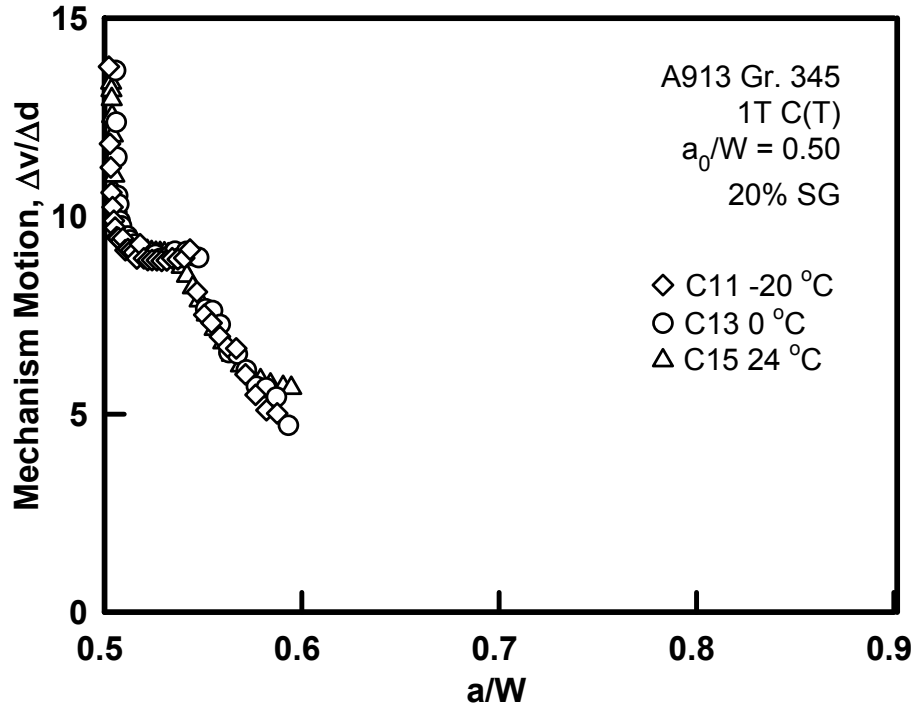


Fig. 6.15 Effect of Testing Temperature on Plastic Tearing Mechanism Motion in C(T) Specimens of A913-345 Steel

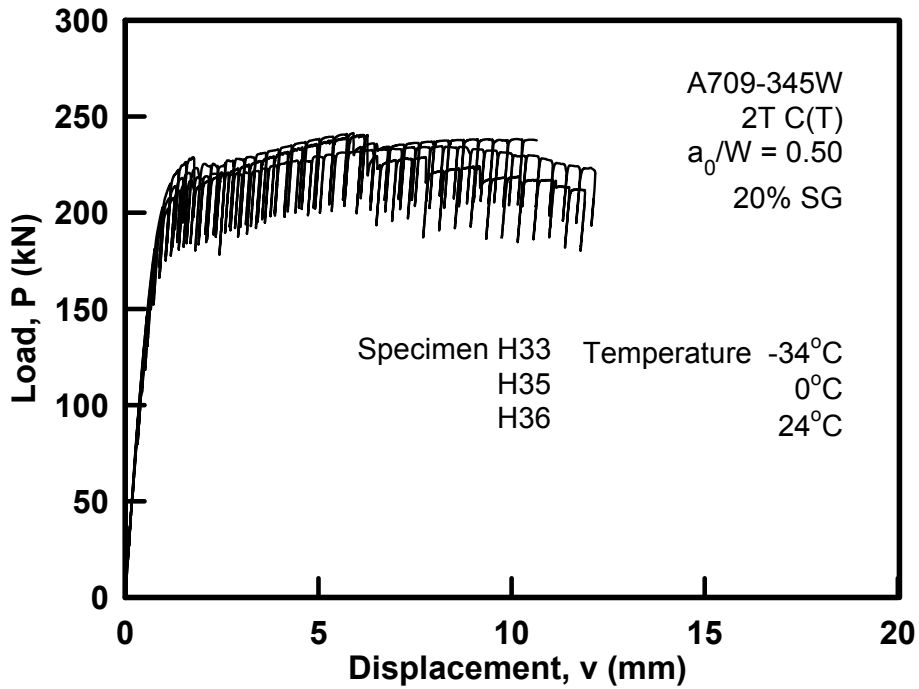


Fig. 6.16 Unloading Compliance Load versus Load-line Displacement for C(T) Specimens H33, H35 and H36

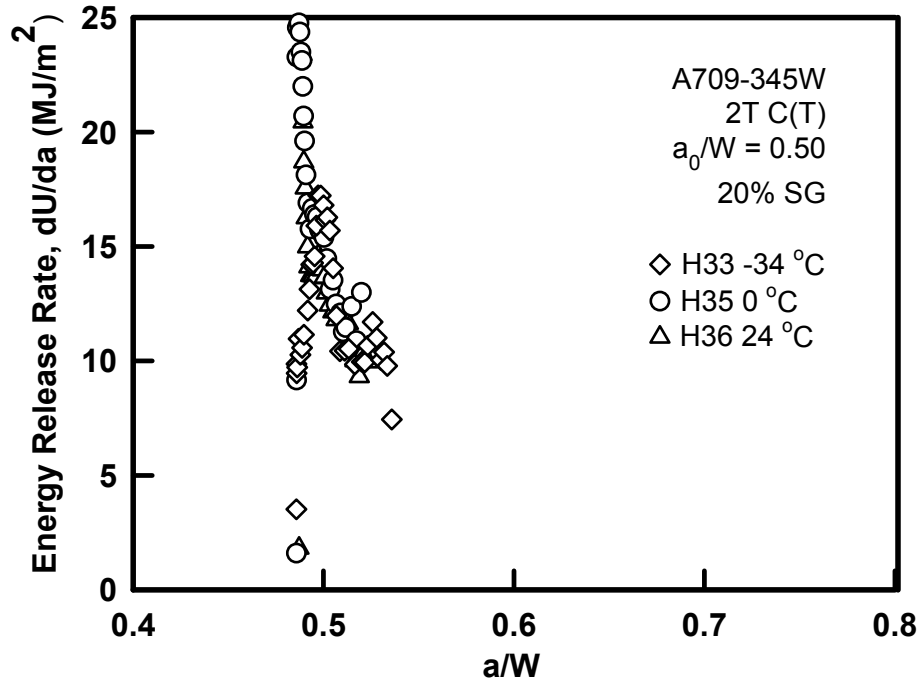


Fig. 6.17 Effect of Testing Temperature on Total Energy Release Rate in C(T) Specimens of A709-345W HPS

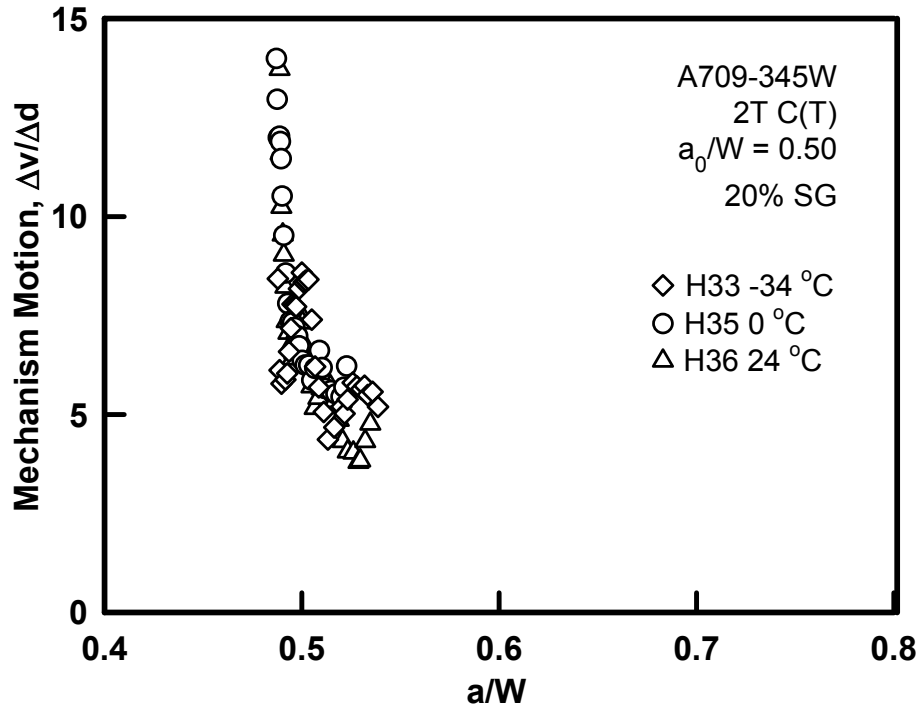


Fig. 6.18 Effect of Testing Temperature on Plastic Tearing Mechanism Motion in C(T) Specimens of A709-345W

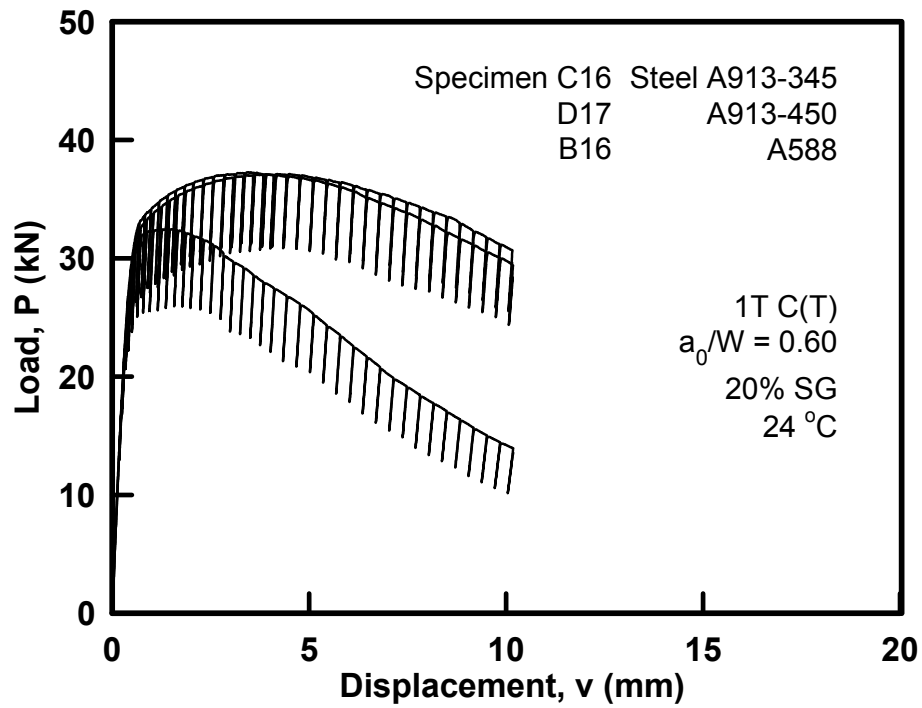


Fig. 6.19 Unloading Compliance Load versus Load-line Displacement for C(T) Specimens C16, D17 and B16

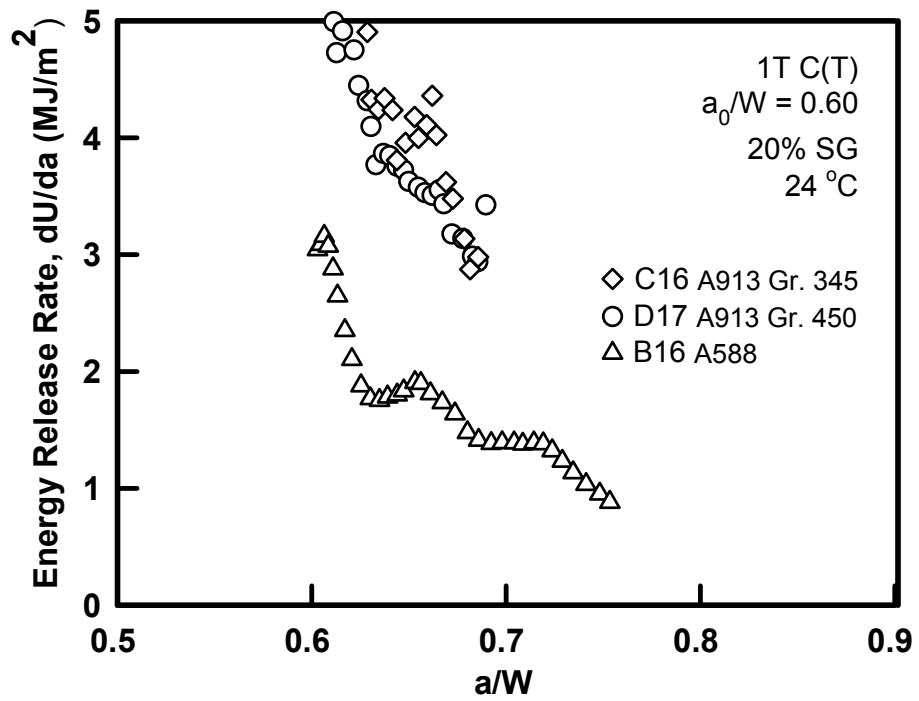


Fig. 6.20 Effect of Steel Type on Total Energy Release Rate in C(T) Specimens of 3 Conventional Steels

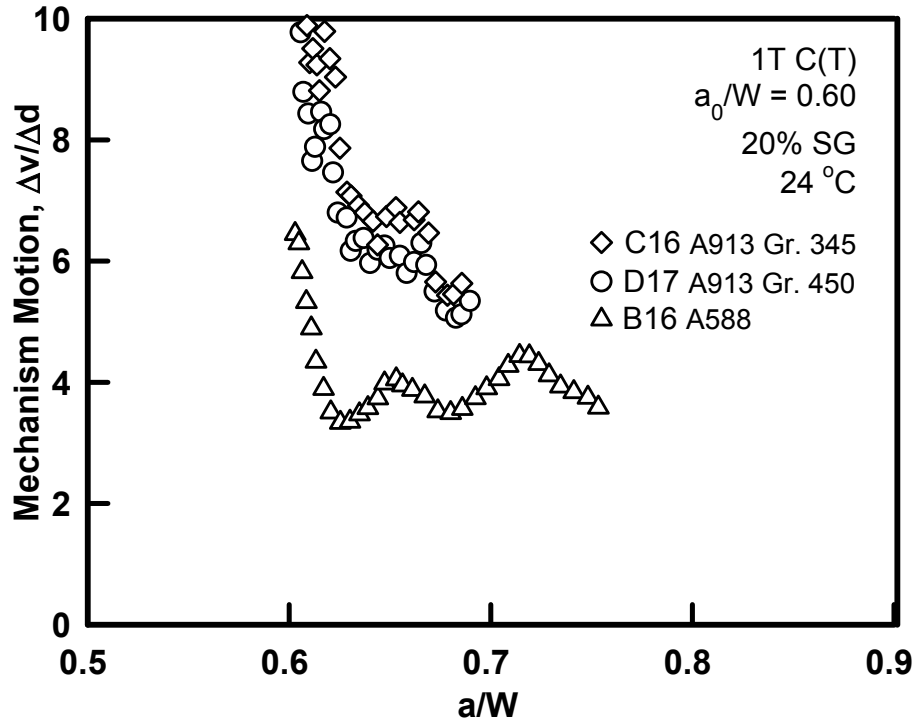


Fig. 6.21 Effect of Steel Type on Plastic Tearing Mechanism Motion in C(T) Specimens of 3 Conventional Steels

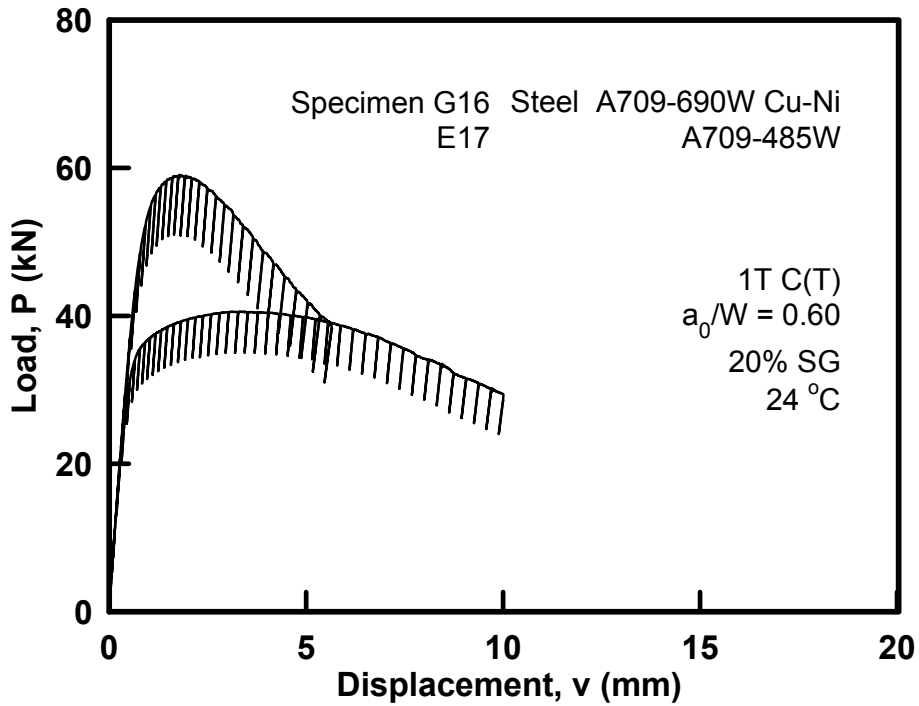


Fig. 6.22 Unloading Compliance Load versus Load-line Displacement for C(T) Specimens G16 and E17

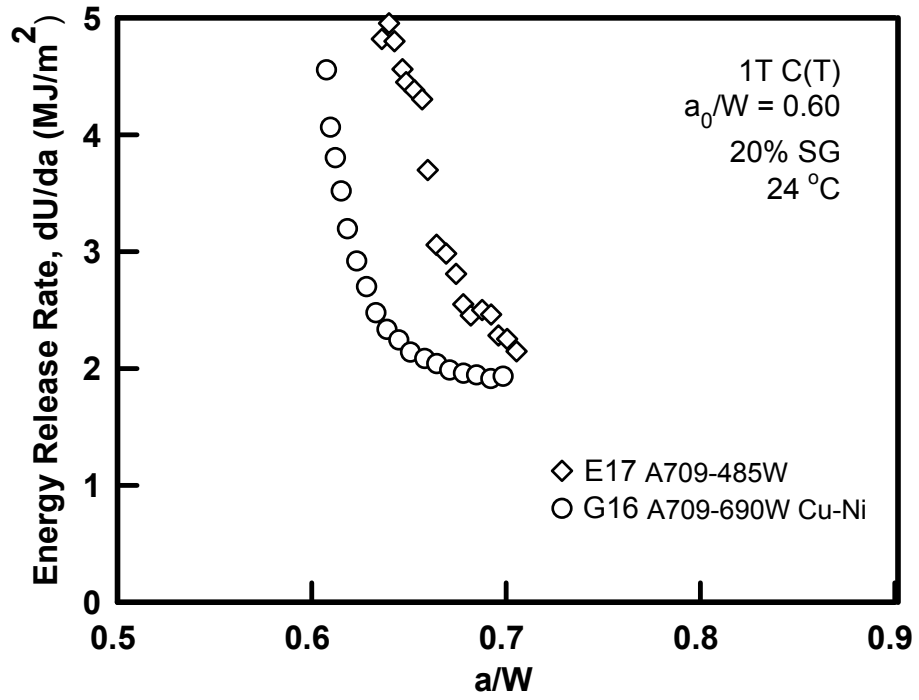


Fig. 6.23 Effect of Steel Type on Total Energy Release Rate in C(T) Specimens of 2 HPS Steels

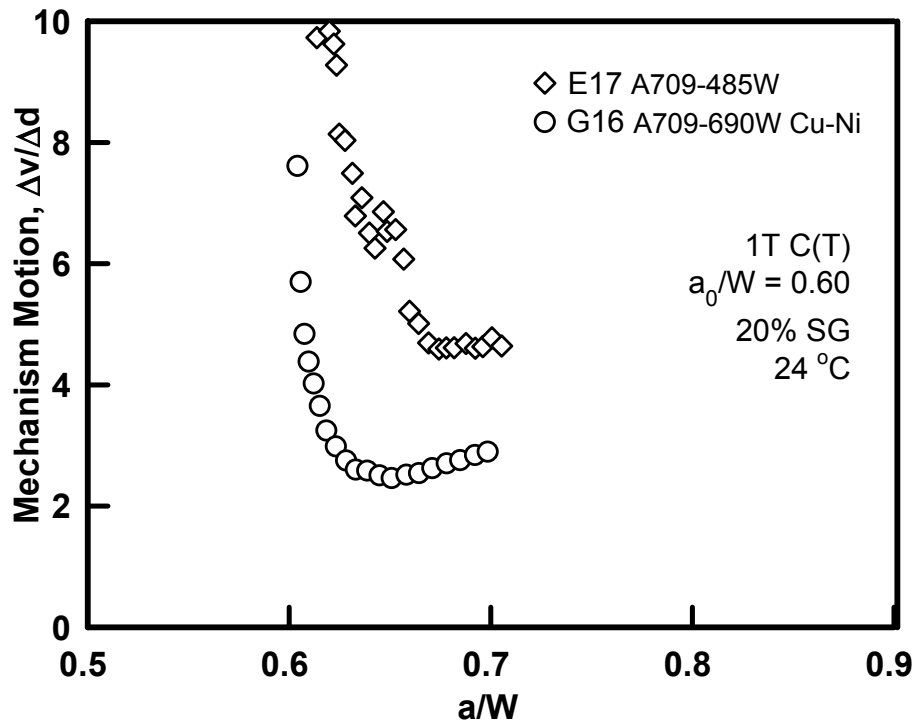


Fig. 6.24 Effect of Steel Type on Plastic Tearing Mechanism Motion in C(T) Specimens of 2 HPS Steels

## CHAPTER 7: DISCUSSIONS AND CONCLUSIONS

The conclusions from the parametric study are that during stable plastic tearing in tough steels the energy release rate is not affected by the initial crack length and is insensitive to a mild range of temperature change. Meanwhile, the plane-strain or plane-stress status in a specimen or in a structural element in application contributes to its rate of dissipation. These facts show that the energy release rate resistance curve is a material property in the fully plastic region of fracture mechanics. Before stating that the energy release rate versus crack extension curve is the right resistance curve to replace the  $J$ - $R$  curve, the valid test data range for the energy release rate must be verified. In Chapter 6, the effect of the initial crack length on the plastic tearing mechanism was analyzed. This analysis shows that after a certain point of long crack extension in very ductile steels such as A533B and HY100, the external loading makes the remaining ligament in the specimen unstable. Therefore, the energy release rate obtained is invalid beyond that point.

The steel type, not the yield strength, controls the performance of plastic tearing in a given degree of tri-axial stress status. Therefore, using a computer simulation to replace the real laboratory testing is impractical because in the finite element modeling of a C(T) specimen test, the stress-strain curve is the only representative input of material properties for a certain type of steel. On the other hand, if the test data are ready and the model can match the original load-displacement curve, the finite element analysis is helpful for investigating the tri-axial status in the macro level because it cannot be observed directly from the experimental data.

The purpose of the discussions in this chapter is to verify the valid data range of the energy release rate resistance curve and to discuss the 3-D finite element modeling by non-singularity elements.

## **7.1 Validation of Test Data Range**

### **7.1.1 Load Drop Between Load-Displacement Curve and CR Curve**

The application of the compliance ratio (CR) method to construct the CR curve (Candra et al. 2002) has been illustrated in Section 3.2 and in Fig. 3.6 and Fig. 3.7. The CR curve is the load-displacement curve provided that crack growth does not exist. By this definition, the load drop between the CR curve and the original load-displacement curve at a given displacement represents the assumed virtual load to reverse the crack extension as if the crack face up to this point is “healed.” This load drop can be defined by

$$\Delta P_i = P_i^* - P_i \quad (7.1)$$

and computed from Fig. 3.7.

Fig. 7.1 through Fig. 7.3 show the load drop versus crack extension curve of A533B steel specimens JB4, E3, and 13A respectively. The material properties of these specimens are listed in Table 6.1, and the energy release rate has been computed in Section 6.2. The load drop in all three specimens starts off linearly following the straight dashed line shown in the figures after the crack initiation but then becomes nonlinear after a certain point of crack extension. Each data point on

the linear part of the curve indicates that the specimen would need the same amount of reversal load to heal a unit area of crack face up to this point of crack length. The data point on the nonlinear part of the curve implies that the specimen would need less of a load to reverse the crack extension. Therefore, the assumed uncracked specimen would have been in a yielding or failing condition at the corresponding displacement. To investigate this transition, it is necessary to accurately locate the deviation point from the linear region to the nonlinear region on the load drop versus crack extension curve.

### 7.1.2 Application of SED Method to the Deviation Point Determination

Lenwari et al. (2004) proposed the strain energy density (SED) method to accurately determine the yield point of stress-strain curves for adhesives and other materials. As shown in Fig. 7.4, on a typical stress-strain curve, the increment of SED  $\Delta u$  can be written as the increment of the triangle area

$$\Delta u = \frac{1}{2} \Delta \sigma \cdot \Delta \varepsilon = \frac{1}{2} (\sigma_{i+1} - \sigma_i) (\varepsilon_{i+1} - \varepsilon_i) \quad (7.2)$$

where  $\Delta \sigma$  = stress increment and  $\Delta \varepsilon$  = strain increment. The material is observed to behave elastically for as long as  $\Delta u$  is linear and inelastically when  $\Delta u$  deviates from a linear trend. The yield strength is taken as the stress at the point where the value of the SED increment deviates from a linear trend, as shown in Fig. 7.5.

This method has been adopted to determine the first deviation point of the load drop curve shown in Fig. 7.1 through Fig. 7.3. The determination process consists of



the following steps. First, for each specimen, the area of the incremental triangle at each crack extension point is calculated by replacing  $\Delta\sigma$  and  $\Delta\varepsilon$  with  $\Delta P$  and  $\Delta(a/W)$ . Second, a fitting straight line is drawn through the first 20 data points in the elastic region. Third, the standard deviation is calculated. Fourth, the lower and upper confidence limits are drawn at three standard deviations from the mean line, as shown in Fig. 7.6. Finally, the first data point to fall outside of the upper or lower bound is chosen as the deviation point. Fig. 7.6 through Fig. 7.8 show that the transition happens at  $a/W = 0.685$ ,  $0.700$ , and  $0.822$  for specimens JB4, E3, 13A, respectively.

### 7.1.3 Valid Data Range for Energy Release Rate Resistance Curve

Fig. 7.9 through 7.11 replot the curves of the plastic tearing mechanism motion and the energy release rate versus crack extension of the three A533B specimens JB4, E3, and 13A. The data points are marked in gray shade where the load drop becomes nonlinear. In each of the three specimens, the transition of the load drop is located almost perfectly at the point where the curve starts climbing again. This result shows that the plastic tearing mechanism successfully predicts the unstable manner of the specimen from the geometric side. In addition, the valid data range for the energy release rate resistance curve can be verified. So the data range beyond those crack length points could be misleading (i.e.,  $a/W$  could be greater than  $0.685$ ,  $0.700$ , and  $0.822$  respectively, as shown in Fig. 7.9 through Fig. 7.11). Note that even though the energy rate level will not be affected, the toughness of the material is not as strong as it appears in these curves. It should be noted that not all specimens have the deviation

point of load drop. For example, 1/2T specimens B1 and C1 have a very limited crack extension; therefore, the data are valid for the full range.

This data validation is conservative in practice because the limit of  $\pm 3$  times the standard deviation is pretty comfortable in the author's opinion. At least five or more data points can be fitted to the linear regression after the first deviation point, as shown in Fig. 7.6 through Fig. 7.8. In this case, the valid data range of the energy release rate will be expanded to the additional crack length of approximately  $0.1W$ .

## **7.2 Discussions on Finite Element Modeling**

In the field of fracture mechanics, most of the research in computer analysis done today is limited to the finite element modeling in 2-D by singularity elements. The most commonly used quarter-point element or special crack tip elements are derived by the same assumption of the stress singularity at the crack tip. This assumption is incorrect because an infinite stress status does not exist in nature. Chen et al. (2002) proposed a new modeling technique, the Meshless Method, which shows that there is no singularity at the crack tip. The maximum principal stress in tri-axial stress status from their analysis was about three times the yield stress and was located ahead of the crack front (Chen et al. 2002).

### **7.2.1 ABAQUS Model by Non-Singularity Element**

The commercial finite element software ABAQUS version 6.4 (HK&S 2003) was used in this research to model the compact tension specimen for the fracture

toughness test. By taking advantage of its double symmetric geometry and by using 8-node brick elements, as shown in Fig. 7.12, a typical 25.4 mm (1T) thickness specimen model with a 1 mm element size in the crack front can have about 8,000 nodes/elements. The nodes at the top of the XY plane are fully fixed and the nodes at the bottom of the XZ plane are fixed up to the initial crack length and can be released during the computer run to simulate the advances of crack front.

A parametric study has been performed by load control with different minimum element sizes close to the crack tip. The program was running on a SGI Octane II workstation with a dual CPU at 400MHz. The stress/strain contour was found to be insensitive when the smallest size was less than 0.35 mm with the use of an 8-node element. A summary of this study is listed in Table 7.1. The 8-node brick element and the 20-node brick element (marked bold in Table 7.1) with a minimum size of 0.25 mm and 1.13 mm respectively were chosen to simulate the fracture toughness test. The 20-node element was later dropped because its performance was not as good as the 8-node element with the same number of total nodes when running in the full experimental data range.

As previously mentioned, the computer simulation has to match the original load versus load-line displacement data to be considered a reliable finite element model and, therefore, to be used as a valid resource in the investigation of stress or energy. In this finite element method study, the material properties are represented by the input of the true stress-strain curve as shown in Fig. 7.13 with a total of six points in the strain-hardening region. Fig. 7.14 and Fig. 7.15 show that the finite element

analysis for specimen C15 matches both the load-displacement curve with crack extension and the compliance ratio curve without crack extension. Specimen C15 is fabricated from A913 Grade 345 steel, has an initial crack length of  $0.50W$ , and was tested at room temperature. Both runs were displacement controlled with an external loading surface of  $1/4$  pinhole to simulate the contact surface in a real test and to avoid the local buckling at the loading nodes. The pre-calculated crack lengths by Eq. (5.10) were released when the node at the load line reached the corresponding displacement.

### 7.2.2 The Tri-Axial Stress State Ahead of the Crack Front

In the computer simulation with crack extension, the highest tri-axial stress status happened in the second row ahead of the crack front. The maximum principal stress was 1,350 MPa, which is about three times the yield stress and which matches the results reported by Chen et al. (2002).

A better parameter to define the degree of plane-strain would be the strain energy density  $\Delta W/\Delta V$ . In a tri-axial loading

$$\frac{\Delta W}{\Delta V} = \frac{1}{2E}(\sigma_x + \sigma_y + \sigma_z)^2 - \frac{\nu}{E}(\sigma_x\sigma_y + \sigma_y\sigma_z + \sigma_z\sigma_x) + \frac{1}{2\mu}(\tau_{xy}^2 + \tau_{yz}^2 + \tau_{zx}^2) \quad (7.3)$$

In Fig. 7.16 and Fig. 7.17 the total strain energy density and its distortional and dilatational components are extracted from the finite element results for specimen C15 modeled without any side groove. Fig. 7.16 shows the SED state ahead of the crack front at the crack length  $a/W = 0.541$  at which the crack has grown by 2.1 mm;

Fig. 7.17 shows the SED state at  $a/W = 0.566$  at which the crack has grown by 3.4 mm. Identical information is shown in Fig. 7.18 and Fig. 7.19, except for the fact that 20 percent side grooves were in the model that was used in the test.

Clearly, the distortional component stays constant in both cases. This result is expected because ABAQUS adopts the Von Mises criterion that should be true both theoretically and practically. The model without side grooves shows a higher SED in the middle plane of the specimen and a lower SED close to the surface, which is reasonable because it is a plane-stress condition on the free surface. Whereas the model with side grooves shows ups and downs along the elements ahead of the crack front. The side grooves are introduced into the C(T) specimen to eliminate the plane-stress condition and to keep the crack front straight while it advances. Although the tri-axial stress level is elevated close to the surface, as shown in Fig. 7.18 and 7.19, there is also a significant increase of the SED in the quarter point of the specimen. The SED in this point is 50 to 90 percent higher than the elements in the middle and on the surface. Although the crack front is assumed to be straight in the model, in reality the huge difference in SED ahead of the crack tip would cause an irregular advancing of the crack front. This could be the reason behind the not good predictions of the energy release rate in some of the specimens analyzed in Chapter 6 (i.e., specimen C1 and C16 shown in Chapter 6, Fig. 6.11).

### 7.3 Conclusions and Future Work

The primary conclusions of this research are:

- The  $J$ -integral and the  $J$ - $R$  curve should not be used anymore as the resistance parameter in plastic fracture mechanics because they are based on a crack tip singularity analysis, and the computational method specified by ASTM for practical purposes is misleading.
- The resistance curve of the energy release rate versus crack extension, in conjunction with the plastic tearing mechanism motion (both of which were derived in this dissertation) can be used as the resistance factor for plastic tearing in tough steels. The energy release rate provides the measurement of the toughness in plastic tearing, while the mechanism motion provides the maximum allowed degree of tearing.
- For a given steel type, testing multiple specimens with different initial crack lengths within one specimen size is not necessary.
- The side grooves, which are highly recommended by the ASTM specification E1820 to ensure the straight crack front, are not necessarily effective.
- The application of the finite element method in plastic tearing problems should be limited. Each modeling should be treated carefully and should match the experimental load versus displacement data.

The author would suggest the following future work:

- Experimentally investigate the effect of side grooves to the energy release rate resistance curve. The test data can be compared with the results from the finite element modeling in this dissertation.
- Experimentally investigate the effect of the fatigue precracking/machinery notch to the energy release rate resistance curve. If the notch type does not affect the energy release rate, the preparation of initial fatigue precracking can be saved.
- Conduct more experimental work on energy release rate resistance curve with C(T) specimens at higher temperature range as to the interest of nuclear industries. This dissertation has shown that mild change from room temperature does not affect the energy release rate. However, the nuclear reactors normally operate at several hundred degrees above room temperature, and it is possible there is a transition temperature that affects the energy release rate.

Table 7.1 Summary of Modeling

Element Type	Min. Ele. Size (mm)	Method in Transition	Number of Node/Element	Running Time @ 60 kN	Comments
8-Node Brick	1.15	Biased	4900/3800	10 Min.	Not Refined Enough
8-Node Brick	0.70	Biased	4900/3800	10 Min.	
8-Node Brick	0.35	Biased	9400/7400	20 Min.	Results Closed to each other, Recommend
<b>8-Node Brick</b>	<b>0.25</b>	<b>Biased</b>	<b>10900/8600</b>	<b>25 Min.</b>	
<b>20-Node Brick</b>	<b>1.13</b>	<b>Biased</b>	<b>10950/2190</b>	<b>35 Min.</b>	More Iterations
20-Node Brick	1.15	Biased	16600/3400	2 Hrs.	Slow Converging, too many iterations
20-Node Brick	0.70	Biased	20100/4100	3 Hrs.	
20-Node Brick	0.35	Biased	35700/7400	Over Night	Unreal Plastic Strain
20-Node Brick	0.25	Biased	40300/8400	Over Night	
8-Node Brick	1.15	Tetrahedron	6600/6600	15 Min.	Stress Contour No Good
8-Node Brick	1.15	None	26600/23200	1 Hr.	Not Economic
20-Node Brick	1.15	Biased,G.L.	16600/3400	30 Min.	Unreal Deformation



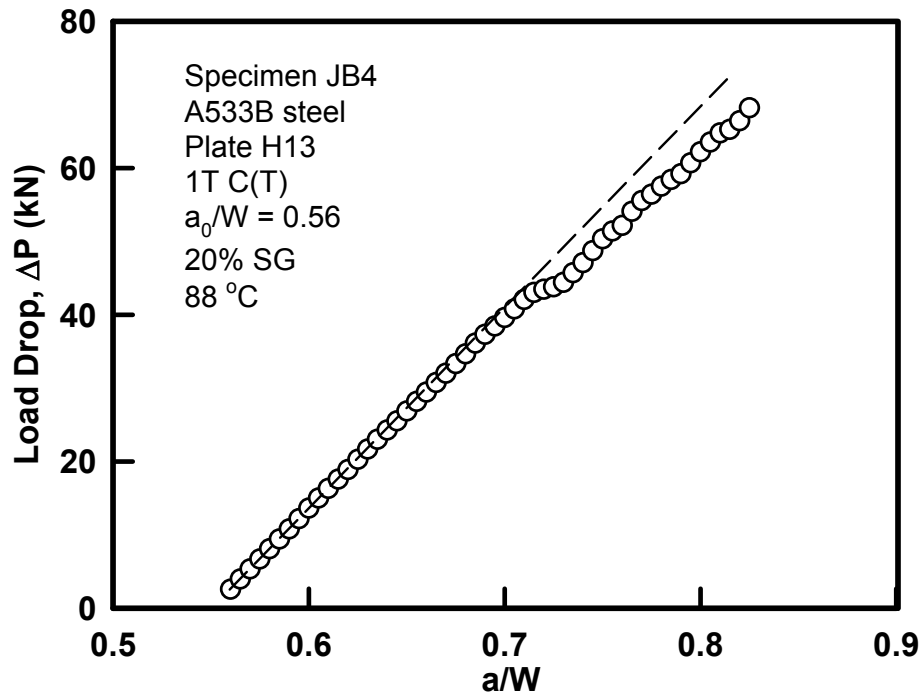


Fig. 7.1 Load Drop vs. Crack Extension; A533B Steel, Specimen JB4, 1T C(T), 88°C,  $a_0/W = 0.56$

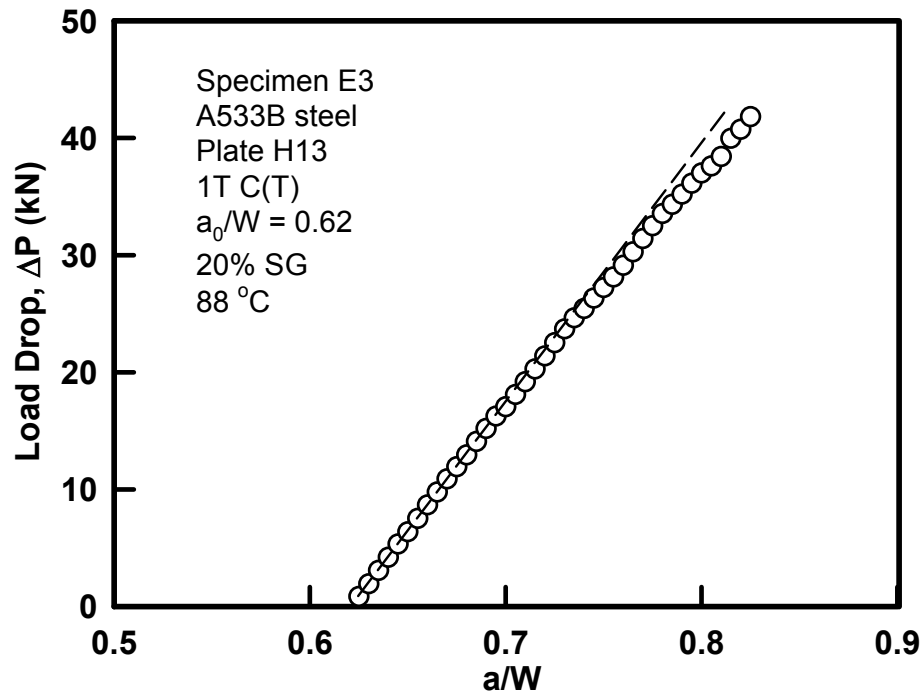


Fig. 7.2 Load Drop vs. Crack Extension; A533B Steel, Specimen E3, 1T C(T), 88°C,  $a_0/W = 0.62$

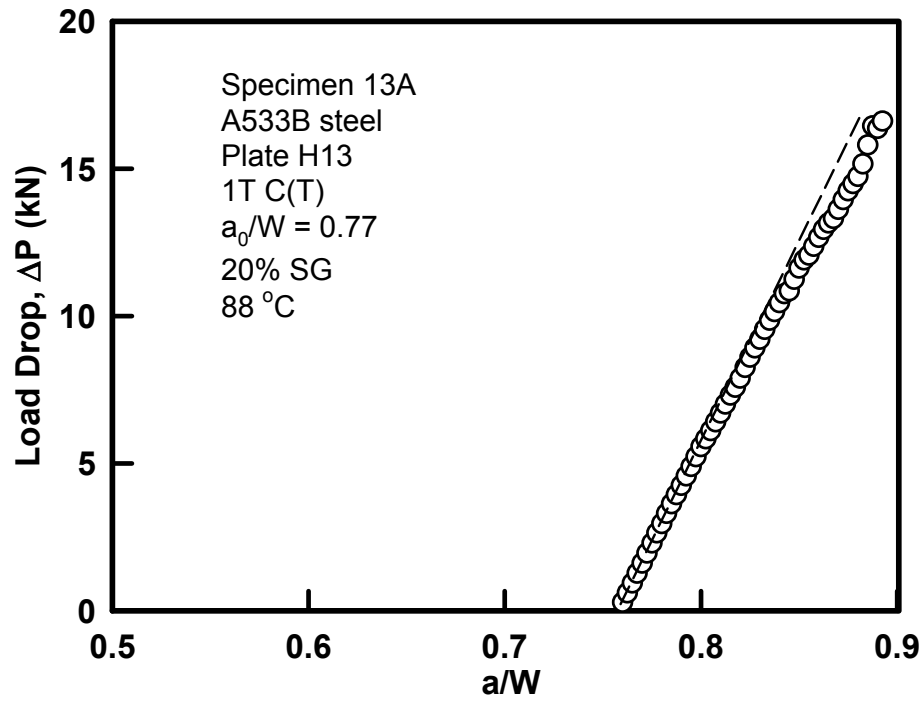


Fig. 7.3 Load Drop vs. Crack Extension; A533B Steel, Specimen 13A, 1T C(T), 88°C,  $a_0/W = 0.77$

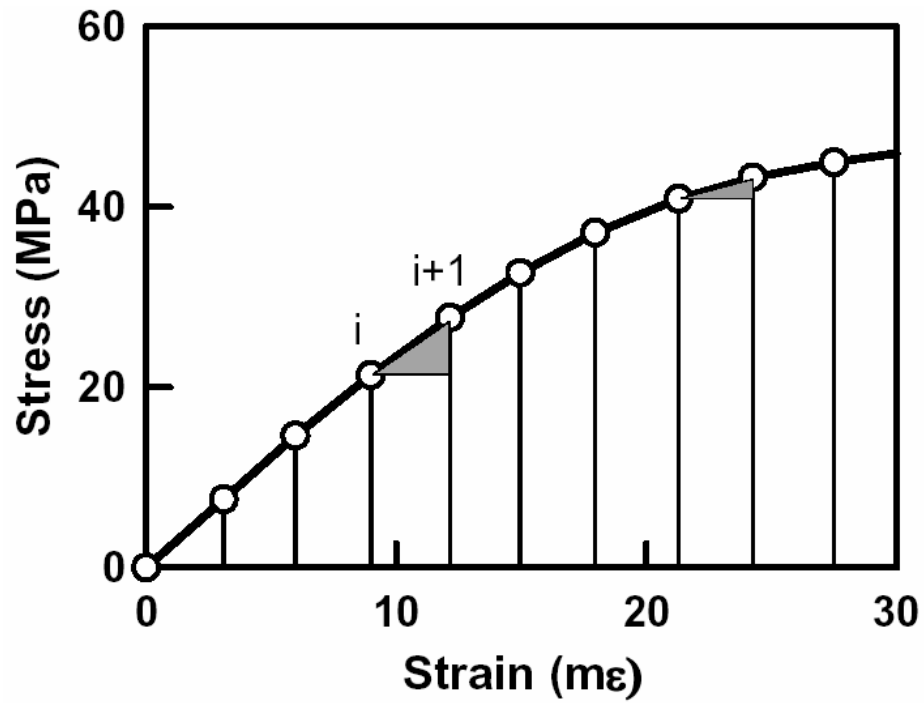


Fig. 7.4 Definition of Strain Energy Density (Lenwari et al. 2005)

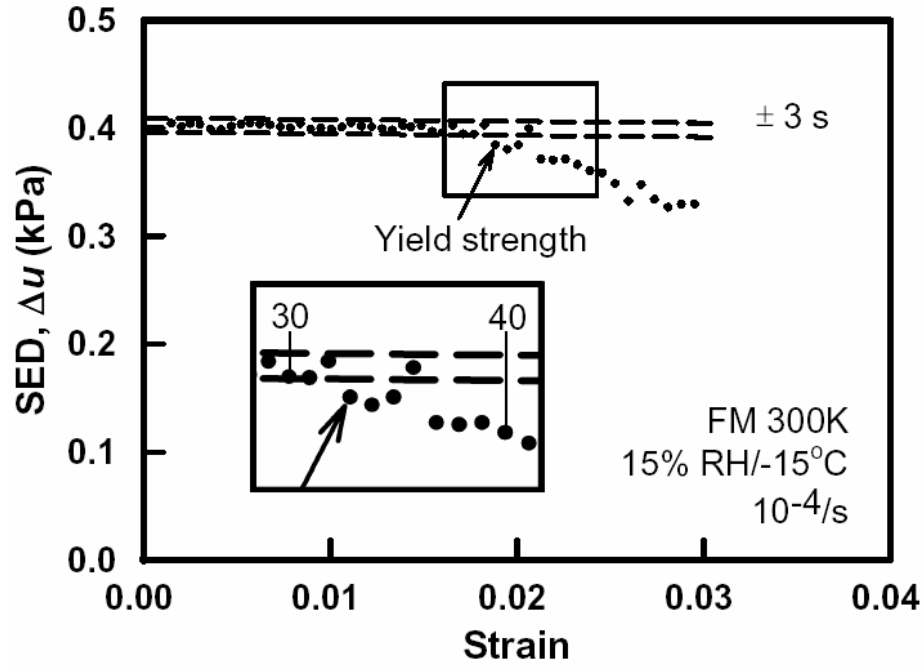


Fig. 7.5 Accurate Yield Point in Adhesive FM 300K at 15% RH, -15°C and 10<sup>-4</sup>/s strain rate (Lenwari et al. 2005)

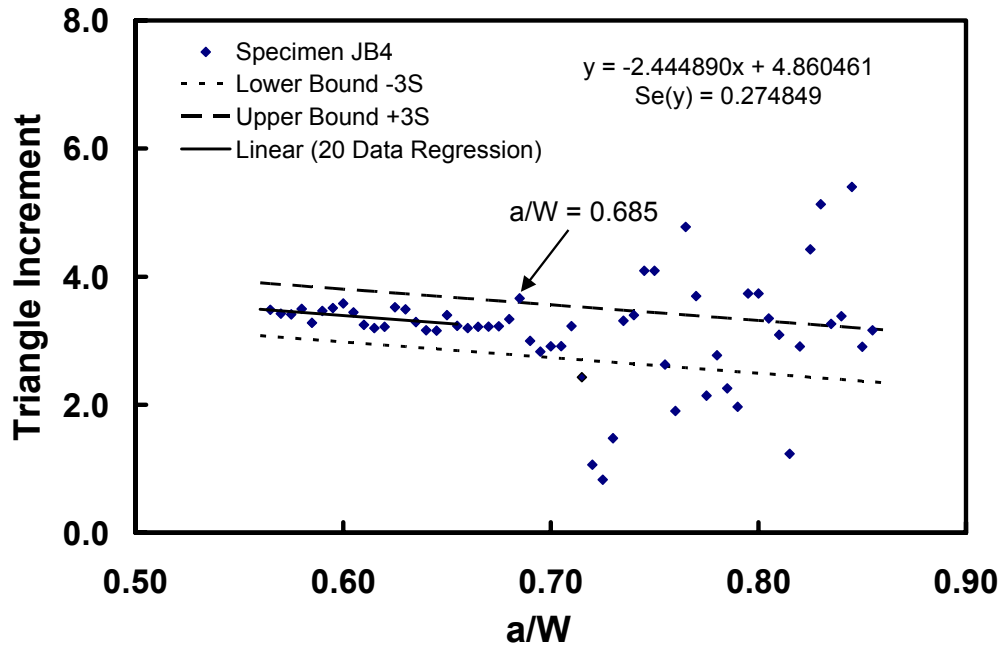


Fig. 7.6 Deviation Point of Load Drop, A533B Steel, Specimen JB4, 1T C(T), 88°C,  $a_0/W = 0.56$

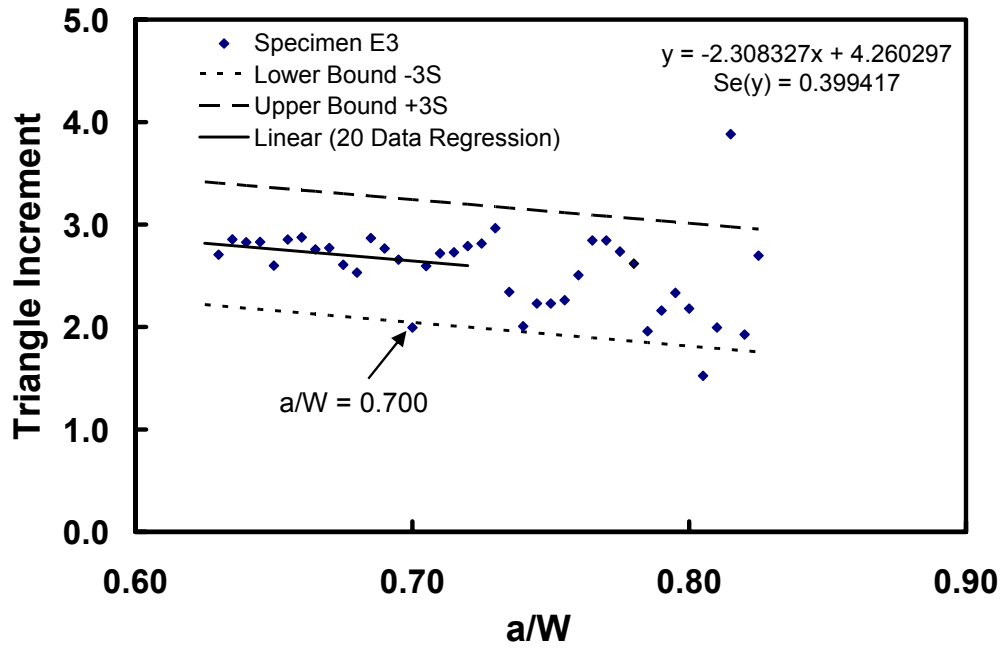


Fig. 7.7 Deviation Point of Load Drop, A533B Steel, Specimen E3, 1T C(T), 88°C,  $a_0/W = 0.62$

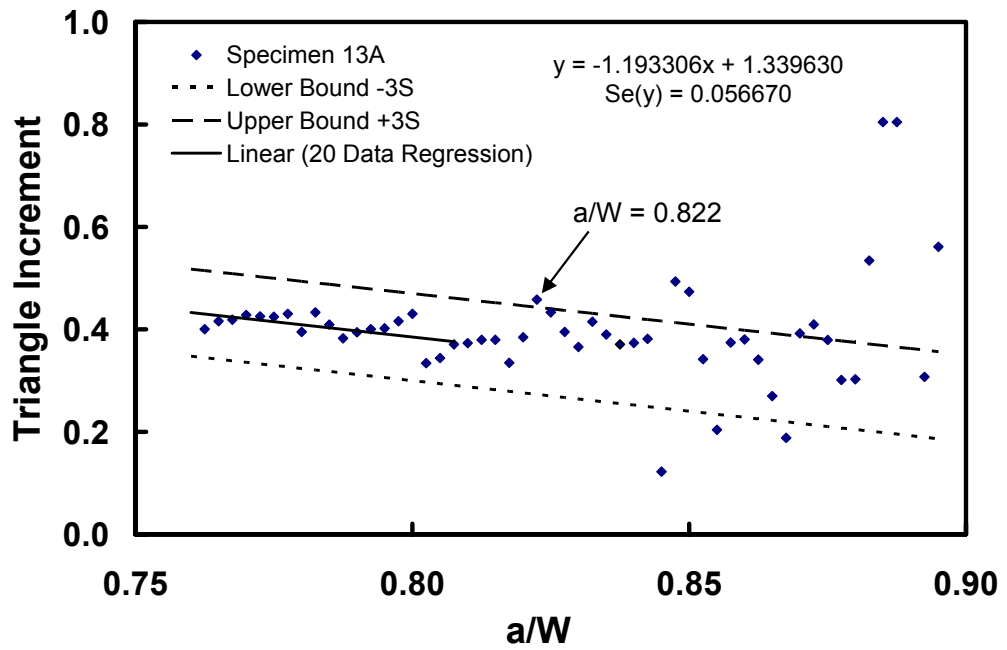


Fig. 7.8 Deviation Point of Load Drop, A533B Steel, Specimen 13A, 1T C(T), 88°C,  $a_0/W = 0.77$

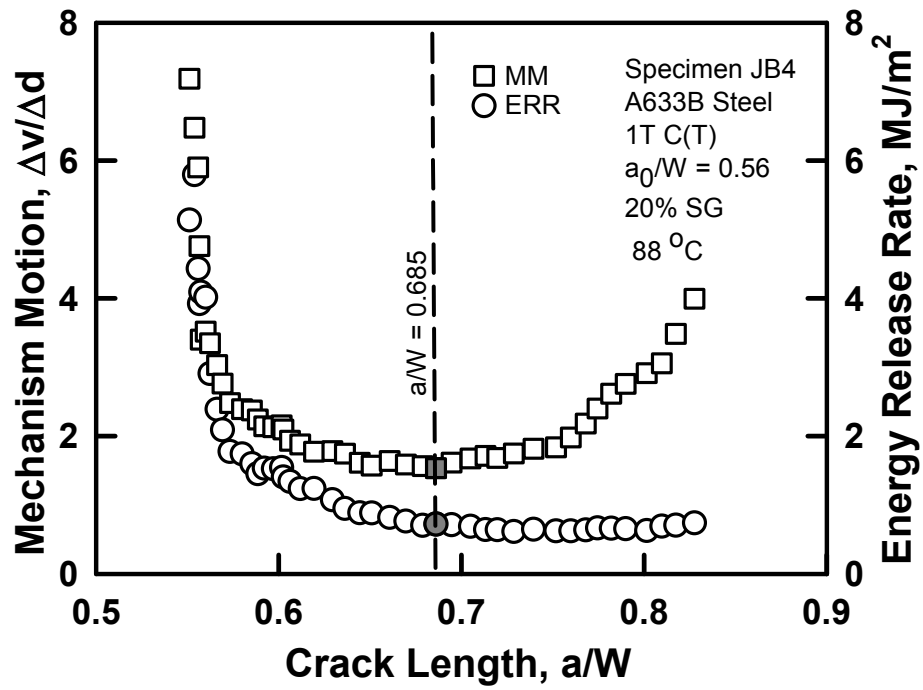


Fig. 7.9 Data Range Validation on Energy Release Rate by Plastic Tearing Mechanism Motion for Specimen JB4

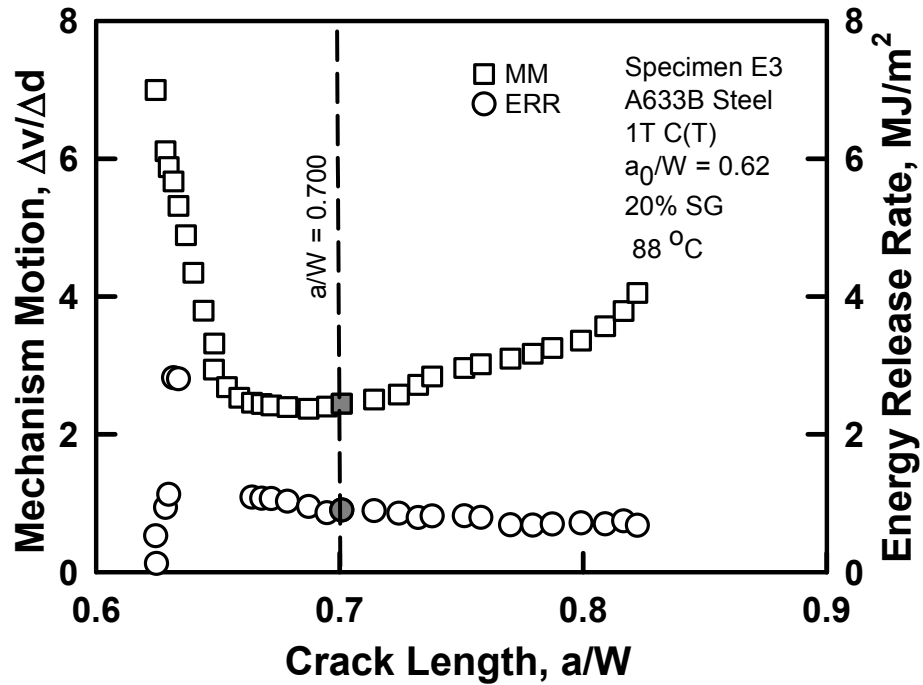


Fig. 7.10 Data Range Validation on Energy Release Rate by Plastic Tearing Mechanism Motion for Specimen E3

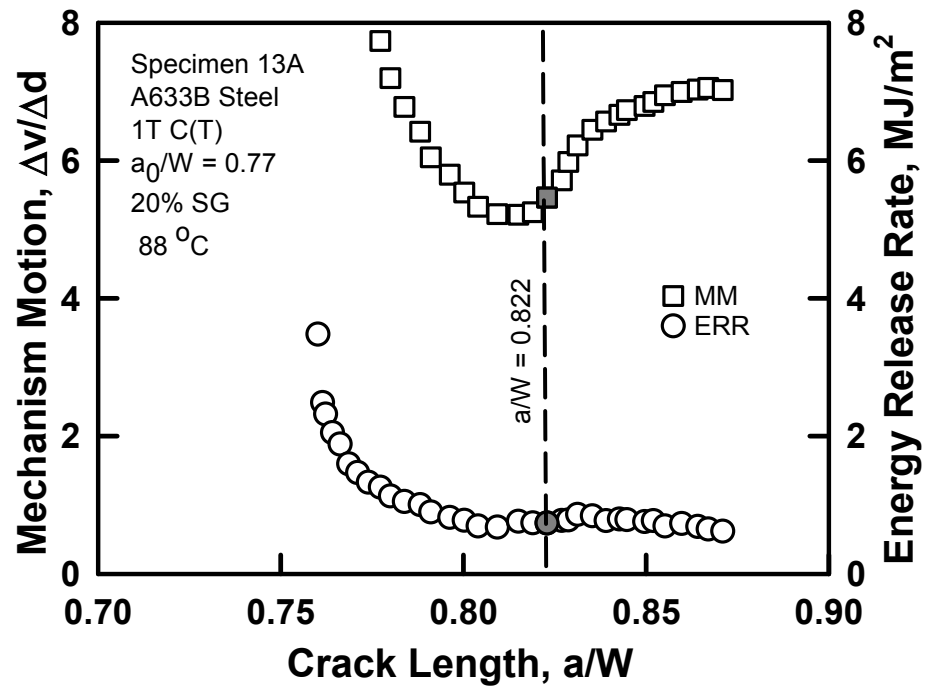


Fig. 7.11 Data Range Validation on Energy Release Rate by Plastic Tearing Mechanism Motion for Specimen 13A

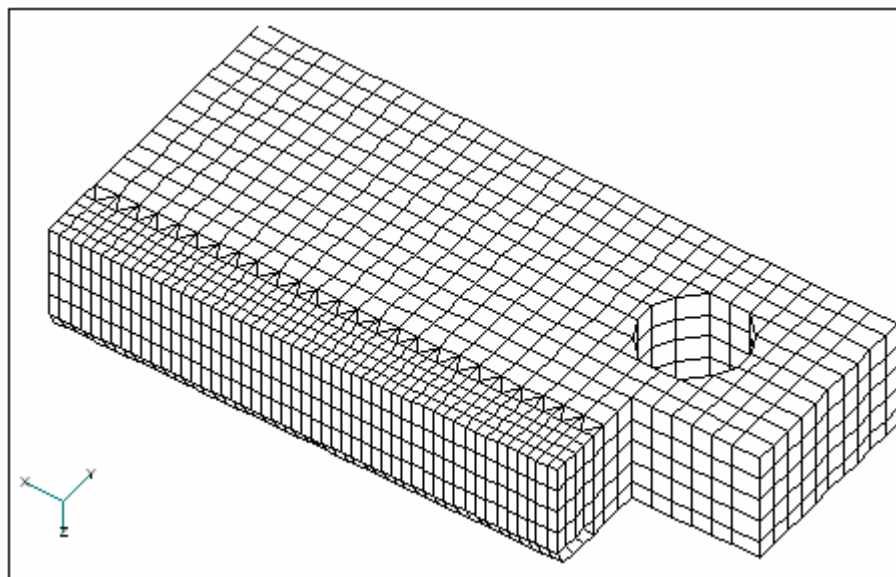


Fig. 7.12 Typical ABAQUS Model of Quarter 1T C(T) Specimen

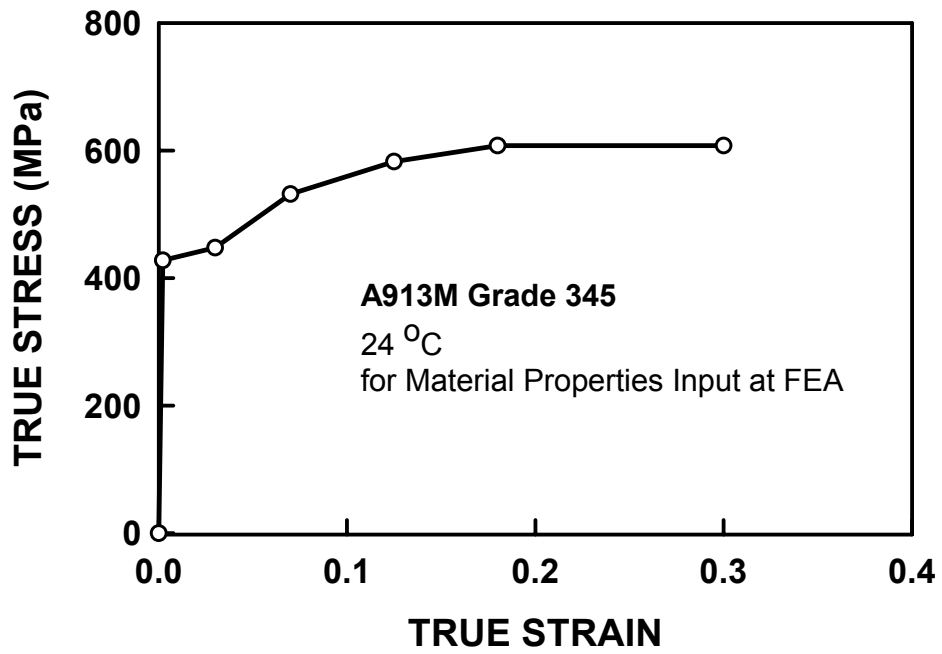


Fig. 7.13 True Stress-Strain Curve in FEA Input

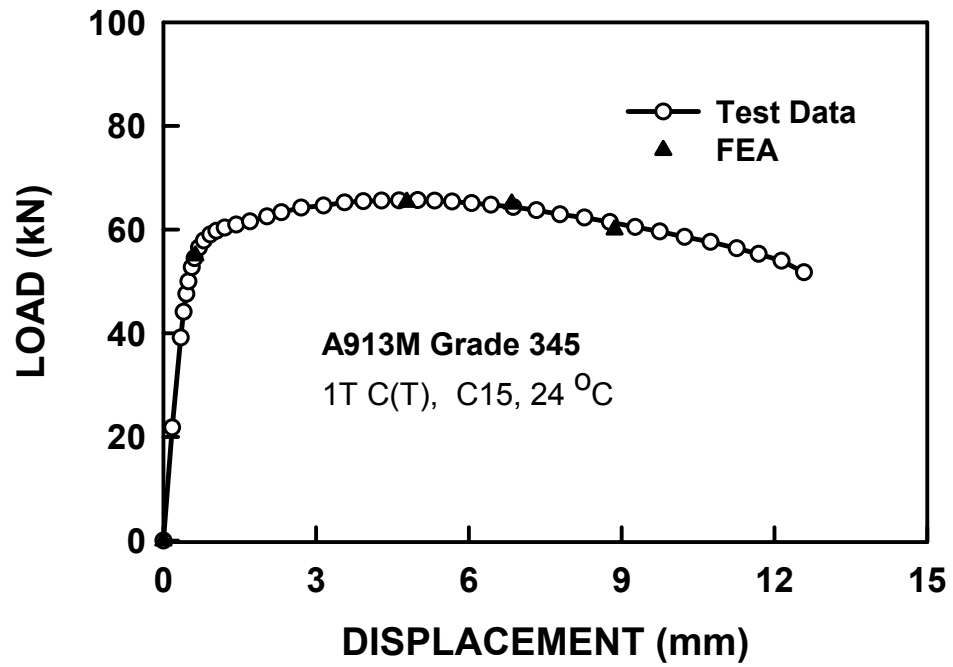


Fig. 7.14 Load-Displacement Verification for FEA Running With Crack Extension; A913-345, Specimen C15, 1T C(T), 24°C,  $a_0/W = 0.50$

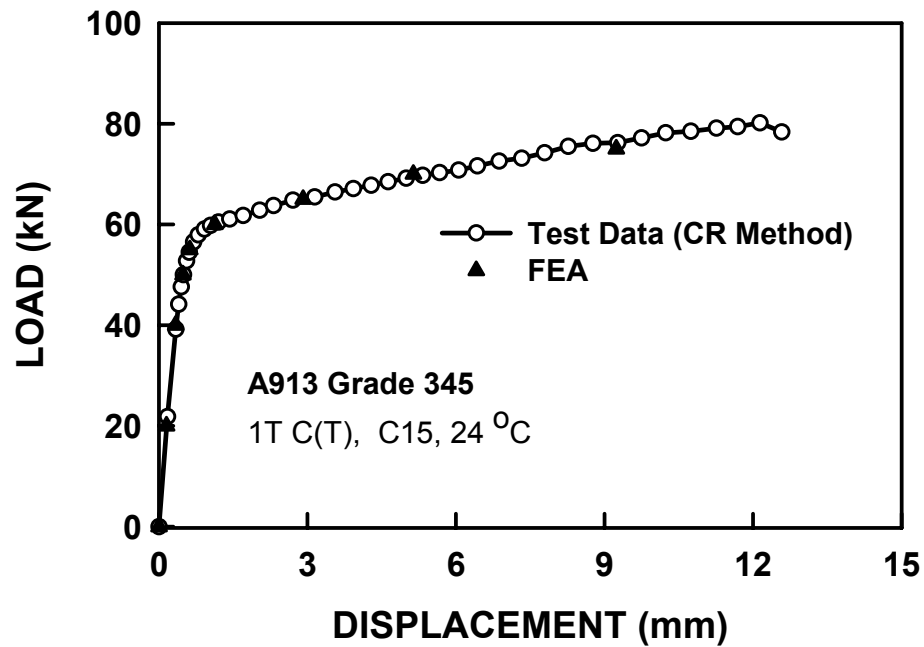


Fig. 7.15 CR Curve Verification for FEA Running Without Crack Extension; A913-345, Specimen C15, 1T C(T), 24°C,  $a_0/W = 0.50$

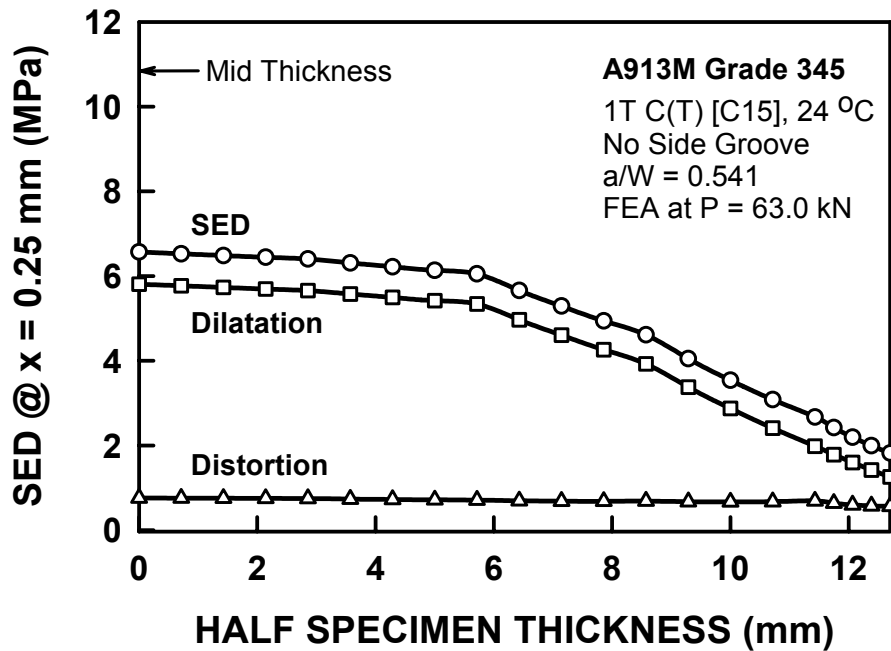


Fig. 7.16 SED From FEA Model Without Side Groove; A913-345, Specimen C15, 1T C(T), 24°C, at  $a/W = 0.541$



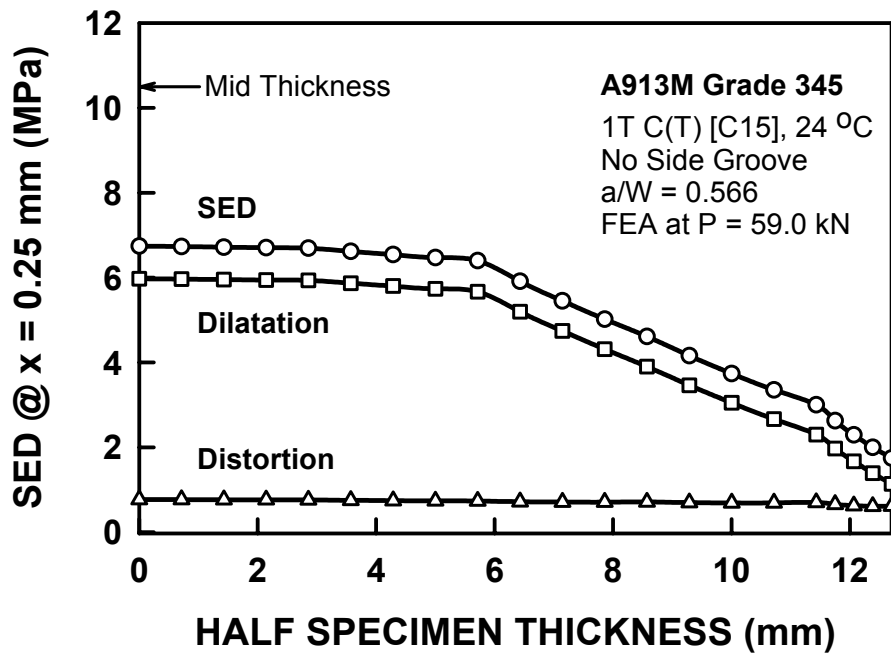


Fig. 7.17 SED From FEA Model Without Side Groove; A913-345, Specimen C15, 1T C(T), 24°C, at  $a/W = 0.566$

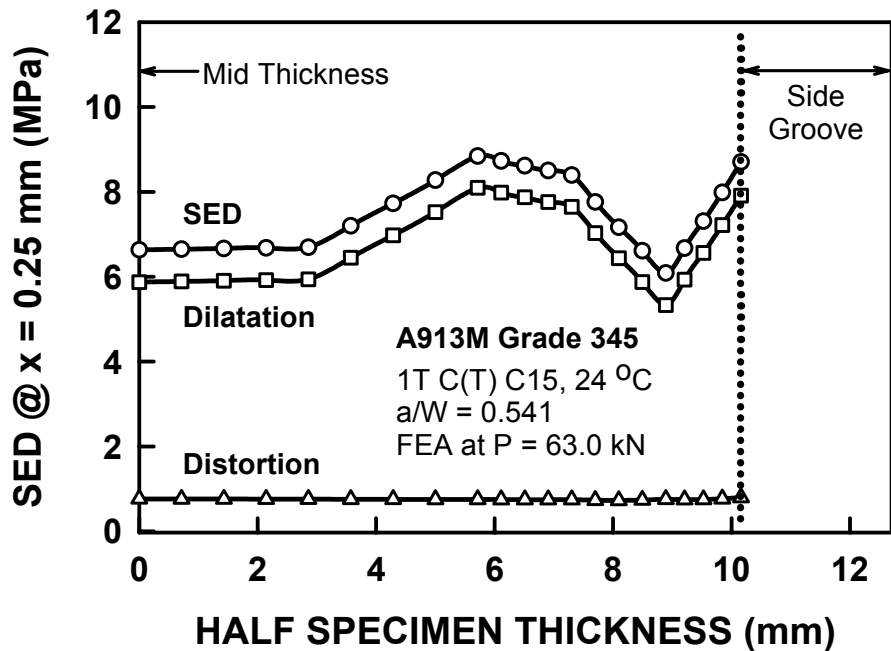


Fig. 7.18 SED From FEA Model With 20% Side Grooves; A913-345, Specimen C15, 1T C(T), 24°C, at  $a/W = 0.541$

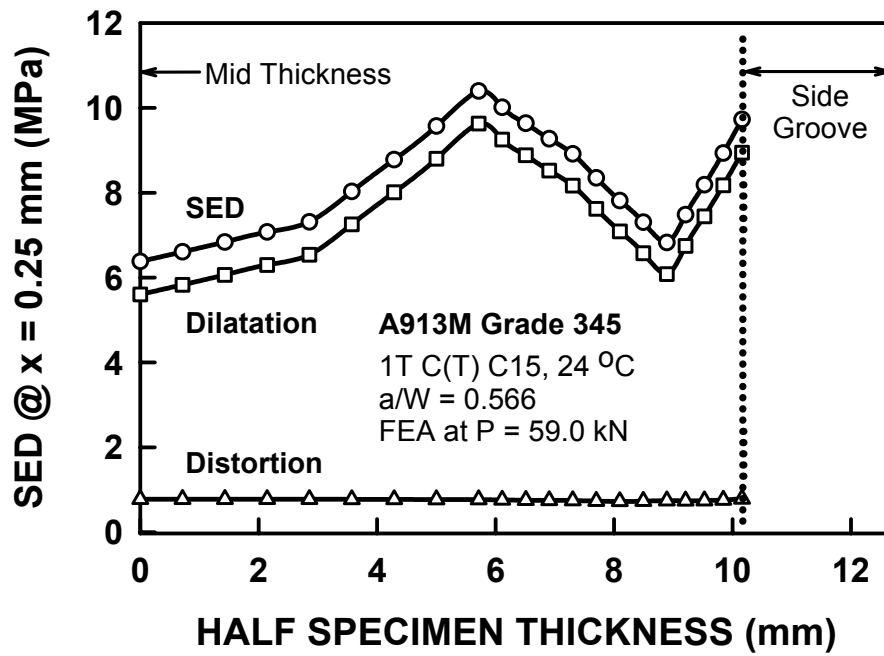


Fig. 7.19 SED From FEA Model With 20% Side Grooves; A913-345, Specimen C15, 1T C(T), 24°C, at  $a/W = 0.566$

## REFERENCES

- ASTM (1988). "Draft Standard Test Method for Crack Tip Opening Displacement (CTOD) Fracture Toughness Measurement." Working Document for E24 Committee, ASTM, Philadelphia, PA.
- ASTM (1990). "Standard Test Method for Plane-Strain Fracture Toughness of Metallic Materials." E399-90 (Reapproved 1997).
- ASTM (1999). "Standard Test Method for Measurement of Fracture Toughness." E1820-99a, Annual Book of ASTM Standards, Vol. 03.01, pp. 1000-1033.
- Bilby, B. A., Cottrell, A. H. and Swinden, K. H. (1963). "The Spread of Plasticity from a Notch." Proceedings, Series A 272, Royal Society, London, pp. 304-312.
- Brocks, W. and Yuan, H. (1991). "Numerical Studies on Stable Crack Growth." Defect Assessment in Components – Fundamentals and Applications, ESIS Pub. 9, pp. 19-33.
- Brocks, W. and Anuschewski, P. (2004). "Parametrizing Ductile Tearing Resistance by Four Parameters." Engineering Fracture Mechanics 71, pp. 127-146.
- Broek, D. (1982). "Elementary Engineering Fracture Mechanics." Martinus Nijhoff, Boston, MA.
- BS7448 Part 4: 1997. "Method for Determination of Fracture Resistance Curve and Initiation Values for Stable Crack Extension in Metallic Materials."
- BSI (1979). "Methods for Crack Opening Displacement (COD) Testing." BS 5762, British Standards Institution, London, England.
- Candra, H. (2001). "Compliance Ratio Method of Estimating Crack Extension in Static and Dynamic Fracture Toughness Tests." Ph. D. Dissertation, University of Maryland at College Park.
- Candra, H., Wright, W. J. and Albrecht, P. (2002). "Experimentally Determined Key Curves for Fracture Specimens." International Journal of Fracture, Vol. 117, pp. 247-267.

Castro, P. M. S. T., Spurrier, J. and Hancock, P. (1979). "An Experimental Study of a/W Dependence of COD Test Using Small-Scale Specimen." Fracture Mechanics: 11th Symposium, ASTM STP 677, ASTM, Philadelphia, PA, pp. 486-497.

Chapuliot, S., Marie, S., and Moulin, D. (2001). "An Energetic Approach for Large Ductile Crack Growth in Components." Fatigue and Fracture Mechanics: 32nd Volume, ASTM STP 1406, pp. 229-246.

Chen, X., Candra, H., Wright, W. J. and Albrecht, P. (2003). "Plastic Tearing Energy of Ductile Steels." Second International ASTM/ESIS Symposium on Fatigue and Fracture Mechanics, November 19-21, Tampa, Florida

Chen, Y., Lee, J. D. and Eskandarian, A. (2002). "Local and Nonlocal Meshless Method of Fracture Mechanics", Proceedings of International Conference of Computational Engineering and Science, July 29 –Aug. 2, Reno, Nevada.

Czoboly, E., Havas, I. and Gillemot, F. (1981). "The Absorbed Specific Energy Till Fracture as a Measure of the Toughness of Metals." Symposium on Absorbed Specific Energy/Strain Energy Density Criterion, Martinus Nijhoff Publishes, Hague, The Netherlands, pp. 107-129.

Dawes, M. G. (1979). "Elastic-Plastic Fracture Toughness Based on the COD and J-contour Integral Concepts." Elastic-Plastic Fracture, ASTM STP 668, ASTM, Philadelphia, PA, pp. 307-333.

Dawicke, D. S., Newman, J. C., Jr. and Bigelow, C. A. (1999). "Residual Strength Predictions for Multiple-Site Damage Using a Three-Dimensional Finite-Element Analysis and a CTOA Criterion." ASTM STP 1332, pp. 815-829.

De Koning, A. U. (1975). "A Contribution to the Analysis of Slow Stable Crack Growth." Report NLR MP 75035U, The Netherlands National Aerospace Laboratory, Holland.

Dugdale, D. S. (1960). "Yielding of Steel Sheets Containing Slits." Journal of Mechanics and Physics of Solids, Vol. 8, pp. 100-104.

Etemad, M.R., and Turner, C.E. (1990). "Unique Elastic-Plastic R-Curves: Fact or Fiction?" Fracture Mechanics: Twenty-First Symposium, ASTM STP 1074, pp. 289-306.

- Garwood, S. J. (1988). "A Crack Tip Opening Displacement Method for the Analysis of Ductile Materials." Fracture Mechanics, 18th Symposium, ASTM STP 945, ASTM, Philadelphia, PA, pp.957-985.
- Green, A. P (1953). "The Plastic Yielding of Notched Bars due to Bending." Journal of Mechanics and Applied Mathematics, Vol. 6, Part 2, pp. 223-239.
- Green, A. P. and Hundy, B. B. (1956). "Initial plastic Yielding in Notch Bend Tests." Journal of Mechanics and Physics of Solids, Vol. 4, pp. 128-145.
- Green, G. and Knott, J. F. (1975). "On Effects of Thickness on Ductile Crack Growth in Mild Steel." Journal of Mechanics and Physics of Solids, Vol. 4, pp. 128-145.
- Griffith, A. A. (1920). "The Phenomena of Rupture and Flow in Solids." See "Fracture Mechanics Retrospective", ASTM RPSI, American Society for Testing and Materials, Philadelphia, Pennsylvania, 1972.
- Gullerud, A. S., Dodds, R. H., Jr., Hampton, R. W. and Dawicke, D. S. (1999). "Three-Dimensional Modeling of Ductile Crack Growth in Thin Sheet Metals: Computational Aspects and Validation." Engineering Fracture Mechanics, Vol. 63, pp. 347-374.
- Hibbit, Karlsson & Sorensen, Inc. (2003). "ABAQUS User's Manual." Version 6.4.
- Hu, J. M. (1989). "Analysis of Ductile Crack Extension in Plastic Fracture." Ph. D. Dissertation, University of Maryland at College Park.
- Hu, J. M. and Albrecht, P. (1991). "Limit Load Solution and Loading Behavior of C(T) Fracture Specimen." International Journal of Fracture, Vol. 52, pp. 19-45.
- Hutchinson, J. W. (1968). "Singular Behavior at the End of Tensile Crack in A Hardening Material." Journal of Mechanics and Physics of Solids, Vol. 16, pp. 13-31.
- Hutchinson, J. W. (1983). "Fundamentals of the Phenomenological Theory of Nonlinear Fracture Mechanics." Transactions of the ASME, Vol. 50, pp. 1042-1051.
- Irwin, G.R. (1956). "Onset of Fast Crack Propagation in High Strength Steel and Aluminum Alloys." Proc. 2<sup>nd</sup> Sagamore Conf. Ordnance Materials. Vol. II: 289-35. Syracuse, NY: Syracuse University Press, and NRL Report No. 4763 (U), May, PB121224.

- Irwin, G. R. (1957). "Analysis of Stress and Strain near the End of A Crack Transversing A Plate." *Journal of Applied Mechanics*, Vol. 24, pp. 361-364.
- Irwin, G. R. and Kies, J. A. (1954). "Critical Energy Release Rate Analysis of Fracture Strength." *Welding Journal, Research Supplement*, Vol. 19, pp. 193-198.
- James M.A. (1998). "A Plane Stress Finite Element Model for Elastic-Plastic Mode I/II Crack Growth." Ph. D. Dissertation, Department of Mechanical and Nuclear Engineering, Kansas State University.
- Janssen, M., Zuidema, J., and Wanhill, R. J. H. (2002). "Fracture mechanics" 2<sup>nd</sup> Edition, Delft DUP Blue Print.
- Joyce, J.A., Davis, D.A., Hackett, E.M., and Hays, R.A. (1990). "Application of *J*-Integral and Modified *J*-Integral to Cases of Large Crack Extension." *Fracture Mechanics: Twenty-First Symposium*, ASTM STP 1074, pp. 85-105.
- Kanninen, M. F. and Popelar, C. H. (1985). "Advanced Fracture Mechanics." Oxford University Press, New York.
- Kumar, V. and Shih, C. F. (1980). "Fully Plastic Crack Solution, Estimation Scheme, and Stability Analysis for the Compact Specimen." *Fracture Mechanics, 12th Conference*, ASTM STP 700, ASTM, Philadelphia, PA, pp. 406-436.
- Landes, J. D. and Begley, J. A. (1972). "The Effect of Specimen Geometry on  $J_{Ic}$ ." *ASTM STP 514, Part2*, 1972, pp. 24-39.
- Lenwari, A., Albrecht, P. and Albrecht, M. (2004). "SED Method of Measuring Yield Strength of Adhesives and Other Materials." *ASTM Symposium on Advances in Adhesives, Adhesion Science, and Testing*, October 4, Washington, D. C.
- Mecklenburg, M. F., Joyce, J. A., and Albrecht, P. (1989). "Separation of Energies in Elastic-Plastic Fracture." *Nonlinear Fracture Mechanics*, ASTM STP 995, pp. 594-612.
- Meyers, M. A. and Chawla, K. K. (1999). "Mechanical Behavior of Materials." Prentice-Hall, Inc., Upper Saddle River, NJ.

- Miller, K. J. and Kfoury, A. P. (1979). "A Comparison of Elastic-Plastic Fracture Parameters in Biaxial Stress State." Elastic-Plastic Fracture, ASTM STP 668, ASTM, Philadelphia, PA, pp. 65-120.
- Milne, I., and Chell, G.G. (1979). "Effect of Size on the J Fracture Criterion." Elastic-Plastic Fracture, ASTM STP 668, pp. 358-377.
- National Transportation Safety Board (1970). "Collapse of U.S. 35 Highway Bridge Point Pleasant, West Virginia." Highway Accident Report, NTSB Number: HAR-71/01.
- Newman, J. C., Jr. (1985). "Prediction of Stable Crack Growth and Instability Using VR-Curve Method." Elastic-Plastic Fracture Technology, ASTM STP 896, ASTM, Philadelphia, PA, pp. 139-166.
- Newman, J. C., Jr., McNeill, S. R. and Sutton, M. A. (1988). "Application of the VR Resistance Curve Method to Fracture of Various Crack Configurations." Fracture Mechanics, 18th Symposium, ASTM STP 945, ASTM, Philadelphia, PA, pp.103-117.
- Newman, J. C., Jr., Shivakumar, K. N. and McCabe, D. E. (1991). "Finite Element Fracture Simulation of A533B Steel Sheet Specimens." Defect Assessment in Components – Fundamentals and Applications, ESIS Pub. 9, pp.117-126.
- Newman, J. C., Jr., James, M. A. and Zerst, U. (2003). "A Review of the CTOA/CTOD Fracture Criterion." Engineering Fracture Mechanics, Vol. 70, No. 3-4, pp. 371-386.
- Paris, P. C., Tada, H., Zahoor, A. and Ernst, H. (1979). "The Theory of Instability of the Tearing Mode of Elastic-Plastic Crack Growth." Elastic-Plastic Fracture, ASTM STP 668, ASTM, Philadelphia, PA, pp. 5-36.
- Rice, J. R. (1968). "A Path Independent integral and the Approximate Analysis of Strain Concentration by Notches and Cracks." Journal of Mechanics and Physics of Solid, Vol. 15, pp. 379-386.
- Rice, J. R. and Rosergren, G. F. (1968). "Plane Strain Deformation Near a Crack Tip in a Power Law Hardening Material." Journal of Mechanics of Physics of Solids, Vol. 16, pp. 1-12.

- Rice, J. R. and Sorensen, E. P. (1978). "Continuing Crack Tip Deformation and Fracture for Plane Strain Crack Growth in Elastic-Plastic Solids." *Journal of Mechanics and Physics of Solids*, Vol. 26, pp. 163-186.
- Schwalbe, K. -H. (1995). "Introduction of  $d_5$  as an Operational Definition of the CTOD and Its Practical Use." *Fracture Mechanics: 26th Volume, ASTM STP 1256*, pp. 763 -778.
- Schwalbe, K. -H., Newman, J. C., Jr. and Shannon, J. L, Jr. (2004). "Fracture Mechanics Testing on Specimens with Low Constraint - Standardisation Activities with ISO and ASTM." *Volume 72, No. 4*.
- Shi, J. (2004). "Stochastic Modeling of Materials with Complex Microstructure." Ph. D. Dissertation, The Johns Hopkins University.
- Shih, C. F., Delorenzi, H. G. and Andrews, W. R. (1979). "Studies on Crack Initiation and Stable Crack Growth." *Elastic-Plastic Fracture, ASTM STP 668*, ASTM, Philadelphia, PA, pp.65-120.
- Shih, C. F. and Hutchinson, J. W. (1971). "Fully Plastic Solutions and Large Scale Yielding Estimates for Plane Stress Crack Problems." *Journal of Engineering Material and Technology*, Vol. 98, pp. 289-295.
- Sih, G. C. (1973). "Some Basic Problems in Fracture Mechanics and New Concepts." *Journal of Engineering Fracture Mechanics*, Vol.5, pp. 365-377.
- Sumpter, J.G.D. (1999). "An Alternative View of R Curve Testing." *Engineering Fracture Mechanics*, Elsevier Science Ltd., Vol. 64, pp. 161-176.
- Sumpter, J.G.D. (2004a). "The Energy Dissipation Rate Approach to Tearing Instability." *Engineering Fracture Mechanics*, Elsevier Science Ltd., Vol. 71, pp. 17-37.
- Sumpter, J.G.D. (2004b). "An Alternative View of R Curve Testing." *Engineering Fracture Mechanics*, Elsevier Science Ltd., Vol. 71, pp. 39-56.
- Thomason, P.F. (1990). "An Assessment of the Validity of  $J$  Controlled Growth and the Stability of Cracks in Incremental Elastic-plastic Solids." *International Journal of Fracture*, Vol. 44, pp. 259-281.



Turner, C. E. (1984). "Method for Post-Yield Fracture Safety Assessment." Post-Yield Fracture Mechanics, G. H. Latzko, Ed., pp. 25-221.

Turner, C. E. and Kolednik, O. (1994). "A Micro and Macro Approach to the Energy Dissipation Rate Model of Stable Ductile Crack Growth." Fatigue. Fract. Engng. Mater. Struct., 17 (9), pp. 1089-1107.

Watson, T. J. and Jolles, M. I. (1986). "Plastic Energy Dissipation as a Parameter to Characterize Crack Growth." Fracture Mechanics: Seventeenth Volume, ASTM STP 905, J. H. Underwood, R. Chait, C. W. Smith, D. P. Wilhem, W. A. Andrews, and J. C. Newman, Eds., American Society for Testing and Materials, Philadelphia, pp. 542-555.

Wells, A. A. (1961). "Unstable Crack Propagation in Metals, Cleavage and Fast Fracture." The Crack Propagation Symposium, Cranfield, pp. 210-230.

Wells, A. A. (1963). "Application of Fracture Mechanics at and beyond General Yield." British Welding Res. Ass. Rept., M13/63.

Wells, A. A., Burdekin, F. M. and Stone, D. E. (1964). "A Written Discussion on Fracture Toughness." Fracture Toughness Testing and its Application, ASTM STP 381, pp. 400-405.

Wilkowski, G.M., Marschall, C.W., and Landow, M.P. (1990). "Extrapolation of C(T) Specimen *J-R* Curves." Fracture Mechanics: Twenty-First Symposium, ASTM STP 1074, pp. 56-84.